

moment of the total sum force about the center point	-	$(1,0)W$
Reynolds number	-	R
drag moment about the center point	-	$R(\theta)$
center of pressure about the center point	-	S_{00}
wave height	-	T
sum of particle velocities in the direction of the wave motion	-	U
velocity gradient along the wave	-	U_w
local acceleration of the wave	-	U/U_0
total wave height	-	W
water depth	-	h
developmental displacement at time t	-	$(1,1);d$
initial displacement at time $t=0$	-	$(1,-1);d_0$
displacement at time t	-	$(1);d$
the integral value of the displacement function	-	$(1)b$
nonlinear initial acceleration	-	$(1,x);I$
translational acceleration	-	\ddot{d}
nonlinear initial position	-	$(1,\dot{\theta},\theta)d$
nonlinear initial velocity	-	$(1,\dot{\theta},\theta)v$
nonlinear initial acceleration	-	$(1,\dot{\theta},\theta)\ddot{d}$
wave number	-	k
distance from center pass to the initial position of center	-	l
boundary condition distance along center, $a = k l$	-	s
time	-	t
initial displacement times used to calculate the primary approximation	-	n, n_0
horizontal component of the sum particle velocity	-	n
$\text{horizontal}(T\backslash H\pi) = n \cos(n - \omega t)$	-	n
horizontal, $n = \text{horizontal}(T\backslash S)(e^{(n-k)t}) \cos \omega t$	-	n^*
horizontal, $n^* = \text{horizontal}(S)(e^{(n-k)t}) \cos(n - \omega t)$	-	n^{**}
vertical component of the sum particle velocity	-	v
$\text{vertical}(T\backslash H\pi) = v \sin(n - \omega t)$	-	v
horizontal displacement, velocity, and acceleration of the center	-	\ddot{x}, \dot{x}, x
vector in phase space	-	x
derivative solution for a set of first order	-	$(1)^*x$
nonlinear displacement $\dot{x} = f(x, t)$	-	f
initial displacement vector at $t=0$ time increment	-	$(1,0)x\Delta$
final displacement vector at $t=\tau$ time increment	-	$(1,\tau)x\Delta$
vertical coordinate	-	z

Изложенија

Δ	disstance from mass center to tower pass	wave length	$V_s = 1/(k_4)^2$
V_s	wave height	$V_s = 1/(k_4)^2$	$V_s = (k_4 - 1)/(k_4)^2$
k_4	$V_s = 1/(k_4)^2$	$V_s = I/(k_4)^2$	$V_s = I/(k_4)^2$
I	moment of inertia of tower about its pass	inertia of drag force return	added mass moment of inertia of tower about its pass
I'	moment of inertia of tower about its pass	mass center	total drag force acting on the tower
F_d	drag force about its pass	inertia of drag force about its pass	drag force about its pass
F_t	total drag force about its pass	inertia of drag force about its pass	drag force about its pass
F_m	the Morison equation	the Morison equation	total drag force due to structure motion
D	total fluid force due to structure motion	drag force due to structure motion	drag force due to structure motion
$D\backslash D$	total fluid force due to structure motion	drag force due to structure motion	drag force due to structure motion
C_w	drag coefficient	inertia coefficient	inertia coefficient
C_a	drag coefficient	drag coefficient	drag coefficient
C_g	drag coefficient	drag coefficient	drag coefficient
C_s	drag coefficient	drag coefficient	drag coefficient
B	drag coefficient	drag coefficient	drag coefficient
A	drag coefficient	drag coefficient	drag coefficient

List of Figures

B.I	Calculation of the largest Lipschitz exponent from time series	31
4.1	Model of the self-organized power spectrum	38
4.2	Fredneucy response of the power using local and total acceleration .	45
4.3	Combination of the power response using total acceleration .	45
4.4	Combination of the power response using local acceleration .	46
4.5	Combination of the power response using local acceleration .	47
4.6	Fredneucy response for different values of C _y .	48
4.7	Fredneucy response for different values of M	50
4.8	Fredneucy response for different values of q	52
4.9	Fredneucy response for different values of B	55
4.10	Fredneucy response for different values of D	56
4.11	Two coexisting $\alpha = 3$ solutions	61
4.12	Period doubling bifurcation	63
4.13	Basins of attraction	64
4.14	Bifurcation diagram	66
4.15	Poincaré maps and power spectra	68
4.16	Poincaré maps and power spectra for chaotic response .	72
4.17	Partial enlargement of bifurcation diagram	74
4.18	Time evolution of the largest nonlocal Lipschitz exponent .	76

List of Tables

V.1	Solutions for $D = \text{Iw}$ using $DU/Dt = gU/gt + UgU/gx$	58
V.2	Solutions for $D = \text{Iw}$ using $DU/Dt = gU/gt + UgU/gx$	59
V.3	Solutions for $D = \text{Iw}$ using $DU/Dt = gU/gt + UgU/gx$	60
V.I	Solutions for $D = \text{Iw}$ using $DU/Dt = gU/gt$	73
V.2	Solutions for $D = \text{Iw}$ using $DU/Dt = gU/gt$	78
V.3	Solutions for $D = \text{Iw}$ using $DU/Dt = gU/gt$	80

Chapter 4

4.1	Response of an Artificially Fed Tower System Parameters	36
4.2	Combination of Solutions of Equations	40
4.3	Fednegec Response	42
4.4	Supplementary Response	47
4.5	Bifurcation to Chaos	69
4.6	Numerical Calculation of Lipschitz Exponent	73

Chapter 5

5.1	Sums and Conclusions	82
-----	----------------------	----

5.2	References	83
-----	------------	----

Appendix A

5.6	Solutions Using Local Acceleration Only	86
-----	---	----

Appendix B

B.1	Numerical Calculation of the Largest Lipschitz Exponent	80
B.2	Definition	80
B.3	Variation for Combining the Largest Lipschitz Exponent γ_1	85

Contents

		Chapter 1
1		Introduction
		Chapter 2
6		Literature Review
7	2.1	Wave Description and Sea States
8	2.2	Wave Loading
13	2.3	Review of Nonlinear Dynamics of Offshore Structures
17	2.4	Useful Tools of Nonlinear Dynamic Analysis
18	2.4.1	Poincaré Section
19	2.4.2	Liaison Exponent
21	2.4.3	Fourier Spectrum
		Chapter 3
23		Formulation of Equations of Motion
24	3.1	Linear Wave Theory
25	3.2	Motion Equations
27	3.3	Equations of Motion of Articulated Offshore Tower

Acknowledgements

I wish to thank my supervisor, Dr. V. W. Lipschutz, for his guidance, advice, and assistance in the preparation of this thesis.

I also wish to express my deep gratitude to my husband, Yann, for his unselfless understanding, encouragement and patience, who has supported both my research and my life.

Apsiract

As simple as it may seem, the concept of a system with a target power is relatively straightforward. One key factor in this thesis is the various ways in which this target power can be achieved. One method is through the use of a feedback loop, where the output of the system is compared to the desired output, and the difference is used to adjust the system's behavior. Another method is through the use of a feedforward controller, which takes into account the current state of the system and adjusts the input accordingly. Both methods have their advantages and disadvantages, and the choice between them depends on the specific application.

The first method, feedback control, is based on the principle of negative feedback. It involves comparing the actual output of the system to the desired output, and then adjusting the input to reduce the error. This method is often used in industrial control systems, such as those used in manufacturing or process control. The second method, feedforward control, is based on the principle of positive feedback. It involves predicting the future state of the system based on its current state and adjusting the input accordingly. This method is often used in robotics or aerospace applications, where the system needs to anticipate future events to maintain stability. Both methods have their own strengths and weaknesses, and the choice between them depends on the specific requirements of the application.

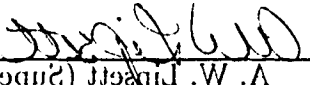
A third method, called "A-B-A-B" control, is based on the principle of alternating between two different control modes. In this mode, the system alternates between two different control modes, A and B, at regular intervals. Mode A is typically used for low-power applications, while mode B is typically used for high-power applications. The transition between modes is triggered by a specific event, such as a change in the system's state or a change in the environment. This method is often used in hybrid vehicles or in systems where power requirements fluctuate over time. The choice between feedback, feedforward, and A-B-A-B control depends on the specific needs of the application, such as power requirements, response time, and cost.

UNIVERSITY OF VIBERIA
FACULTY OF GRADUATE STUDIES AND RESEARCH

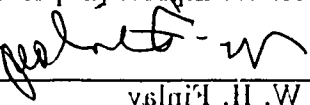
The undersigned certify that they have read, and recommend to the Faculty of
Graduate Studies and Research for acceptance, a thesis entitled:

Moulinet Response of an Artificial Olfactory Tower

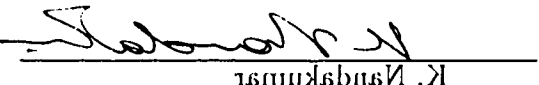
Submitted by **Yan Wang** in partial fulfillment of the requirements for the degree of
Master of Science.



V. W. Pidgeon (Supervisor)



M. H. Huijala



K. Nasarwanji

Aug. 3 1983

Date: _____

UNIVERSITY OF ALBERTA

RELEASE FORM

Name of author : Yan Wang

Title of thesis : Nonlinear Response of an Articulated

Offshore Tower

Degree : Master of Science

Year of this degree granted : Fall 1993

Permission is hereby granted to the University of Alberta Library to produce
single copies of this thesis and to lend or sell such copies for private, scholarly or
scientific research purposes only.

The author reserves all other publication and other rights in association with
the copyright in the thesis, and except as permitted by law, may not be reproduced
nor any substantial portion thereof may be printed or otherwise reproduced in any
material form without the author's prior written permission.

Yan Wang

Date:

Aug. 23



National Library
of Canada

Acquisitions and
Bibliographic Services Branch

325 Wellington Street
Ottawa, Ontario
K1A 0N4

Bibliothèque nationale
du Canada

Collection des acquisitions et
des services bibliographiques

325 Wellington Street
Ottawa, Ontario
K1A 0N4

ISBN 0-312-88145-3

ISBN 0-312-88145-3

L'auteur a accordé une licence
irrévocable et non exclusive
à la Bibliothèque et à la
National de Canada de
reproduire, bref, distiller ou
 vendre des copies de sa thèse
de manière raisonnable et sans
duplisme tout en ce soit pour
mettre des exemplaires de cette
thèse à la disposition des
personnes intéressées.

The author has granted an
irrevocable non-exclusive license
allowing the National Library of
Canada to reproduce, loan,
distribute or sell copies of
this/her thesis by such means and
in such form or format, making
this thesis available to interested
persons.

L'auteur conserve la propriété
droit d'auteur du protégé sa
thèse. Ni la thése ni des extraits
supplémentaires de celle-ci ne
doivent être imprimés ou
autrement reproduits sans son
autorisation.

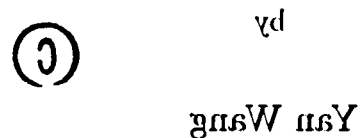
The author retains ownership of
the copyright in this/her thesis.
Neither the thesis nor substantial
extracts from it may be printed or
otherwise reproduced without
this/her permission.

ISBN 0-312-88145-3

Canada

UNIVERSITY OF ALBERTA

Nonlinear Response of an Artificially
Towered Tower



A thesis

submitted to the Faculty of Graduate Studies and Research
in partial fulfillment of the requirements for the degree of

Master of Science

in

Department of Mechanical Engineering

Eduardo A. Peralta

Fall, 1993

La durabilité de cette microtolerance dépend grandement de la durabilité de la théorie soumise au microtolimide. Nous avons tout fait pour assurer une durabilité supérieure de l'époxidation.

Si l'absence des badges, venus de communiquer avec l'université, a contribué à dégrader le grade.

La durabilité d'impression de certaines badges peut laisser à désirer, surtout si les badges originaires sont sortis ou ont été affecté par la photocopie à l'aide d'un tampon usé ou si l'université nous a fait suivre une photocopie de la durabilité intérieure.

La répudiation, même partiellement, de cette microtolerance est soumise à la Loi canadienne sur le droit d'auteur, SRC 1970, c. C-30, et ses amendements suspendus.

335 Wellington Street
Ottawa, Ontario
K1A 0N4
335 Wellington Street
Ottawa, Ontario
K1A 0N4
Acquisitions and
Bilingual Services Branch
Direction des acquisitions et
des services bilingues
du Canada
Bibliothèque nationale
National Library of Canada
of Canada
National Film Board
335 Wellington Street
Ottawa, Ontario
K1A 0N4
335 Wellington Street
Ottawa, Ontario
K1A 0N4

National Film Board
of Canada
Bibliothèque nationale
du Canada
Acquisitions and
Bilingual Services Branch
Direction des acquisitions et
des services bilingues
du Canada
Bibliothèque nationale
du Canada



AVIS

NOTICE

The durability of this microtolerance is heavily dependent upon the durability of the original thesis submitted for microtolimide. Every effort has been made to ensure the highest durability of repudiation possible.

If badges are missing, contact the university which granted the degree.

Some badges may have indistinct print especially if the original badges were filed with a book binder or if the university sent us an inferior photocopy.

Repudiation in full or in part of this microtolerance is governed by the Canadian Copyright Act, R.S.C. 1970, c. C-30, and suspended amendments.

fluid inertias force.

A discussion above, the values of the drag and inertia coefficients and bottom shear to each case need to be used as the Morison equation is empirical. For a cylinder moving in waves, because of the lack of leeway data the two coefficients, drag and inertia coefficients, are usually considered to be equal to those of a fixed cylinder in waves or a sailing cylinder in still water. This method is often used, but it is not fully considered as previous studies have shown that the aerodynamic coefficient of the saildrift of the relative form of the Morison equation has not been made to compare the effects of various forms of sailing acceleration.

2.3 Review of Nonlinear Dynamics of Offshore Structures

Previous studies concerning the nonlinear dynamic behavior of various types of offshore structures have focused on obtaining a good approximation of dynamic wave loading as well as the harmonic response of the structure, and developing the various techniques to simplify the nonlinearities arising in these systems. To do this various linearization techniques have been used by many researchers, for example, Spasov et al. [10], McNamara et al. [20], and Charkiewicz et al. [31]. A comparison of various linearization methods and a brief introduction to deal with the nonlinear drag force is given by Lipsett [22]. It is well known that the solution of a linearized system, though very useful in some cases, can not provide all the nonlinear phenomena which can occur in real systems. Consequently the simulation of environmental conditions by linearization may only give partial results and can not determine the actual system behavior which governs the system response and sensitivity to the initial conditions. Because of this reason there is interest in nonlinear phenomena and stability analysis of nonlinear systems. Complex responses have been observed in various models of offshore systems. For most models of nonlinear offshore systems some assumptions and simplifications are

applicable to the form of the Morison equation from which they are obtained. Results of these two configurations have been obtained for fixed body problems by the work of many researchers. However, for the case of a body moving in waves the experimental data is rare. A good review on this topic is given by Sarpkaya and Imberger [15]. An attempt to investigate this area was also made by Williamson and Coker [16]. Their results showed that the relative velocity form of the Morison and Coker is generally applicable. The work by Williamson [16] has also indicated that wave conclusion except for a small region near the first resonance in which the two force coefficients C_w and C_a for flexible cylinders decrease significantly from those for fixed cylinders. Kogeyasins and Nakamura [17] have also investigated the variation of relative velocity form of the Morison equation. It was shown from their work that the relative velocity form of the Morison equation is applicable only in the case that the frequency of the motion of a structure is the same as that of incident waves. The redundancy of the motion of a cylinder is needed to determine the appropriate values of C_w and C_a . Further investigation is needed to determine the relative velocity form model in waves.

Different forms of DU/Dt can be considered for the fluid inertia term in Equations 2.6. For a body moving in an accelerating flow, DU/Dt in Equation 2.4 can be evaluated by several ways. In the case that the positional displacement x of a cylinder is small compared to the wave length, the local form of fluid particle acceleration $DU/Dt = gU/gx$ can be used. In this case the relative velocity form of the Morison equation will be nonlinear only in the drag force.

Newman [18] has shown that for an accelerating flow and flexible structure, the total fluid particle acceleration is given by $DU/Dt = gU/gx + (U - \dot{x})(gU/gx)$, which includes both local and convective acceleration terms and is the most accurate form for the fluid particle acceleration. In the case of $\dot{x} < U$, the total fluid acceleration expression becomes $DU/Dt = gU/gx + UgU/gx$, where again both local and convective terms are present. In these two cases, the relative velocity formulation of the Morison equation is nonlinear in both the drag force and the

the inertial force due to the motion of the cylinder; and the third term is the drag force due the relative velocity between the fluid and cylinder.

If the acceleration and velocity of the cylinder are small, that is ≈ 0 and $\dot{x} \approx 0$, the neglecting terms involving \ddot{x} and \dot{x}^2 and letting $DU/Dt = g/(g_f)$, Equation 2.6 becomes identical with Equation 2.3 which is for the case of a fixed cylinder in an accelerating fluid.

Several reviews have been made in the area of wave forces and structural resonance in the recent past. Saripaksa and Isaacson [13] have reviewed the literature made in many aspects of wave interaction with offshore structures. Chikraborty [13] has discussed the advancements made in this area, in particular, the various extensions and modifications of the Morison equation were discussed and their implications investigated.

For large body problems in which the diffraction effect is important, that is the ratio of the lateral dimension of the structure to wave length is greater than 0.2, the hydrodynamic forces will include the force component arising from this diffraction effect and the theory should be employed to predict the hydrodynamic forces. This effect is not considered here.

If should be mentioned that the inertia coefficient C_i in Equation 2.4 and the drag coefficient C_d in Equation 2.5 depend mainly on the Reynolds number R_c , defined as $R_c = U_w D / \nu$, and Kutta-Joukowski number K_c , defined as $K_c = U_w T / D = 2\pi A / D$ which is proportional to the ratio of the fluid particle displacement to the cylinder diameter, where U_w is the maximum fluid particle velocity, A is the fluid particle diameter, T is the wave period, and ν is the kinematic viscosity. Usually these two coefficients are determined from experiments by the method of Fourier analysis as detailed by Keulegan and Carneget [14]. The research in this field has suggested that the values shown only determined by appropriate experiments and their values are affected by

these two forces together, which gives

$$(2.3) \quad F = bC_w \frac{\pi}{4} \frac{D_s^2}{D_t^2} \frac{gU}{gC_q D U / U_1}$$

This is the original form of the Morison equation, valid only for fixed cylinders, with two empirical coefficients C_w and C_q determined by appropriate experiments. For a cylinder moving in a unidirectional, two-dimensional, accelerationing fluid, in this case the inertia force, due to the fluid inertia and the acceleration of the cylinder, and the drag force, due to the relative velocity between the fluid and the cylinder, become

$$(2.4) \quad F_i = bC_w \frac{\pi}{4} \frac{D_s^2}{D_t^2} (\dot{x} - \ddot{x}) + bC_q D \frac{\pi}{4} \frac{D_s^2}{D_t^2} gU$$

and

$$(2.5) \quad F_d = \frac{1}{2} bC_q D (U - \dot{x}) |U - \dot{x}|$$

respectively, where \dot{x} and \ddot{x} are the velocity and acceleration of cylinder in the horizontal direction, and D/U is the total fluid acceleration in the same direction. For small body problems, in which the ratio of the lateral dimension of the structure to wave length is less than about 0.2, combining these two forces gives the relative velocity formulation of the Morison equation for a flexible cylinder in an accelerationing fluid as

$$(2.6) \quad F = bC_w \frac{\pi}{4} \frac{D_s^2}{D_t^2} D \dot{x} - bC_w \frac{\pi}{4} \frac{D_s^2}{D_t^2} \dot{x} + \frac{1}{2} bC_q D (U - \dot{x}) |U - \dot{x}|$$

where C_w is the added mass coefficient, with $C_w = C_q + 1$. For a cylinder moving in a unidirectional accelerationing flow, theoretically the added mass coefficient $C_w = 1$ (see for example, Strokas and Isaacson [13]), so that the theoretical value of the inertia coefficient is $C_w = 2$. The first term on the right-hand side of Equation 2.6 represents the inertia force due to the total fluid acceleration; the second term is

2.2 Wave Loading

Offshore structures are subjected to both steady and time dependent forces due to the action of winds, waves and currents. Of these, wave forces are usually the most significant for offshore structures. Waves account for most of the structural loading and, because they are time dependent, produce dynamic effects leading to increase the stresses.

The force on a submerged structure is a result of the hydrodynamic pressure exerted by the fluid around it. In the case of ideal inviscid fluid, the total fluid force acting on this structure is obtained by integrating this pressure around the surface. For a fixed circular cylinder in an accelerating flow, the component of this fluid force per unit length on the horizontal direction is given by

(see for example, Saripakaya and Isaacson [13])

$$(2.1) \quad F_x = \frac{1}{4} C_w \frac{\pi D^2 g U}{g}$$

where ρ is the fluid density, D is the diameter of cylinder, C_w is the inertia coefficient, and gU/gt is the local fluid particle acceleration in the horizontal direction. This force is often called the inertia force as it is due to the fluid acceleration.

Now consider the case of a fixed cylinder in a real fluid. The cylinder will also experience a resistance due to the separation of flow and the formation of wake behind the cylinder in addition to the fluid inertia force. This drag force, for a fixed cylinder, is usually given by (see for example, Saripakaya and Isaacson [13])

$$(2.2) \quad F_d = \frac{1}{2} C_d D |U|,$$

in which C_d is the drag coefficient, and U is the velocity of fluid particle in the horizontal direction. Note that if the cylinder is not fixed, then the relative velocity between the fluid and cylinder is often used in Equation 2.2.

Based on the above discussion, the well known Morison equation [13] given as follows first the total fluid force on the cylinder can be obtained by summing

specificed to represent the extreme loading conditions in a long interval known as wave period. The design wave is usually specified by statistical analysis of the long-term period. The design wave can be defined as the largest design waves over the height, period, and direction such that it gives the largest design waves over the site. With this specified design wave, the use of a linear loading calculation method, such as the Morison equation which will be discussed in Chapter 3, and the approximate wave theory will give the final forces. This method is relatively slow than the design point of view because it is considered in the long wave. However, it does not permit taking due consideration of the wave characteristics such as so-called design wave which is not the design point for many offshore structures this so-called design wave period is called wave period of the wave. Waves will smaller waves helping to reduce the wave period of the wave in the long case. Waves will have higher frequencies than the highest excite the resonance motion which increases larger structures than the highest design wave. They can be considered in the future, however.

The second approach is a stochastic method which is based on the random loading conditions. In this method all the data for wave forecasting are presented in the form of a complete wave spectrum. The method uses the stochastic spectral analysis to determine the frequency and dynamic response of structures. The drawback of this method is that it is very difficult to superposition principle is applicable. In the deterministic model is based on the design wave, the wave is generated by long-period regular waves with a single frequency component. In the stochastic approach there are different types of waves in the sea state. In the stochastic approach, waves of different periods are followed to be superimposed on one another to form the wave spectrum. It actually describes the irregular waves in the sea state. Allowing for regular waves harmonic state which closely approximates a real sea state. Waves are laterally oscillated in nature, a series of them leaves certain basic concepts which are fundamental to wave motion as well as the response of offshore structures. In this thesis, only the response of the articulated tower in regular sea waves will be studied.

out encountered in linear systems, have been operated in various nonlinear dynamics systems and experiments. Much in this landmark paper [7] has discussed the nonlinear dynamics features of the logistic equation, showing that even very simple systems can exhibit very complex behavior. Moon [8] has discussed the nonlinear dynamics of many systems and performed experimental work on forced vibrations of a packaged beam and investigated many of the characteristics of chaotic motion. Thompson and Stewart [8] have published an excellent book on chaotic dynamics which includes an example of the complex response of an offshore structure. Recent research on the phenomena of complex offshore structures has revealed that the response of these structures is very complex because of the inherent complex nonlinearities in these structures even for the very simple models [9, 10, 11].

In this chapter, we will review the descriptions of waves, and the methods to calculate the fluid forces acting on slender offshore structures. Also the current research on the complex behaviors of complex offshore structures will be discussed. Some universal features of chaotic systems and useful tools used to study nonlinear dynamics problems will also be summarized here.

2.1 Wave Description and Sea States

In order to provide the kinematical properties of waves necessary for calculating the wave loading on the structure, various wave theories have been developed. Such wave theories allow a description of a wave in terms of the wave height, period, and water depth to be translated into the values of fluid velocity, acceleration and pressure at any point under the wave. This describes an adequate knowledge of the wave data. There are two distinct approaches, corresponding to either a regular or irregular sea state, to describe the wave parameters which are used as an "input" to the structural design.

The first approach is a deterministic method which is based on a single wave

Literature Review

This section is specifically focused on large-scale environmental phenomena in the form of wind and waves and current. These phenomena directly influence the environment leading to significant structures. The main objective is to understand the importance of offshore systems such as oil platforms and wind turbines. Wind energy has become a major source of electricity worldwide due to its low cost and reliability. Wind energy is also considered as a sustainable alternative to fossil fuels. When the demand for energy increases, these systems are able to provide clean and renewable energy. Wind energy is also used for desalination purposes, which is becoming increasingly important due to water scarcity. The main focus of this review is to analyze the impact of wind energy on the environment, particularly on coastal ecosystems. This study aims to evaluate the effects of wind energy on marine life, including fish populations, marine mammals, and seabirds. The review also discusses the potential risks and benefits of wind energy, such as noise pollution, visual impact, and habitat disruption. Overall, the aim of this review is to provide a comprehensive overview of the environmental impacts of wind energy and to highlight the need for further research and monitoring.

The dynamics of nonlinear systems has attracted significant attention in recent years due to the extremely complex behaviors exhibited by even very simple systems. Complex responses such as superharmonic and chaotic responses, which are

form of total fluid particle acceleration expression, $DU/Dt = \dot{U}/g_f + U\dot{g}_f/g_f$ or $DU/Dt = \dot{U}/g_f + (U - \dot{x})\dot{g}_f/g_f$, where U is the velocity component of the fluid particle in the direction of the structure motion and \dot{x} is the velocity component of the structure in the same direction. In order to compare the effects of these two quantities on the behavior of the system, the local acceleration due to the $DU/Dt = \dot{U}/g_f$ alone is also used so that in this case the dominant drag force is the only nonlinearity in the equation of motion.

The solutions of the various systems are obtained by numerically integrating the equation of motion for a large variety of system parameters to provide a comprehensive understanding of the behavior of the compressing air-driven power. In order to investigate the response of real structures in regular waves, the system parameters typical for a real air-driven power are chosen.

An outline of the remaining parts of this thesis is as follows. Chapter Two is a review of literature relevant to the current research on the nonlinear dynamics of compressible offshore structures, including the ocean environment and hydrodynamics loading acting on the offshore structures. Also some useful tools for analyzing linear dynamics problems as well as some universal features of chaotic systems are reviewed. The equation of motion of the air-driven power is then formulated from Chapter Three. Chapter Four includes the discussion of the results obtained from numerical simulations. The effects of different values of various system parameters on the system response are discussed and the possible route to chaos by period doubling is identified. To test the sensitivity of the system to initial conditions, the largest Lyapunov exponent for some cases is computed. The calculated positive Lyapunov exponent further verifies observed chaotic response. In addition, the solutions of various equations of motion are compared each other to identify the dominant nonlinearity of the system studied here. Finally a summary and conclusion of this work as well as the direction of future research are given in Chapter Five.

Unintended capitalistic structures design should avoid the system barrier where chaotic responses may occur.

It is the intent of this thesis to investigate the nonlinear phenomena of an air-circulated tower subjected to the regular harmonic ocean wave excitation for a variety of tower geometries in deep water. The influence of various nonlinearities will also be studied. The aim of this thesis is to gain insight into the dynamic response of this structure, to explore the possibility of dynamic instabilities and chaotic motion, and to provide useful information for the design of these compliant structures.

Air-circulated towers are being designed and installed in many offshore areas. They are employed as mooring towers for oil tankers as well as for drilling and production operations. A air-circulated tower is usually buried at seabed, and remains vertical due to its own buoyancy or the hydrostatic of specific modulus. A simple and useful model of an air-circulated tower is a single-degree-of-freedom system in which the tower itself is taken as an upward rigid cylinder. The dynamics of this system can be described by a single-degree-of-freedom which is the model used in this thesis.

The equations of motion of the air-circulated tower are formulated by assuming that linear wave kinematics are applicable and that the fluid forces acting on the structure are given by the well known Morison equation [6]. The hydrodynamic drag force will be made to investigate the nonlinearities arising from the wave kinematics being computed numerically and the nonlinearities arising from the response of the air-circulated tower. The nonlinear wave kinematics are often nonlinearities due to the use of either nonlinearities or other nonlinearities on the response of the tower will be made to investigate the influence of other nonlinearities on the response of the air-circulated tower. The nonlinear wave kinematics terms arise from the use of either

states. Nonlinearity also arises in wave kinematics even for the range in which linear wave theory is valid part for which the convective terms, antisipation of fluid acceleration with respect to their spatial coordinates, cannot be neglected. These convective terms provide salient nonlinearities to the system. An example of such a case is when the motion of the structure is very large and the wave kinematics need to be computed at the displaced position of the structure. In addition to this, there are other possible nonlinearities. The example nature of the structure itself, the initial displacement is caused by large amplitude structures and the interaction between structure and boundary condition may result in a nonlinear stiffness for these structures. These effects will not be considered here. The inherent nonlinearity of coupling of systems of different subsystems implies that the full range of nonlinear responses such as superharmonic, subharmonic, and chaotic responses as well as the applicability properties occur in these systems and is the focus of this research in this thesis.

In a linear single degree of freedom system with harmonic forcing, the ratio of response is always the same as that of the excitation and the response amplitude is linearly proportional to the exciting amplitude. However in nonlinear systems, as is well known, the response of the system can be superharmonic, subharmonic, even chaotic in addition to the more typical harmonic response. Under certain conditions two or more than two different motions can coexist, depending on the initial conditions.

The recently found chaotic motion [6] is a random-like response exhibiting a perfectly deterministic system that has been observed in many physical systems by both numerical simulations and experimental measurements. Here the distinction has to be made between random chaotic motion and random motion people in which the random forces or system parameters are not known exactly but only have a statistical description. It consists of motion can result from those problems in which the input to the system is unpredictable in shape or parameters to result in motion of random motion. The main distinguishing feature of

in 1863 or water on the Bonito River in the Mediterranean Sea; in 1888 a revision by Isidoro was undertaken in Green Canyon area of the Gulf of Mexico in a second water depth of 60 m. Several reviews of marine benthos including the oil industry studies from the use of compilation offshore structures as well as the solutions to these problems are given by Thornton [3] and Palet [3]. New oil fields, such as the Marlin and Alpaca oil fields have been found in deep water ranging from 600 m to 1100 m in Campos Basin, offshore Brazil. As a result much oil companies have initiated projects to investigate the application of compilation offshore structures in water depths up to 1500 m.

This new generation of offshore structures, characterized by very low natural frequency and large working displacement, creates new challenges for both engineers and geologists. Low natural frequency, which may fall into the wave frequency range, usually, immediately lessens response of these structures which are excited and good damping may occur. Successful compilation structure design depends upon a good understanding of the dynamic behavior and accurate prediction of the response of such structures, and is key to safe, economic and efficient design.

There exists another important interaction mechanism between ocean waves and offshore structures which makes the dynamic analysis of offshore structures extremely complex. The wave force acting on a slender structure is nonlinear and unsteady if the structure motion and the wave kinematics. However, the motion of the structure is in turn determined by the wave forces. This is the so-called wave-structure interaction. In addition to the resonance of this interaction, there is a comprehensive review of the relevant literature [4] has given a comprehensive review of this wave-structure interaction. One of nonlinearities in this wave-structure interaction is the hydrodynamic separation of flow from separation point, which is due to the presence of trailing free surface separation point. This force is predominantly modeled by a superelevation structure fundamental member. This force is relatively velocity between the hydrodynamic elevation depending on the relative velocity especially being a structure. Wave kinematics are another source of nonlinearity especially when nonlinear waves are used to give the wave properties in extreme sea

Chapter I

Introduction

One of the major topics being discussed in the hydrology of Mexico is the development of [1] exfiltration processes in coastal areas in order to understand the relationship between precipitation data showing the drainage basin characteristics of water bodies for different which indicates the process of infiltration in the coastal area. Specifically, in 1973, the first serial publication was installed in open water, in the water body of the Potrero coast. From the 1950s to the early 1970s, water depth for infiltration studies increased from 30 m to about 130 m and in 1976 a piezometered steel jacket-type piezometer was installed in 200 m of water in the San Bartolomé Channel of California. By the year 1978, the water depth increased to 310 m where a fixed jacket structure was installed in the Gulf of Mexico. To meet this challenge, the technology of the piezometer design and the techniques of installation have advanced rapidly in the past few decades. Now the offshore industry has turned to flexible or compliant structures to reduce the cost which increases significantly with water depth. Examples of this new generation of offshore structure are tension leg platforms, buoyed tower platforms, compliant tower platforms, articulated towers, and floating production systems. For example, in 1983 a buoyed tower was installed in 30 m of water in the Tuna Field of the Gulf of Mexico; in 1987 a partially integrated column was installed

1	measured response amplitude	Poincaré points of the solution	and singular points of the solution	points of singularity	coercive	the Lipschitz exponents	the system basins	the water density	the solution of order δ on periodic impulse	the width of steady window associated with periodic impulse	a sequence of impacts showing the convergence to Feigenbaum's a sequence of impacts showing the convergence to Feigenbaum's a logistic equation $g = 4.6692... \text{ for logistic equation } g = 4.6692... \text{ for logistic equation } g = 4.6692...$	responsible for the power	wave frequency	logarithmic map $g = 4.6692... \text{ for logistic equation } g = 4.6692... \text{ for logistic equation } g = 4.6692...$	logarithmic map $g = 4.6692... \text{ for logistic equation } g = 4.6692... \text{ for logistic equation } g = 4.6692...$	to the power of water	system basins of attraction	the ratio of the power	system basins of attraction	of the power	of the power
---	-----------------------------	---------------------------------	-------------------------------------	-----------------------	----------	-------------------------	-------------------	-------------------	--	---	---	---------------------------	----------------	---	---	-----------------------	-----------------------------	------------------------	-----------------------------	--------------	--------------

It is common to assume that these fixed cylinder coefficients also apply to the flexible cylinder case for the apposite Reynolds number. However, it is a typical case for the apposite Reynolds number.

3.3 Equations of Motion of Atticulated Offshore Tower

The articulated tower considered in this thesis is modeled as a rigid body with circular cross section shown in Figure 3.1. The tower is pinned at sea floor, standing vertically under its own weight. Mechanically, it is acceleratedly an inverted pendulum with the pivot angle θ being the only degree of freedom. As shown in Figure 3.1, F_B is the buoyancy force of the tower acting at point B, M is the buoyancy center, which is located at a distance Y_B from the tower base, W is the total tower weight, G and Y_G are the mass centre of the tower and the distance from the tower base to G.

The equation of motion of the articulated tower can be written as

$$(3.3) \quad I\ddot{\theta} + C\dot{\theta} + R(\theta) = W(0, \dot{\theta}, t)$$

where I denotes the differentiation with respect to time, $\dot{\theta}$ is the moment of inertia of the tower about its base, C is the structural damping coefficient including the friction at joint O, $R(\theta) = (F_B - MW) \sin \theta$ and $W(0, \dot{\theta}, t)$ is the restoring moment and the moment of total fluid forces about the base of the tower respectively. It is assumed in this thesis that the tower undergoes small so that the presence of the tower does not affect the wave field and that the total fluid force acting on an infinitesimal structural element dy , located at a distance y from the tower base, can be approximated by the relative velocity formulation of the Morison equation (equation 3.8). Thus the restoring moment, $W(0, \dot{\theta}, t)$, can be

written by integrating the fluid force along the tower, that is

$$(3.10) \quad \left. \int_0^L F(y) dy \right\} = (\dot{z}, \dot{\theta}, \theta) M$$

disimenter of structure to the wave length. For slender structures where $D/t < 0.5$, the lateral dimension of structure is small enough in relation to the wave length so that the incident wave characteristics remain unchanged. In this case diffraction effects become unimportant and the Morison equation can be applied to estimate the force due to wave action. The second parameter is the Keulegan-Carpenter number K_c , which is proportional to the ratio of amplitude of water particle motion

to the structure disimenter and is defined as

$$(3.7) \quad K_c = \frac{A}{D} = \frac{T_w U}{D}$$

where U_w is the velocity amplitude of the flow, and A is the amplitude of water particle motion. The importance of K_c is based on the fact that the drag forces on the structure in an oscillatory wave flow are dominated by the separation of flow passing the structure and the formation of large vortices. For small values of K_c , the flow does not separate from the structure. In this case, drag forces are very small, inertial forces dominate and the potential flow diffraction theory will be necessary to predict the wave forces. For large values of K_c , on the other hand, the wave flow separates from the structure eventually resulting in the development of vortices. Drag forces will then be large and the Morison equation is applicable for calculating the wave forces acting on the structure.

As previously discussed in section 3.3, for a flexible cylinder with diameter of D subjected to regular wave excitation, the relative velocity formulation of the Morison equation gives the wave loadings per unit length as

$$(3.8) \quad F = \frac{\rho}{4} C_w D t \frac{DU}{Dt} - \frac{\rho}{4} (C_w - 1) \ddot{x} + \frac{1}{2} \rho D C_d |U - \dot{x}| (U - \dot{x}),$$

where ρ is the fluid density, C_w and C_d are the inertia and drag coefficients, U and D/t are the velocity and total acceleration of the fluid particle respectively. The dependence of the coefficients C_w and C_d as a function of the Reynolds number, Keulegan-Carpenter number have been measured by many researchers for fixed

cylinders as summarized by Sarıkaya and İsaçsoy [13].

For deep water, $\lambda_d > \pi$, so that $\sin(\lambda_d) \approx \cos(\lambda_d) \approx 1$, with the result that the above two equations become

$$(3.3) \quad ; \quad \frac{H\pi}{T} = u$$

$$(4.3) \quad .(1) \omega - \frac{H\pi}{T} = v$$

Note first in above equations the components of fluid velocity are a function of time -
time of the horizontal displacement.

The relationship between wave number k and wave frequency ω is obtained
from the linear dispersion relation

$$(5.3) \quad k_d = \frac{\omega}{\sqrt{g}}$$

which for deep water is simply

$$(6.3) \quad k_d = \frac{\omega}{\sqrt{g}}$$

where g is the gravitational acceleration, and wave number k is given by

where T is wave period.

In this linear wave theory will be used to obtain the wave properties.

3.2 Morison Equations

An empirical equation due to Morison et al. [6] has been widely used in both research and offshore engineering to obtain the wave loading for slender structures since it was first proposed in 1950. The Morison equation is based on the assumption that the presence of the structure does not affect the wave load and the waves act as if they were free surface waves. The forces on a fixed structure can be expressed as the sum of a drag force which is quadratic in the fluid velocity and an inertia force which is linear in the fluid acceleration. There are several parameters which affect the validity of the Morison equation. The first parameter is the diffraction parameter D/L , the ratio of the

3.1 Linear Wave Theory

A wave theory which provides the kinematics of fluid motion in a wave will be necessary in order to calculate the wave loading acting on structures. There are two main difficulties in developing such a wave theory. The first is that the boundary conditions need to be satisfied at an initial time such as the wave profile at the initiation of the wave. The second is that the boundary conditions are themselves nonlinear. The nonlinear boundary conditions arise from the convergence terms in Euler's equations in boundary conditions need to be satisfied at their steady state. They can be approached by neglecting the gradients of the velocity field in the boundary conditions if the wave height is small enough compared to other terms in the kinematics of the wave. This is the basic assumption of linear theory. This is due to the neglecting of the nonlinearity of the wave profile and the corresponding convergence terms. This is the same as the neglecting of the wave profile and the corresponding convergence terms in the linear wave theory. After this is done it is necessary to solve the linear wave equation with respect to the wave height, hence the name linear wave theory. Also it is necessary to consider the effect of the water depth, since the water depth is proportional to the wave height. Also it is necessary to consider the effect of the water depth on the wave profile, since the water depth is proportional to the wave height.

For a wave with wave height, H , water depth, a , and wave number, k , the vertical components of the water surface given by linear wave theory (see for example, Sarpkaya and Isaacson [12]) are

$$(3.1) \quad u = \frac{\pi H \cos(kz)}{T \sinh(kd)} \cos(\omega t - kz);$$

$$(3.2) \quad v = \frac{\pi H \sinh(kd)}{T \sinh(kd)} \sin(\omega t - kz).$$

Here u and v are the horizontal and vertical velocity components of water surface respectively, z and x are the vertical and horizontal coordinates respectively with origin at seabed, T and ω are the wave period and frequency, where $\omega = 2\pi/T$, and t is time.

Chapter 3

Formulation of Equations of Motion

The equations of motion of an articulated tower are formulated in this chapter. The relative velocity form of the Morison equation is used to estimate the wave loading on the articulated tower and linear wave kinematics is assumed. The local and different total acceleration expressions are used to evaluate the acceleration of fluid particles. If the local acceleration expression $D\dot{U}/Dt = gU/gt$ is used, the only nonlinearity in the equation of motion is the quadratic drag force which depends quadratically on the velocity of fluid particle as well as the velocity of the tower. However, when either form of total acceleration expression, $D\dot{U}/Dt = gU/gt + UgU/gx$ or $D\dot{U}/Dt = gU/gt + (U - \dot{x})gU/gx$, is used, the resulting total acceleration of the fluid particle is characterized by both a nonlinear quadratic drag force and a noninert wave exciting force, the latter arising from the convective terms in the noninert wave exciting force. The noninert wave exciting force are a function of both the tower displacement and time so that the resulting system is a coupled parametric and externally excited system.

with periodic eddies to that of periodic motion, along with the superimposition of this component. A plot of $\sin \theta$ versus time shows that the motion is random and considerably chaotic for a deterministic system. This signal indicates the beat frequency route to chaos could correspond to the appearance of an incoherent periodic oscillation due to the random component when varying a parameter of superimposition or a fundamental frequency component component when varying a parameter. The Fast Fourier Transform technique (FFT) is an efficient way to combine the Fourier Transform. Details of this algorithm can be found in any book on digital processing of numerical analysis such as reference [3].

order continuous dissipative system (time dimension system) has three Liapunov exponents. If the system does not have a fixed point, then one Liapunov exponent is zero and one must be negative. The remaining Liapunov exponent can either be zero, positive, or negative. As discussed by Wolf et al. [36], a chaotic system will be a strange attractor that has the following set of Liapunov exponents $(+, 0, -)$, while the so called two-torsas has the set $(0, 0, -)$, and a limit cycle has the set $(0, -, -)$. Note that if the system has an attractive fixed point all Liapunov exponents are negative corresponding to the set $(-, -, -)$.

Various algorithms for calculating the Liapunov exponents are available. Two algorithms, one for data generated by a known set of differential or difference equations, and the other for experimental time series data, or calculating all of the Liapunov exponents have been discussed and studied extensively by Wolf et al. [36]. For second order continuous, dissipative differential systems, at least one of the Liapunov exponents is negative, and one is zero if the system does not have a fixed point so that the largest nonzero Liapunov exponent can be used to determine whether a system response is chaotic or not. One method to calculate the unique largest nonzero Liapunov exponent is by using the variational method. Appendix B gives the algorithm of this method. Also see references [8, 36] for details about this method.

2.4.3 Fourier Spectrum

One of the characteristics of chaotic motion is the appearance of a broad band spectrum of frequencies in the response even though the system input is a single frequency harmonic excitation. From the theory of Fourier series, or its extension Fourier Transform, it is well known that for harmonic motion, the frequency spectrum will have a single component at the frequency equal to that of the harmonic motion. For periodic motion, the frequency spectrum consists of a component

exponents that tell how long it is until a measure changes in the phase space. This is called the Lyapunov exponent, which has to be the most useful dynamical test for chaotic systems (see for example, Moon [6]), are the average exponents of states of divergence or convergence of nearby orbits in the phase space. Since nearby orbits correspond to almost identical initial states, exponents measure the rate at which systems will soon become quite different, implying the loss of the information contained in the initial state. A system containing at least one positive Lyapunov exponent or periodic orbit is often defined as being chaotic (see for example, Moon [6]).

In general, for a n-dimensional system, the time evolution of a particular axis will just depend on its monotonous exponents measure in the same way that Lyapunov exponents measure in the direction of these principal axes after some time. If $\lambda_{\text{int}}(t-k)$ is the initial difference between two nearby points at time $t-k$ and evolves to $\lambda(t)$ at a later time t , the Lyapunov exponent, γ , is defined as (see for example, Moon [6])

$$(7.2) \quad \frac{(\lambda(t); b)}{(\lambda(t-k); b)} \text{ in } \sum_{i=1}^n \frac{1}{\lambda_i - \lambda} = \gamma$$

where b is the initial point. λ is the sum of time increments. For continuous time-dependent dynamical systems without fixed point Haken [35] has shown that at least one Lyapunov exponent is identically zero, corresponding to slow changing magnitude of a principal axis. Axes that are on average to the slow changing magnitude correspond to negative exponents respectively. A consequence is that for a dissipative system at least one Lyapunov exponent must be negative, ensuring that the sum of all the Lyapunov exponents is negative because of the dissipation. The signs of the Lyapunov exponents provide a quantitative measure of the dynamics of a system. In a one-dimensional discrete system, there is only one Lyapunov exponent which is positive for chaos, zero for a monotonic stable orbit, and negative for a periodic orbit. The well known logistic equation (see for example, Moon [6]) is an example of a one dimensional discrete system. A second

sense only if the system motion reaches the steady state, in other words, assuming that the transient part is lost in time. Although some initialisation is done after the transient has died out. Although this technique is useful especially for complexed passive linear systems, so this technique is not suitable for circuiting cyclic, and strictly comparable series. These sampled points, fixed in each forcing cycle, are typically comparable (see for example, Thompson [8] since the phase of the periodic motion is measured at these points.

The Point-to-section sampling rates may still reflect the main features of the dynamical system. In general, the sampling period is usually taken as half of the excitation. Then the number of points on the Point-to-section reflects the order of solution. A finite number of points on the Point-to-section indicates a periodic response since the response will repeat after some time. For example, a periodic response with same period as that of forcing, usually called harmonics or periodic response over one solution, only one point will be shown on the Point-to-section response to period over one solution, only one point will be shown on the Point-to-section response after every forcing period; for a periodic response with a period as motion repeats after every forcing period; for a periodic response with two different points on twice that of forcing, called a period motion process between these two points. The Point-to-section, indicating that motion process between these two points, repeats every two forcing periods. Similarly for a period motion it shows two different points on motion repeats after every a forcing period and there are different points on the Point-to-section. For chaotic motion, in which the response is initially the Point-to-section will contain infinite number of points which do not repeat. The Point-to-section will contain infinite number of points which do not repeat. The high organisation of these points, often called stable attractor showing the stereopicture, showing a definite configuration of the system in phase space, is a characteristic of chaotic motion.

2.4.2 Trajectory Exponents

Lyapunov exponents provide a way to test the sensitivity of the system to changes in initial conditions. For every dynamical system, there is a spectrum of Lyapunov

Some useful tools for studying dynamic systems and the methods to approach them will be described in the following. These tools will be used to describe the response of a system to a forcing with periodic wave packets in the time domain.

2.4.1 Police Sector

A very useful plot to show the properties of dynamic systems is the phase plane diagram in which the velocity is plotted as a function of the displacement. Generally, this diagram consists of a continuous curve which shows the evolution of the system state in the phase space. Alternatively, if instead of looking at the motion continuously, we look at it at discrete times, then it is possible to construct a series of points representing the trajectory at specific times, for example, this diagram shows the position of a particle better than a sequence of snapshots of the motion because it will appear as a sequence of dots on the phase plane.

continuous phase trajectory is “cut” periodically. These sampled points will make contiguous sample phase plane is called a Poincaré section as the diagram for the sample phase plane is called a Poincaré section as the

One of conclusions that Liao claimed is that the complex responses will likely occur only if the wave propagates at the elevated position of the atmosphere, which means the wave exciting forces includes the convectional conduction. However, complex responses were also observed when the wave propagates at the convective position of the atmosphere power in the model used by Gottlieb et al. [3]. Note that the wave angular displacement was assumed to be small in this model so that the nonlinear drag force is the only effect in the model. This is due to the nonlinearity of motion. The conclusion by Gottlieb et al. [3] is opposite: nonlinearity leads to the drag force has a dominant effect on the occurrence of complex responses since this is the only nonlinearity in this model. This seems to be in contrast to the conclusion of Liao [3]. It is this opposite discrepancy that will be discussed in this paper.

The existing current research indicates the need for further investigation of the complex dynamic system behavior to provide a comprehensive understanding of the system response. Although complex perturbations have been observed in different models, the system parameters play a key role in structural response. Also, multiple research is required to identify the effects of various nonlinearities on the system behavior.

2.4 Useful Tools of Nonlinear Dynamic Analysis

As mentioned before, chaotic responses has a very strong dependence on initial conditions. This makes long term prediction response impossible. However, some universal features, such as self-similarity, have been found to identify chaotic motion in nonlinear dynamic systems. These features, such as Feigenbaum numbers, amplitude scaling, superattracting specific scaling, all discovered by Feigenbaum [33, 34] as well as Liao's own experiments, are universal in the sense that they do not depend on any particular system. One of the routes to chaos, perhaps

to some systems. Due to the nonlinear dynamics of traffic, some quantification is usually made when applying these methods to estimate traffic structure systems. The primary purpose of this paper is to compare the local traffic analysis was applied to a model single-point system developed by cubic polynomials by Choi and Lee [36] and higher order polynomials by Li and Sager [32]. The traffic flow in the study area is divided into two components of free and a linear composition of the two components and the traffic velocity was measured. Other examples of using primary traffic analysis method to estimate local was proposed. The multilevel series classes quantification system used to estimate the traffic structure was proposed [10] and Gottlieb et al. [35]. This model includes two basic features a single toll model by Nagel et al. [30, 31]. This model includes two basic features a single toll model by Nagel et al. [30, 31]. This model includes two basic features a single toll model by Nagel et al. [30, 31].

The effort has also been made to determine which nonlinearities has a dominant influence on the occurrence of the complex behavior of coupled oscillating structures. So far two nonlinearities arising in addition to motion of offshore mooring lines. As far as these nonlinearities extend: (a) geometrical nonlinearities and structural systems have been studied extensively; (b) the nonlinear drag force. Discussion will be made of mooring restoring force; (c) the nonlinear drag force is usually in order to analyze the nonlinear restoring force, the nonlinear drag force is usually simplified by using various linearization techniques. The studies by Thompson et al. [11], Choi and Jon [26], Bishop and Vrigui [6] have indicated that the geometrical nonlinearity and structural discoupling in restoring force can induce superharmonic and chaotic responses for certain values of system parameters. The model used by Gottlieb [10] of a multi-point mooring system incorporates the nonlinear restoring force, nonlinear damping drag force, and the nonlinear convective inertia force. Liaw [33] has compared the solutions obtained from several models of discretized

Choi and Jon [36]. In this model, the nonlinear drag force term is introduced and the wave exciting term proportional to the displacement fluid velocity in the drag force is neglected. The discontinuity in the nonlinear restoring moment is approximated by a smoother continuous function. This is the only nonlinear effect in this model and the resulting equation is a Duffing type oscillator. This has operated first as the amplitude of excitation increases. In addition, higher-order approximation techniques and damping motion will appear. In addition, jump phenomena, convergence of multiple solutions will appear. Also the motion and higher-order harmonics occur as the damping decreases. Also the motion of harmonic balance and the Hill's vibration definitions have been compared to obtain the analytical solution and the stability criteria for this system. A good agreement has been found between the analytical results and direct numerical integration results. The values of wave height used by Choi and Jon were $W = 7.05\text{m}$ to 45.7m.

In the model of the articulated tower used by Gottliep et al. [37], the exact form of the restoring and hydrodynamic excitation moment were obtained. Since the tower displacement was assumed small, the only nonlinear effect in this model is the nonlinear drag force. This [38] has also studied a model similar to this one used by Gottliep et al. [37] except that the convective terms in fluid particle acceleration expression were included in this model. Therefore this model includes the expression drag force and the nonlinear exciting force arising from the convective terms in the fluid acceleration. Both models consider the nonconservative strictioned forces in the fluid acceleration. While complex responses have been operated in both models. The work by Fujino and Sagata [39] has also indicated the existence of the complex response of the articulated tower. The nonlinearities in their model include a nonlinear restoring force and a nonlinear fluid damping which is then expressed by finite terms of Fourier series in their stability analysis.

While numerical time domain simulation has been the primary tool for the solutions of offshore nonlinear systems, analytical methods such as harmonic balance

inaccessibly unsafe. These include the use of the deterministic forcing which models a regular or safe state. Also the inertia and drag coefficients are usually taken as constants determined by typical Reynolds and Keulegan-Carpenter numbers from fixed cylinder experimental tests. Finally, only a single degree of freedom model of the structure is considered in general.

Nonlinear systems of the Duffing type with parametric and external excitation have been studied by Yagasaki [24], and Hoang et al. [25]. Their results obtained by both analytical methods have shown that the dynamics of such systems is extremely complex and various nonlinear responses including beating damping and chaotic motion have been observed. It was also shown that the work by Hoang et al. [25] that such systems can exhibit nonlinear characteristics in their response even at very small amplitudes of the excitation and show enlivened regions of instabilities and chaotic motion compared to the systems with external excitation only.

Bispolat and Vrigut [9] have described a complete numerical and geometrical analysis of steady dynamic perturbations of a mounted semi-supernumerary. The main objective of this study is to analyze a constant drift component. The beat frequency route to chaos has been identified. Gottlieb [10] has studied the wave-stirracture interaction chaos in a multi-point mounting system and has analyzed the stability analysis of this system. The method of harmonic balance and Hill's variational equations have also been employed. The model used by Thompson et al. [11] has shown that for this simple system the response to an alternating load is modeled by a linear system which includes a geometrical and physical stiffness. This results in a significant nonlinear stiffness for this system. Thompson et al. [11] have shown that for this simple system the response to the harmonic force can be very complex; various superharmonic responses and chaotic response as well as coexistence of the multiple solutions have been predicted. By response as well as coexistence of the multiple solutions have been predicted. By introducing additional nonlinearities in restoring force to the primary oscillators, a more realistic model for the stick-slip system has been studied by

have not been found in any of these cases. The frequency response for one of these cases is shown in Figure 4.1(a). The system parameters used for this figure are $a = 100\omega$, $H = 10\omega$, $D = 3\omega$, $C_a = 0.5$, $C_b = 0.05\omega/\alpha$, and $\beta = 1$, as shown in this figure only one resonance, the fundamental resonance at $\omega/\omega_n = 1$, is seen and the response below is always the same as the forcing below. Consequently the solution for the frequency ratio is investigated here in this case at all forcing frequencies, or parametric solution of order $n = 1$. On the other hand, the solutions shown in Figure 4.1(b), obtained from the equation of motion using the total finite particle acceleration $D\dot{U}/dt = \dot{U}\dot{U} + U\ddot{U}/\omega$, with same set of parameters as in indicate a wide variety of solutions with response ranging from one time ($\alpha = 1$) to twelve times ($\alpha = 12$) that of the forcing. Also shown in Figure 4.1 (b) are the supplemental resonances near $\omega/\omega_n = 2$ and 3 respectively, which are not seen in Figure 4.1 (a), in addition to the fundamental resonance. It can be seen from this figure that if the total acceleration is used to evaluate the finite acceleration approximation supplemental parametric responses are predicted, implying that the nonlinear term also plays an important role on the appearance of supplemental and convective terms in the equation of motion. Therefore it is important to include the convective term in the chaotic response. The latter is due to include the convective term in the equation of motion for articulated power system.

Note that when the local acceleration expression \dot{U}/ω is used to evaluate the finite acceleration, the drive force is the only nonlinearly in the system. It turns out that for the system parameter range that has been investigated in this paper the nonlinearly in drive force is not important for complex responses of the articulated power system. The results shown here are in contrast to those obtained by Gottlieb et al. [2], who studied the same articulated power problem and claimed that the system can exhibit complex responses when the local finite acceleration is used. For reference all the solutions computed for the articulated power using the local acceleration expression in a large variety of system parameters are listed in Appendix A. As can be seen from these results only $n = 1$ solutions have been found for this

degree. $D = 1m, 3m, 5m$ are used here.

Note that often parameters such as initial speed v_0 , parameters B , and μ will also be changed for less strictures when the outer diameter D is changed since it applies explicitly in expressions for these parameters. However, in this thesis these two parameters are treated as independent system parameters.

4.3 Comparison of Solutions of Equations

Numerical simulation has been carried out for the equation of motion of an uncoupled rotor using different initial particle acceleration expressions. In this section the solutions obtained from numerical simulation for these cases will be compared and discussed. In each case, the mass amplitude, θ , or the system response over one response cycle is plotted with respect to nondimensionalized time, ωt , in all figures ratio of forcing frequency to natural frequency of structure in m^{-1} , in all figures to determine response presented in this chapter. The n in each figure represents the order of the solution and different solutions of different order are plotted with a different symbol.

A response is called harmonic if period one solution, or response of order $n = 1$ is the same as that of the forcing. A response will be called supharmonic response of order $n = 2$, or period two solution if the period of response is two times that of the forcing. This is also called $1/2$ supharmonic response since the response frequency is half that of the forcing frequency. Similarly a response with a period equal to three times that of the forcing will be called period three solution, or supharmonic response of order $n = 3$, or $1/3$ supharmonic response, and so on.

First, for the equation of motion using the local linear particle acceleration, over two hundred cases of different values of system parameters have been investigated numerically. However, nonlinear responses such as supharmonic or chaotic response

The lowest value of forcing frequency that can be used here is determined by water depth limitation to ensure that water depth is in the range of deep water, that is, $a/L < 0.5$ (see for example, Sarpkaya and Janssen [15]), where a is the water depth and L is the wave length given by $L = 2\pi/\lambda$, and λ is the wave number. The diffraction parameter D/L , which is the ratio of the power diameter to the wave length, puts another limitation on the effect of the forcing frequency. Specifically the condition $D/L > 0.3$ needs to be met to force the diffraction effects are not important. This point discussed so far is the diffraction coefficient D . It is also discussed in Chapter 3. As will be discussed below structure dimensions of L_w , and λ_w , and a_w are used in this thesis. This gives the forcing frequency range from about 0.5 rad/s to 2.0 rad/s , or the corresponding non-dimensional forcing frequency range of 0.33 to 3.33 for water depth $a = 100\text{m}$; and the ratio range of 0.14 to 3.33 for $a = 500\text{m}$. Note that it is the ratio of the forcing frequency to the natural frequency that is the important parameter here.

• Power diameter D

Power diameter D appears explicitly in drag force term in equations of motion of the power (Equations 3.15, 3.18). With other parameters being fixed, changing power diameter only affects the amplitude of this drag term. As can be seen in each of the equations of motion, Equations 3.15, or 3.18, both the drag term and nonlinear forcing terms will depend on the wave height H . This implies that increasing wave height will increase the amplitude of both the drag term, which mainly provides large fluid damping, and the nonlinear forcing terms. The magnitude of the drag term can be classified by varying forcing terms. Since the range of drag coefficient or the power diameter. Since the range of drag coefficient is very limited (0.5 to 2.0), changing power diameter provides a way to significantly change the main damping term which is of interest in this

$\eta = 200 \text{ m}$. Note that the other system parameters are chosen such that, for each of these two values of water depth, the articulated tower system is in the range of deep water for linear wave theory.

• Natural frequency ω_n

Natural frequency ω_n is the natural frequency of the articulated tower in water and is given by $\omega_n^2 = (FBL - MW)(I + I_a)$, where F , B , L , and T_w are defined before. It changes with the superimposed height of the structure and this superimposed height of the structure changes when tower oscillates in response to the wave excitation. Therefore, it is a function of the tower displacement θ as is shown in this small diagram in this figure, as will be seen in the numerical results, so that changes of ω_n varying θ with θ will be small and the natural frequency ω_n can be taken as constant. In this figure, $\omega_n = 0.07\sqrt{g}$ is assumed.

• Focusing frequency ω_f

Focusing frequency, or wave frequency, is one of the most important parameters in the investigation of nonlinear phenomena of offshore structures. In nature, a large number of periodic wave components with different wave heights, e.g., and different rates of travel occur at the same time in a given sea area. So the real sea state is a random varying surface elevation of superposition of all of these wave components. Although the model of the wave kinematics is based on this process is based on a design wave with a single frequency, it provides a good mathematical model for the so-called regular sea state. In order to understand how this parameter affects the system response, the focusing frequency is used as a basic parameter which is allowed to vary over a realistic range in numerical simulations for each combination of other parameters.

- **Interfa and drag coefficients C_w and C_d**

As already mentioned in the Chapter 3, the interfa and drag coefficient C_w and C_d both are a function of the Reynolds number R , Keulegan-Carpenter number K , as well as the relative surface roughness of structure. If R is follows the interfa coefficient C_w will be set to 2.0, as the change of C_w will Reynolds number and Keulegan-Carpenter number is relatively constant and close to 2 except for a narrow region of Keulegan-Carpenter number (see for example, Sarpkaya and Isaacson [15]). Three values of drag coefficient will be considered; $C_d = 0.5, 0.8, 1.0$. Note that for real structures, drag coefficient C_d typically varies from 0.2 to 2.0. The value 0.2 is not typical for a real offshore structure. It is chosen here so that some basic knowledge is gained about how the system behaves when the drag coefficient is extremely small.

- **Wave height H**

Wave height H is an important parameter of interest and usually contributes to the amplitude of wave excitation forces. Large wave height means large exciting force. However, increasing wave height also increases the wind damping effect as well (see Equation 3.35 in Chapter 3). In order to see which one of these two has a dominant effect on the response of the tower, changing wave height is very important in studying the response of the tower as it will allow us to see changes in response of the system when wave height is varied. The values of wave height used in this thesis are $H = 5\text{m}$, 10m , and 20m .

- **Water depth a**

Water depth a is another parameter important for the wave kinematics. Since the effect of a wave with same wave height on the structures in different water depth is different, it is also important to study the response of the system to different water depths. Here the water depth is set to either $a = 100\text{m}$ or

4.1 System Parameters

There are nine independent parameters in the definition of the structure-lifted power. They are: parameter η , which is proportional to the structural damping coefficient, parameter β , the inertia and drag coefficients C_w and C_d , which arise in the Motion equation, wave height H , water depth d , natural and forcing frequencies ω_n and ω_f , and the tower diameter D .

In order to obtain some preliminary knowledge for the response of real structures, typical values of system parameters are chosen here. Occasionally a parameter value not commonly encountered, is used for illustrative purposes. Each parameter with its values which are used in this thesis will be discussed in turn as follows:

• Parameter η

Parameter η is the ratio of the structural damping coefficient C to the sum of inertia moment of the tower I , and eddy current inertia moment of water displaced I_w ; that is $\eta = C/(I + I_w)$. The structural damping coefficient C accounts for the structural damping including the friction of joint O shown in Figure 3.1. In general, the structural damping is very small compared to that of fluid damping, and η is set to 100.0 to turn off this physics so that the effect of fluid damping can be studied alone.

• Parameter β

Parameter β , given by $\beta = I/(I + I_w)$, is a dimensionless which is a measure of the ratio of the tower weight to the weight of water displaced by the tower. Parameter β takes larger values for lighter structures and smaller values for heavier structures. Note that β is always less than one. Three values, 0.5, 0.5, and 0.5, of β are used here in order to see how this parameter affects the response of the articulated tower.

tion is expensive to evaluate, such as the one for the arithmetic mean power consumption per unit which includes the evaluation of an integral in a range in each evaluation. Here we can use the method of a Runge-Kutta method or the combination of different numerical methods. However, the Adams predictor-corrector methods are preferable in this case as they need less evaluations of differential equations. It is for this reason that the Adams predictor-corrector method has been chosen to integrate the equation of motion of the articulated power in this thesis.

Numerical simulations have been carried out for a pruned and fully case of different parameters for the evaluation of motion using the total fluid particle acceleration expression $DU/Dt = gU/gt + UgU/gx$. At least two pruned case for the evaluation of motion using the local fluid particle acceleration expression $DU/Dt = gU/gt$ have also been investigated. Several runs have also been performed for the total acceleration form of $DU/Dt = gU/gt + (U - \dot{x})gU/gx$ to give a comparison of the effects of different forms of the total fluid particle acceleration on the vibration response. The stable steady state motions of the system are depicted by using the Poincaré section that samples the solution at integer multiples of the forcing period after the transient have died out. Each of these sampled Poincaré points is compared to the previous ones and it is thought that a steady state periodic motion is reached if a Poincaré point repeats a previous one within the desired accuracy of 10^{-6} . Once the steady state motion is identified, the mean amplitude, denoted by θ^* , which is the average of the amplitude over a positive part and the amplitude in negative part over one response period, and the period of solution are recorded. Multiple coexisting solutions, if they exist, are searched for by using different initial conditions. The forcing frequency is varied for each set of system parameters so that the frequency response of system can be obtained.

In this chapter the system parameters with their values and results obtained from numerical simulations will be presented and discussed.

Chapter 4

Response of an Artificialized Tower

The solutions of various editions of motion are obtained by numerical integration. Integration of the edition of motion includes evaluating the definite integral in the drag force term. Evaluation of this integral is obtained by using a subroutine from QUADPACK [3] which uses 31 point Gauss-Kronrod procedure with error control. An Adams predictor-corrector adaptive step size and adaptive order numerical method is employed to obtain the solutions of different initial conditions. The method uses an Adams-Basforth procedure as the predictor, and an Adams-Moulton formulas as the corrector. Further details about this numerical method are given by [4].

All calculations are performed in double precision. In addition, to check the accuracy of numerical simulation, numerical results obtained from the Adams predictor-corrector numerical method for a number of cases were compared to those obtained from a fourth order Runge-Kutta-Heun's method with adaptive step size and global error assessment. As a result, the solutions computed from both methods in all cases were the same.

In general, the fourth order Runge-Kutta methods need four evaluations of the differential equation to obtain the solution for each step. When a different initial

form of the total fluid particle acceleration expression is both a barometric and externally excited system since the amplitude of wave exciting force and damping coefficient are a nonlinear function of the power displacement θ as well as time t . Also, the wave exciting force includes the higher order component of wave frequency. With the assumption of a dispersive element of the form θ being small the inclusion of the nonlinearity, sin θ , on the left hand side of Equation 3.18, is not important here. It can be seen from Equation 3.18 there are two significant nonlinearities, namely the nonlinear wave force which is a nonlinear function of the angular displacement θ of the tower, and the nonlinear damping force which is a nonlinear function of both wave velocity or fluid particle velocity $\dot{\theta}$ of the tower in space directions. In order to compare the effect of these two nonlinearities on the complex responses of the tower it is worthwhile to discuss the nonlinear drag force further. Defining this drag term as F_D , from Equation 3.17 we have

$$(3.35) \quad F_D = Y K_y \int_0^{\pi} \left[\left(\frac{\dot{\theta}}{\omega} - \frac{d}{\omega} \right)^2 - \frac{d}{\omega} \right] d\theta$$

where a^* and K_y are given by Equations 3.24 and 3.30. As it can be seen in Equation 3.35, the first term in the surface pressure [] is basically a forcing term while second and third terms are linear and damping terms. Thus F_D provides forcing as well as the damping to the system. They both increase with the wave height and the drag coefficient and decrease with the diameter of tower since y is proportional to C_d and K_y is inversely proportional to D as given by Equations 3.28 and 3.30.

The assumptions in Equations 3.17 to Equations 3.25 are defined as below

$$\begin{aligned}
 (3.26) \quad & \ddot{\theta} = a \\
 (3.27) \quad & \ddot{\theta}^* = \frac{kH}{S} e^{(a-kq)} \cos \omega_l t, \\
 (3.28) \quad & \ddot{\theta}'' = \frac{C}{I + I_o}, \\
 (3.29) \quad & \ddot{\theta}''' = \frac{FB - MW}{I + I_o}, \\
 (3.30) \quad & \ddot{\theta}'''' = \frac{I_o}{I + I_o}, \\
 (3.31) \quad & \ddot{\theta}''''' = \frac{C_w - J_{\text{eq}}}{J}, \\
 (3.32) \quad & \ddot{\theta}''''' = \frac{\pi D^3 q_s}{4 \cdot 3}, \\
 (3.33) \quad & \ddot{\theta}'''''' = \frac{J}{(kq)^2}, \\
 (3.34) \quad & \ddot{\theta}''''''' = \frac{kH}{S} e^{(a-kq)} \cos(\omega_l t - \omega_l t).
 \end{aligned}$$

The linear dispersion relation (Equation 3.6) has been used in above equations.

Note first in finding inertial force functions $\ddot{\theta}(\theta, \dot{\theta}, t)$, the angular displacement of the tower θ appears alongside with nondimensional factor kq in sine and cosine functions. Note that for very deep water, θ is large so that the term kq can also be large. Consequently the term $kq\dot{\theta}$ can be a significant term even though kq for small oscillations θ may be very small. The result is that neglecting $kq\dot{\theta}$ in expressions of the fluid velocity as well as fluid acceleration is not appropriate in this case. It is for this reason that convective acceleration terms play a crucial role in resulting in complex responses of the anticipated tower system.

As can be seen in above equations, the resulting motion using either

Using the local acceleration to estimate the final position leads to

The following definition of motion of the articulated power

$$(71.8). \lambda \omega \min(1/\lambda), \lambda \geq -\text{sgn} \left| \frac{\dot{\theta}_2}{\dot{\theta}_1} - \gamma \right| \left(\frac{\dot{\theta}_2}{\dot{\theta}_1} - \gamma \right)^{\frac{b_2}{b_1}} \Bigg|_0^{\infty} \lambda \lambda = \theta_1^{\xi} \omega + \theta_2^{\eta} + \theta_3^{\zeta}$$

Note that this is equivalent to the definition of $\text{End}(E)$ given above.

If either form of the total acceleration expression is used, then the definition of

በዚህ የዚህ አገልግሎት ስምምነት

$$(81.8) \quad , (1, \dot{0}, 0) \mathbf{v} + z \omega \left| \frac{\partial \mathbf{e}}{\partial \omega} - \mathbf{u} \right| \left(\frac{\partial \mathbf{e}}{\partial \omega} - \mathbf{u} \right)^{-1} \lambda = \theta \pi i s_n \omega + \theta u + \theta$$

which force acceleration expression is used. If Equation 3.15 is used, then $a(\theta, \dot{\theta}, t)$

yद नेविं सि

$$(0.1.8) \quad ;(\mathbf{i}, \dot{\mathbf{0}}, \mathbf{0})_{\mathbf{1}\mathbf{0}} = (\mathbf{i}, \dot{\mathbf{0}}, \mathbf{0})_{\mathbf{0}}$$

alternatively, if Edition 3.16 is used instead, then

$$(0\Omega.\mathcal{E}) \quad ,(\mathfrak{z},\dot{\theta},\theta)_{\mathfrak{L}\mathfrak{P}} + (\mathfrak{z},\dot{\theta},\theta)_{I\mathfrak{P}} = (\mathfrak{z},\dot{\theta},\theta)\mathfrak{P}$$

where functions $\phi(\theta)$ and $\psi(\theta)$ are given by

$$(j_1\omega - \theta b\lambda) \sin \frac{(s\theta - 1) - (s\theta + 1)b\lambda}{s(s\theta + 1)} \Big] (H\lambda)^{j_1} \chi_3 = (j, \dot{\theta}, \theta)_{18}$$

$$\left[(\zeta \omega - \theta b \dot{x}) \cos \frac{(s\theta + 1)\theta b \dot{x} - \theta s}{s(s+1)} + \right.$$

$$(j_1\omega - \theta b\lambda) \sin \left[\frac{(s_0 - 1) - (s_0 + 1)b\lambda s}{s(s_0 + 1)} \right] s(H\lambda) \frac{\partial}{\partial} -$$

$$(3.31) \quad ; \left[\frac{\cos \Im(kq\theta - \omega_1 t)}{(1 + \theta s)^2} + \frac{s\theta - 2kq\theta(1 + \theta s)}{s^2} \right]$$

$$\left[\frac{(\zeta_0 \varepsilon - 1)\zeta + (1 - \zeta^4)h\zeta^2 + \zeta(\zeta\theta + 1)\zeta(h\zeta)}{\varepsilon(1 + \zeta^2)} \right] \frac{\dot{\theta}}{\omega} (H\zeta)^{-1} \lambda_3 = (\dot{z}, \dot{\theta}, \theta, \varphi)$$

$$(\mathfrak{f}_1\omega - \theta b\lambda)\pi i s$$

$$\frac{(\varepsilon\theta - \varepsilon)\theta\varepsilon - (\varepsilon\theta + 1)\theta b\lambda^2 + \varepsilon(\varepsilon\theta + 1)\theta\varepsilon(b\lambda) - }{\varepsilon(\varepsilon\theta + 1)} +$$

$$(\mathfrak{Z}\mathfrak{Z}.3) \quad \cos(\omega_0 t - \omega_{\frac{1}{2}}) \cdot [$$

and convective terms are included in this edition. However, if the assumption of $\hat{x} < U$ can be satisfied, a simpler expression for fluid particle acceleration can be obtained by neglecting the term involving \hat{x} , which results in Eq. (3.15). This expression, which again includes both local and convective terms, is a good approximation for researchers, for example, Tians [32]. Finally, if the horizontal displacement x of the structure is small compared to the wave length λ , a linearized expression, which simply includes the local acceleration term and is the simplest form for the fluid particle acceleration, can be given by Equation 3.14.

As will be seen later in numerical simulations, neglecting the convective terms in either Equation 3.15 or 3.16 mean neglecting all interesting nonlinearities in the system response. Also it will be shown that the response of the ship to total acceleration expressions will exhibit a critical power using either form of the total acceleration expression as well as a complex response including sympathetic and chaotic responses, as well as a large number of coexisting stable competing solutions. This considerably complicates the important role of the convective terms in resulting complex responses. It should be noted that the fluid particle acceleration given by Equation 3.14 is a function of time and distance, only as it is evaluated at the undisturbed environment position. This is true when the wave height is small and the horizontal displacement x , here, $x \approx 0$, of the tower is negligibly compared to the wave length λ . However, the fluid particle acceleration given by either Equation 3.15 or Equation 3.16, on the other hand, is a function of time, distance, as well as the horizontal displacement x between these two for increasing wave height. Lasscoson [38] has also studied the geometrical influence of convective acceleration terms on the inertial force for fixed body problems, showing that the effective inertia coefficient is generally less than or equal to the true inertia coefficient so that the inertia forces calculated in the convolutional manner will generally overestimate the actual inertia force.

with θ being given by Equation 3.8. Substitution of θ and $\dot{\theta} \approx 1$ into Equation 3.10 gives

$$(3.11) \quad W(\theta, t) = \frac{6}{4} \frac{\pi D_s}{C_w} \int_0^q \frac{DU}{Dt} \left(1 - \frac{6}{4} \frac{\pi D_s}{C_w} (C_w - 1) \right) dt + \frac{1}{2} b D C_q \int_0^q \left| U - 1 \right| \dot{\theta} dt.$$

The velocity of fluid particle in the direction of the wave motion, U , is given by linear wave theory as

$$(3.12) \quad U = a \cos \theta + a \sin \theta$$

which for small θ becomes

$$(3.13) \quad U \approx a.$$

There are several ways that can be used to evaluate the fluid particle acceleration DU/Dt in above equation. It can be given by the local acceleration expression

$$(3.14) \quad \frac{DU}{Dt} = \frac{gU}{\dot{\theta}},$$

which can be justified only if the convective terms in the total acceleration expression are small compared to local acceleration. When convective terms are not small, therefore can not be neglected, the total acceleration expression of either form

$$(3.15) \quad \frac{DU}{Dt} = \frac{gU}{\dot{\theta}} + \frac{gU}{\dot{x}}$$

or

$$(3.16) \quad \frac{DU}{Dt} = \frac{gU}{\dot{\theta}} + \left(U - \dot{x} \right) \frac{gU}{\dot{x}},$$

can be used to evaluate the fluid acceleration. Here \dot{x} is equivalent to $\dot{\theta}$. As mentioned earlier in Chapter 3, the most accurate form for the fluid particle acceleration, Equation 3.16, was derived by Newman [18]. Note that both local

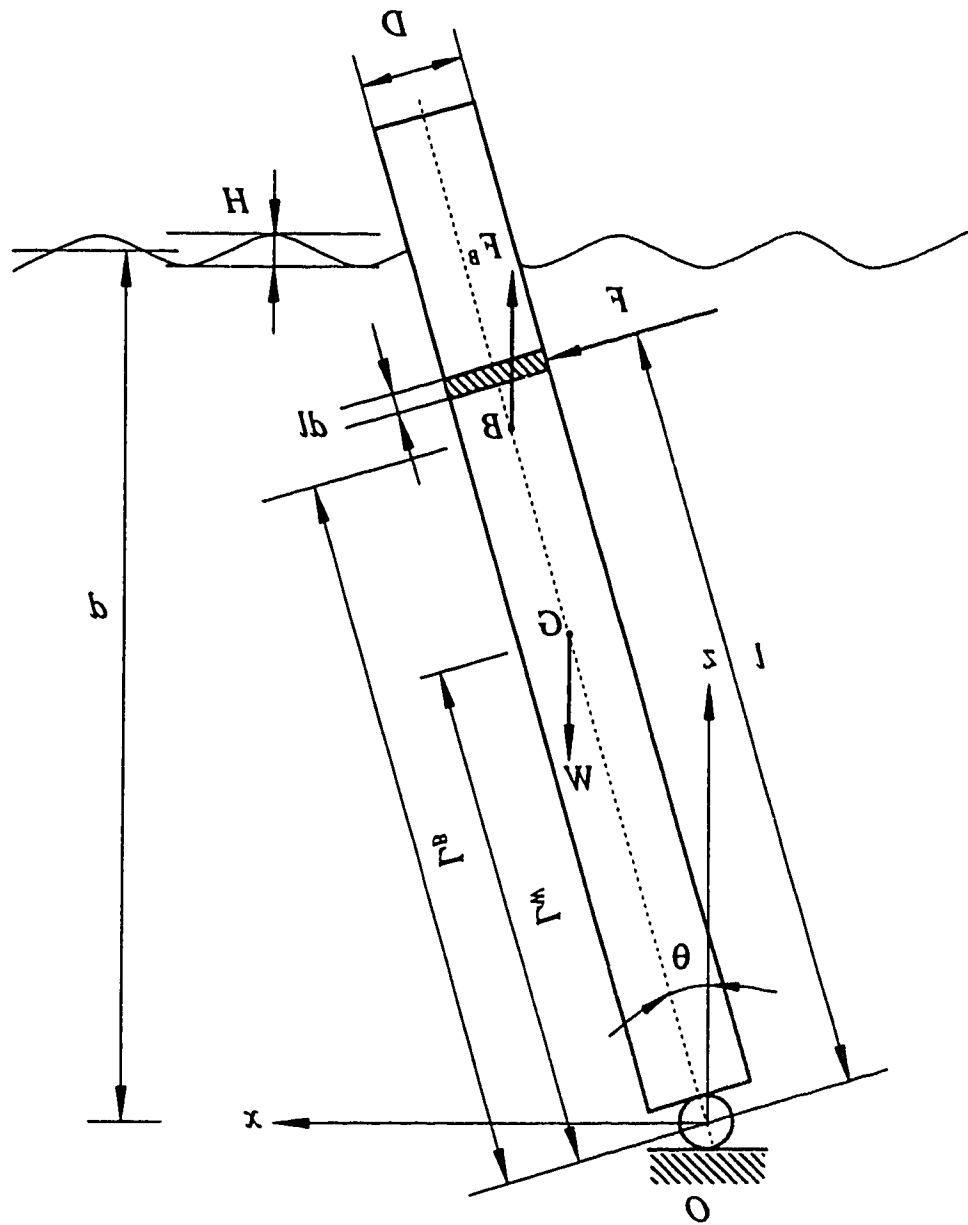
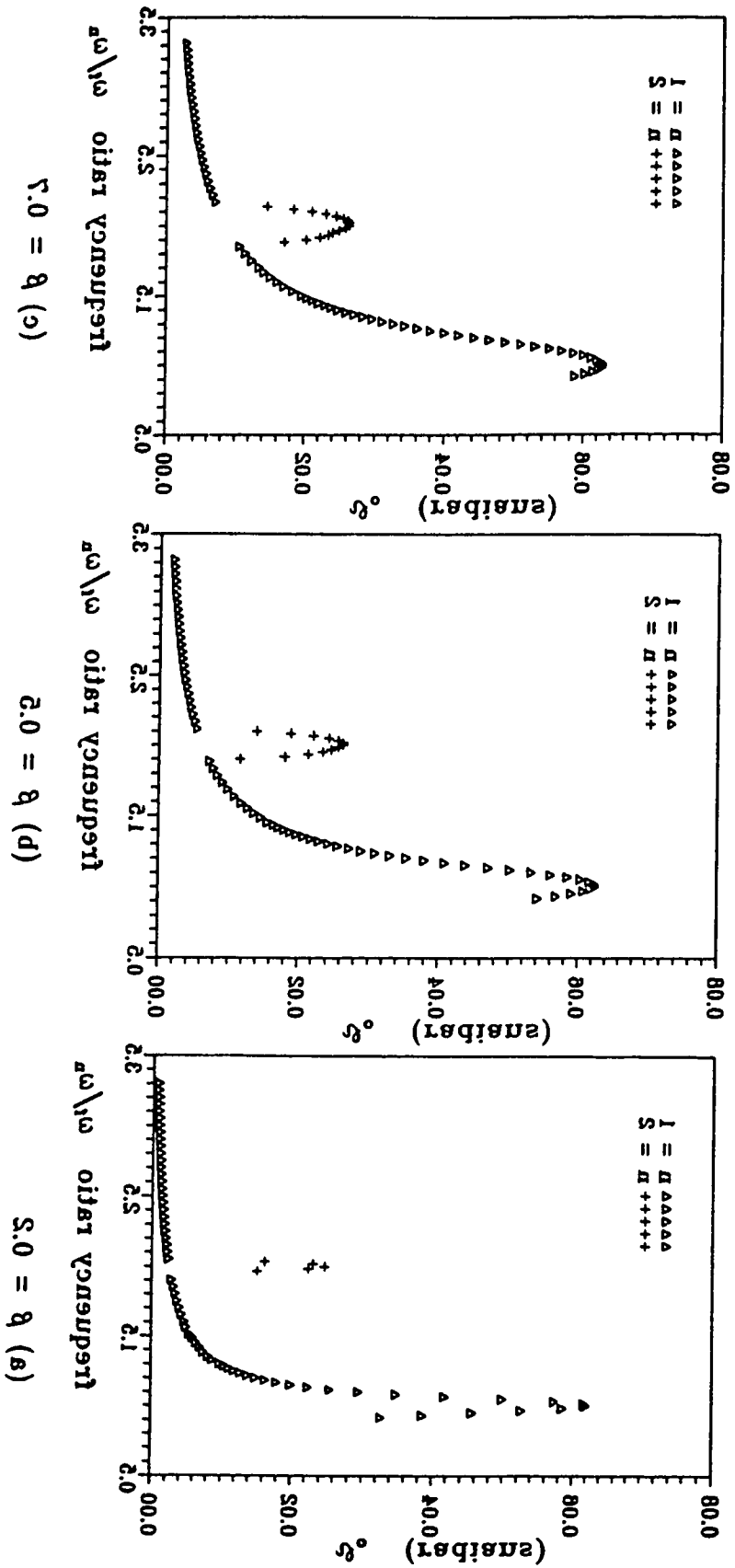


Figure 3.1: Model of the surface-irradiated power system

Figure 4.8: Evidence of resonance desorption for different initial states
parameter: $\eta = 100\pi$, $H = 100\pi$, $C_a = 0.5$, $C_w = \pi$, $D = \pi$, $\omega = 0.01\pi$.



The second integral on the right hand side of Equation 4.3 contains a damping term which does not contribute to the excitation. Hence this damping increases significantly when water depth is increased and supharmonics become less prominent. Note that as water depth increases very little change in the model of the excitation power presented in this thesis, which neglects the deformation of the water surface system as a rigid single-degree-of-freedom system, may not be appropriate since the higher modes of deformation of the water itself could become significant. From this point of view the effect of water depth on the system response needs further investigation.

Figure 4.8 shows the frequency response curves of the system for varying values of parameter β . The values of the used rate: 0.1 , 0.5 , and 0.3 and other system parameters values are: $a = 100\text{m}$, $H = 5\text{m}$, $C_w = 2.0$, $C_d = 1.0$, and $\omega_n = 0.0704/\text{s}$. This figure shows that variations of β do not significantly influence the system response in each case. The fundamental and supharmonic resonance curves all have almost the same peak value. The only difference between these response curves in this figure is that width of each resonance becomes broader as β increases. This is because the fluid damping increases with parameter β . As already mentioned earlier in this chapter, parameter β is a measure ratio of the water weight to the weight of water displaced by the tower. Since β appears explicitly in both nonlinear drag and nonlinear forcing terms, increasing β will significantly reduce the damping of both damping terms (with larger values) resulting in very little difference between fundamental frequency response curves of each other power (with smaller value of β). However overall results (see Tables 4.1 and 4.3 below) show that a chaotic response is more likely to occur for relatively higher structures.

The variations of the power response with power dissimeter D are shown in Figure 4.9 with other system parameters being: $a = 100\text{m}$, $H = 5\text{m}$, $C_w = 2.0$, $C_d = 0.5$, $\beta = 0.3$, and $\omega_n = 0.0704/\text{s}$. As can be expected, the mean response amplitude

$D = 3\text{m}$, $C_w = 2.0$, $C_d = 0.5$, $\omega'' = 0.04\text{rad/s}$, and $\theta = 0.7$. Note that change of vertical scale between these two figures. When water depth is increased from 100m to 500m the peak value of the first resonance decreases from about 1.0 to about 0.1 and as all peak values of the subsequent resonance become less than 0.1. This indicates that fluid viscosity increases significantly with the water depth so that sympathetic resonance tends to be less significant in deeper water because of the large fluid viscosity. The increase of fluid viscosity with increasing water depth can be seen by considering the drag coefficient formula in terms of the friction factor. For example, if the friction in deeper water is given by equation 3.18 is defined as 1.4, then

$$(3.4) \quad \left. \frac{\partial}{\partial} \left(\frac{\dot{s}}{\omega} - \omega'' \right) \right|_0 = 1.4$$

Recall that $s = 0$ corresponds to the seabed while $s = \infty$ corresponds to the still water surface.

From the results of linear wave theory [1] for deep water the maximum orbital velocity at a distance s below the free surface is given by

$$\omega_s(s) = \omega'' \sqrt{1 + \frac{4}{\pi^2} \sin^2 \theta} \sin(\theta s)$$

where $\theta = \sqrt{\omega''/g}$. For example, if the water depth is 100m the orbital velocity at a distance s below the free surface is given by

$$\omega_s(s) = \omega'' \sqrt{1 + \frac{4}{\pi^2} \sin^2 0.7} \sin(0.7 s) = 0.04 \sin(0.7 s) \text{ rad/s}$$

which is 0.04 rad/s for $s = 0$ and 0.02 rad/s for $s = 100$ m. The orbital velocity at the seabed is given by

$$\omega_s(0) = \omega'' \sqrt{1 + \frac{4}{\pi^2} \sin^2 0.7} = 0.04 \text{ rad/s}$$

which is 0.04 rad/s for $s = 0$ and 0.02 rad/s for $s = 100$ m. The orbital velocity at the seabed is given by

$$\omega_s(100) = \omega'' \sqrt{1 + \frac{4}{\pi^2} \sin^2 0.7} \sin(0.7 \times 100) = 0.04 \sin(0.7 \times 100) = 0.04 \sin(49.3) = 0.04 \times 0.15 = 0.006 \text{ rad/s}$$

$$(3.4) \quad \left. \frac{\partial}{\partial} \left(\frac{\dot{s}}{\omega} - \omega'' \right) \right|_{\pi/2} = 1.4$$

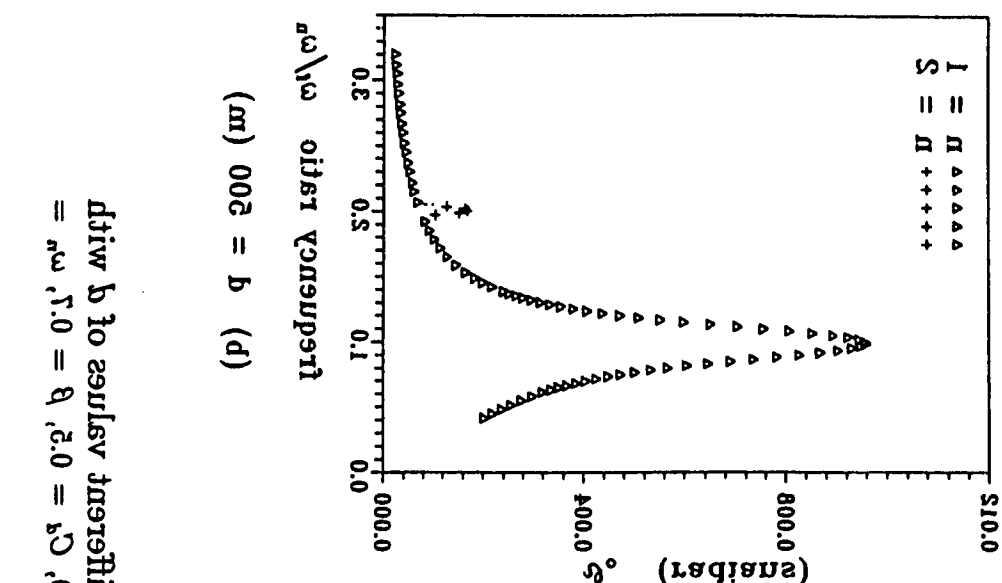
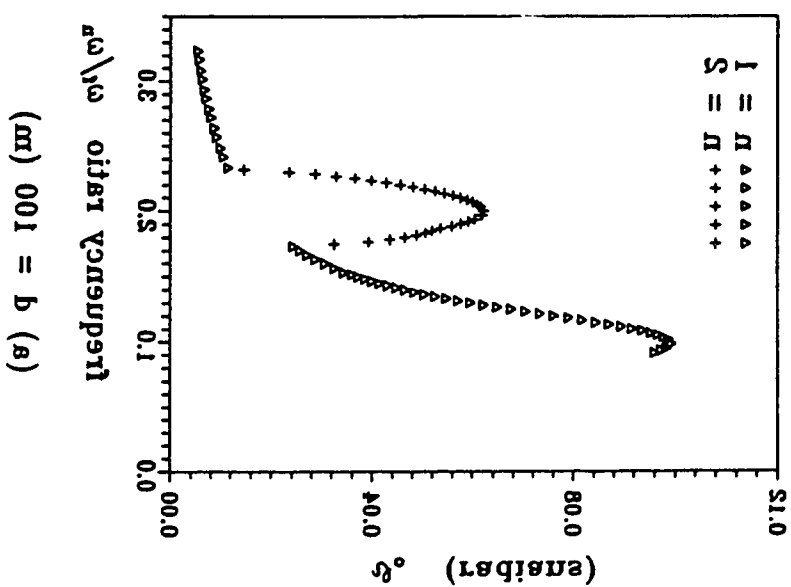


Figure 4.2: Performance measures for different models = 0.0, 0.5, 1.0, 1.5, 2.0, 2.5, 3.0, 3.5, 4.0, 4.5, 5.0, 5.5, 6.0, 6.5, 7.0, 7.5, 8.0, 8.5, 9.0, 9.5, 10.0.

in which no change in response belief to be more complicated in their shape and simplicity problems tend to arise. In Figure 4.(g), all resonance are regular ones, however, in which no change in response belief to be simple phenomenon occurs. However, in Figure 4.(p) and (c) the jump phenomena and belief coupling are seen in some of the resonant peaks. For the third resonance in Figure 4.(p), the belief solution with a probability of 0.12500000000000001 is found when the belief solution becomes unstable as inverse belief coupling appears from belief to period six, and finally to belief solution. Notice that there is a collapse of belief one, belief three, and belief six, coexist at frequency ratio close to 3.0. In Figure 4.(c), the second resonance starts with a sequence of belief two solutions, then jumps to another belief two solution and belief four appears to believe two solution cascade, which may lead to chaotic motion. A unique belief coupling cascade, which may lead to chaotic response, follows after, and finally ends with an inverse superimposed cascade from belief six, to belief eight, to belief four and to belief two solutions. The belief sixteen, to belief eight, to belief four and to belief two solutions. The superimposed phenomena happens at frequency ratio close to 1.6. While a pair of different frequency phenomena has been at frequency ratio of different six to belief twelve solution peaks are just beside the belief eight solution at the frequency ratio about 2.1. The third resonance is only an inverse superimposed cascade with coexisting belief one solution. Figure 4.g shows first as wave height in resonances, the response of the system becomes very interesting, large response and all other nonlinear phenomena can be expected for these system parameters. In the case of small wave height, superimposed response can also be expected for these system parameters.

Shown in Figure 4.7 is the frequency response of the system for water depths $a = 100\text{m}$ and $b = 500\text{m}$ with other system parameter values being: $H = 10\text{m}$,

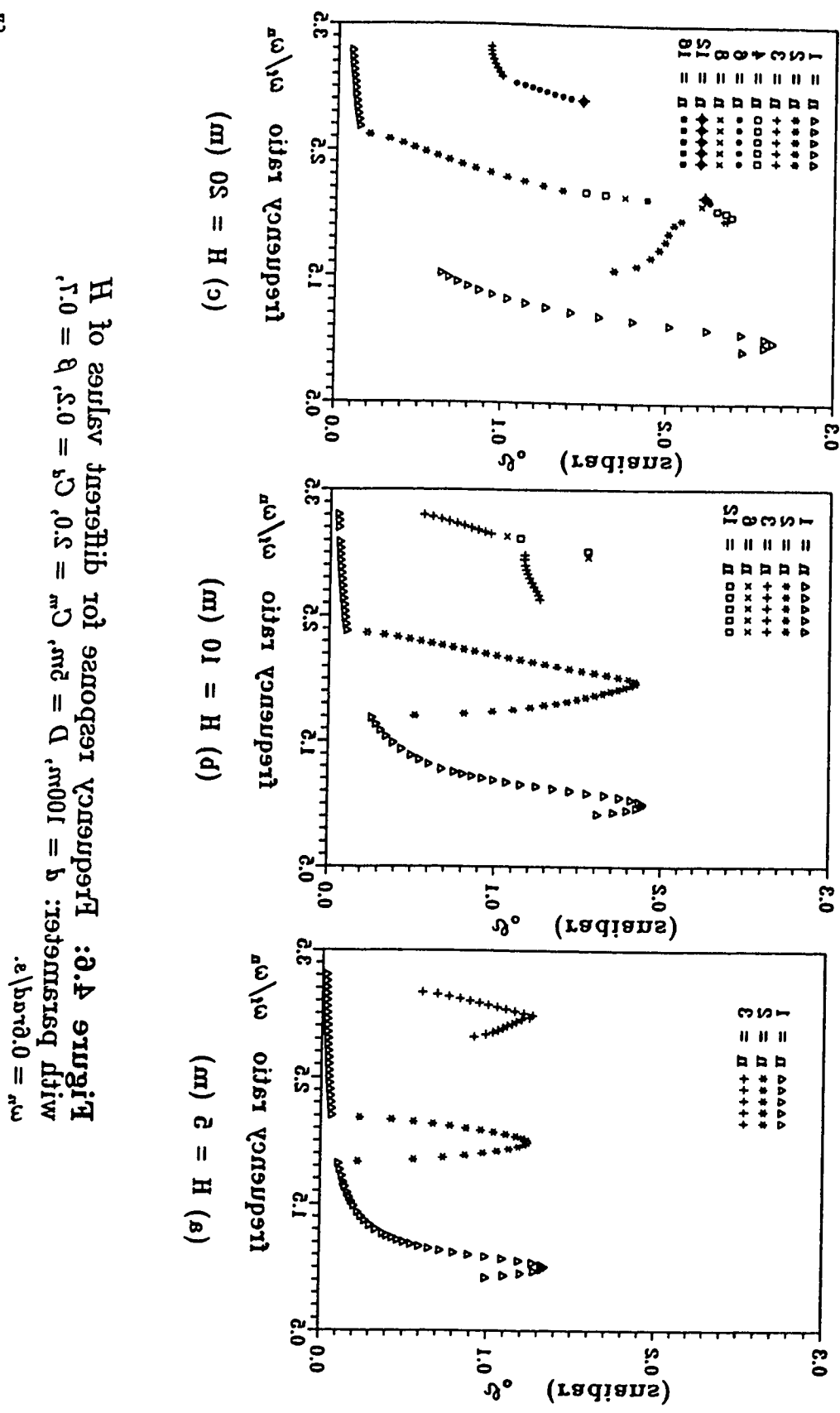
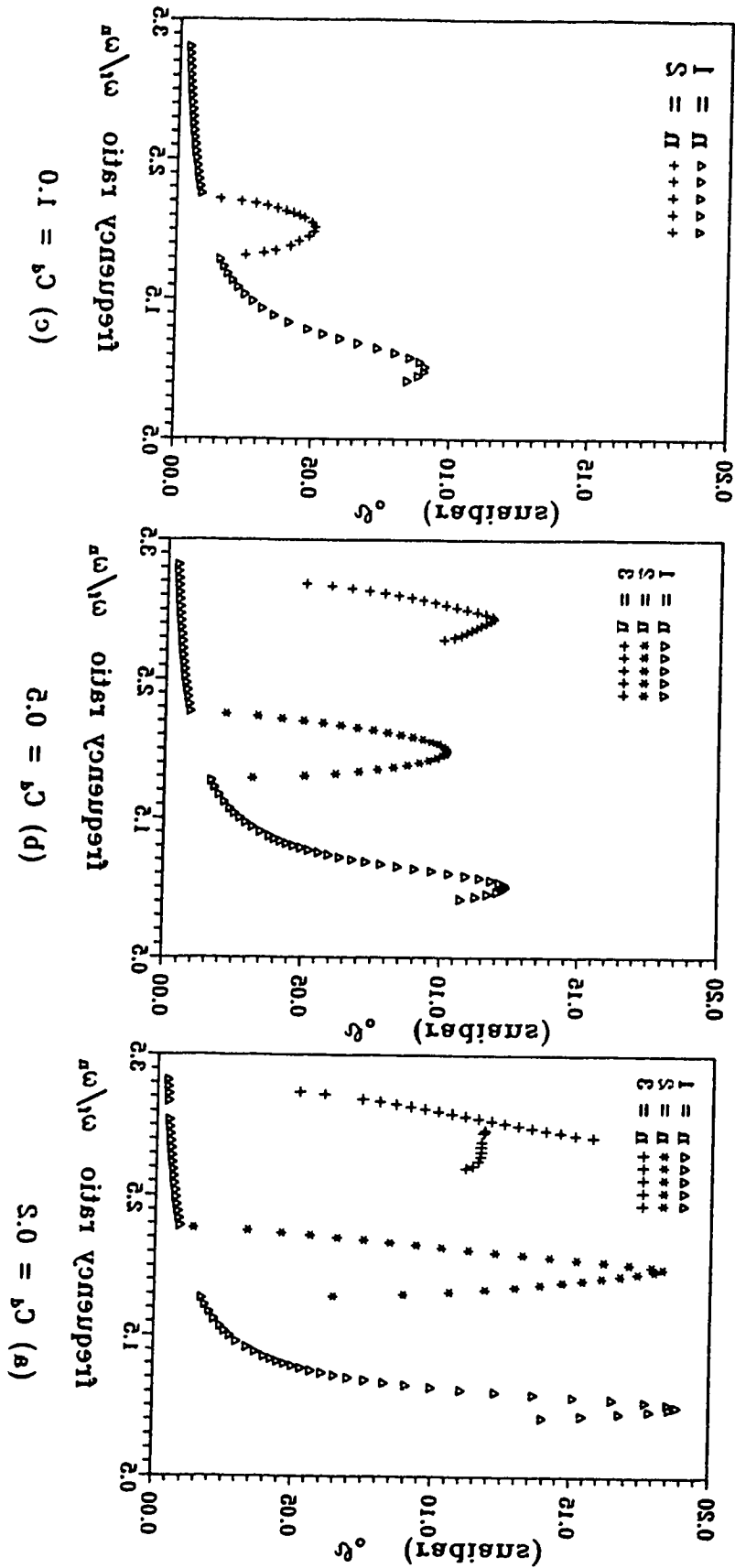


Figure 4.6 shows the endemic threshold H as a function of the parameter γ_0 for different values of β . The plots are for $\gamma_0 = 0.05$, $\gamma_0 = 0.1$, and $\gamma_0 = 0.2$. The x-axis is γ_0 and the y-axis is the endemic threshold H . The legend indicates symbols for β values: 1 (open square), 2 (asterisk), 3 (plus sign), 4 (cross), 5 (filled circle), 6 (filled triangle), 7 (filled diamond), 8 (filled square), 9 (filled circle with cross), 10 (filled triangle with cross), 11 (filled diamond with cross), 12 (filled square with cross), 13 (filled circle with asterisk), 14 (filled triangle with asterisk), 15 (filled diamond with asterisk), 16 (filled square with asterisk), 17 (filled circle with plus sign), 18 (filled triangle with plus sign), 19 (filled diamond with plus sign), and 20 (filled square with plus sign).

$\omega/\omega_0 = \omega$

Figure 4.2: Dependence of the differential measurement ratio ω/ω with parameter C_a for different values of C_b .



analysis for some representative variables will be discussed.

Figure 4.5 is the frequency response for different values of the drag coefficient, $C_d = 0.2, 0.5, 1.0$. Other system parameters remain unchanged for each of these responses curves in this figure and their values are: $a = 100\text{m}$, $H = 5\text{m}$, $C_w = 2.0$, $\omega_r = 0.02\pi/\text{s}$, and $\theta = 0.5$. For small drag coefficient supharmonic responses (the second and third responses) are prominent and are of the same magnitude as the fundamental resonance (the first response). As drag coefficient increases the peak value of responses decreases and the width of each resonance becomes broader similar to linear systems for increasing damping. Note that all responses shown here are regular ones in which no jump phenomena or other stability phenomena occur except the supharmonic resonance associated with periodic three solutions shown in Figure 4.5(a), where a jump phenomena is shown after three solutions are all periodic steady state corresponding to responses due to the frequency ratio $\omega_r/\omega = 2.5$. There is one change in response period at or before this jump and again after this jump corresponding to the coexisting one solution with respect to this resonance. Notice the coexistence of periodic three solutions with the third resonance. It is clearly shown in this figure that the drag coefficient with the third resonance. The large initial amplitude of three solutions in Figure 4.5(a) and (b) is the frequency ratio steady state associated with the supharmonic response. The large initial amplitude causes significant reduction in peak value of responses and damp out all supharmonic responses if it is large enough. Although other parameters do affect the occurrence of supharmonic and chaotic responses, obviously, the drag coefficient is a very important parameter.

Figure 4.6 shows the system frequency response for different values of the wave height, $H = 5\text{m}$, 10m and 30m respectively. Other system parameters are the same as in Figure 4.5. Since $a = 100\text{m}$, $D = 5\text{m}$, $C_d = 0.5$, $C_w = 2.0$, $\omega_r = 0.02\pi/\text{s}$, and $\theta = 0.5$. Since large wave height means large amplitude of the excitation, and consequently large response amplitude, the effect of wave height on the response of the system is obviously important as shown in these figures. As wave height increases, the response

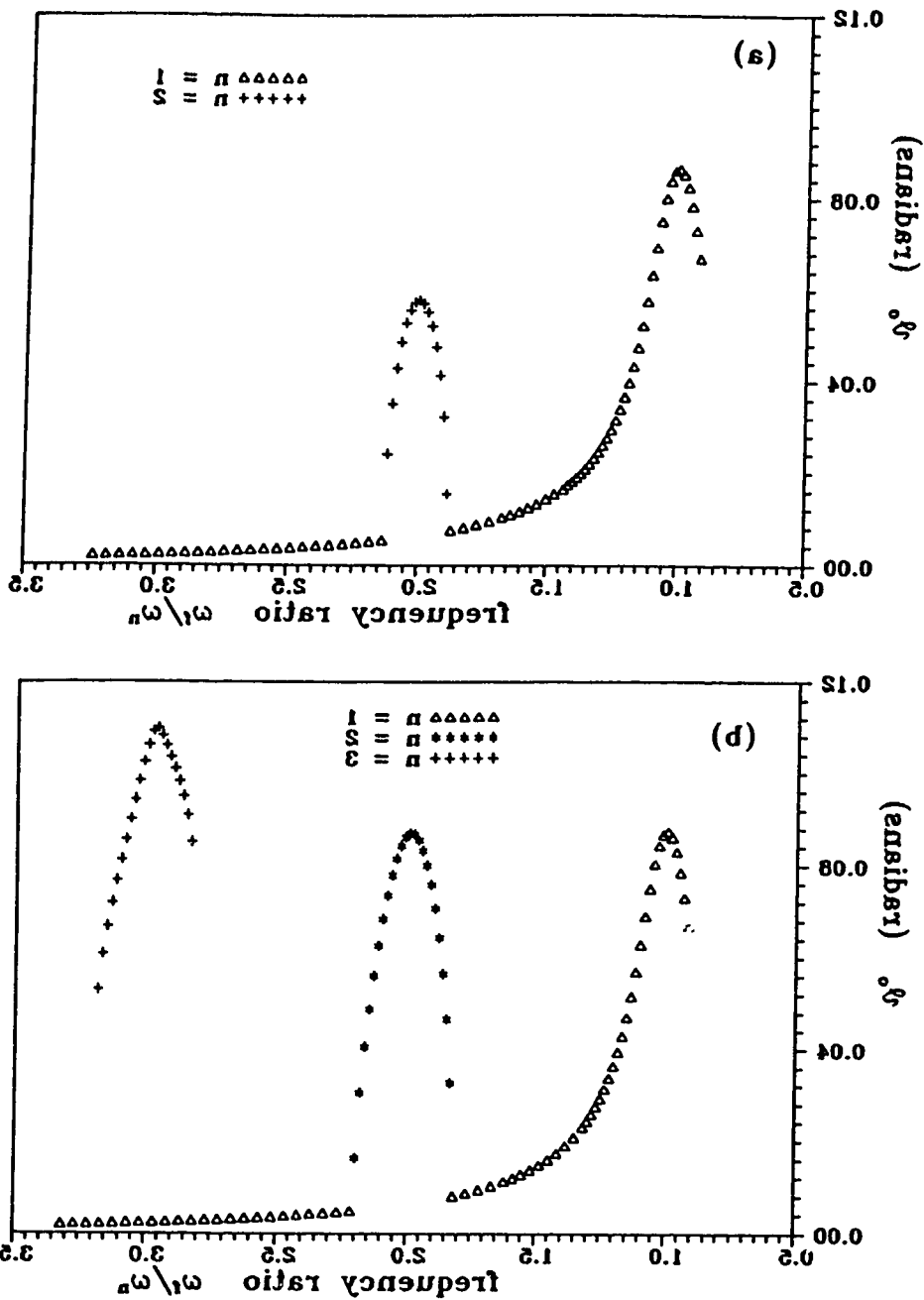


Figure 4.4: Comparison of the lower response using total acceleration versus linear acceleration. Subplot (a) shows results for $U = \frac{1}{2} \dot{x}^2 + U_0 \dot{x}$ and $S = \frac{1}{2} \ddot{x}^2 + S_0 \dot{x}$. Subplot (b) shows results for $U = \frac{1}{2} \dot{x}^2 + U_0 \dot{x}$ and $S = \frac{1}{2} \ddot{x}^2 + S_0 \dot{x}$.

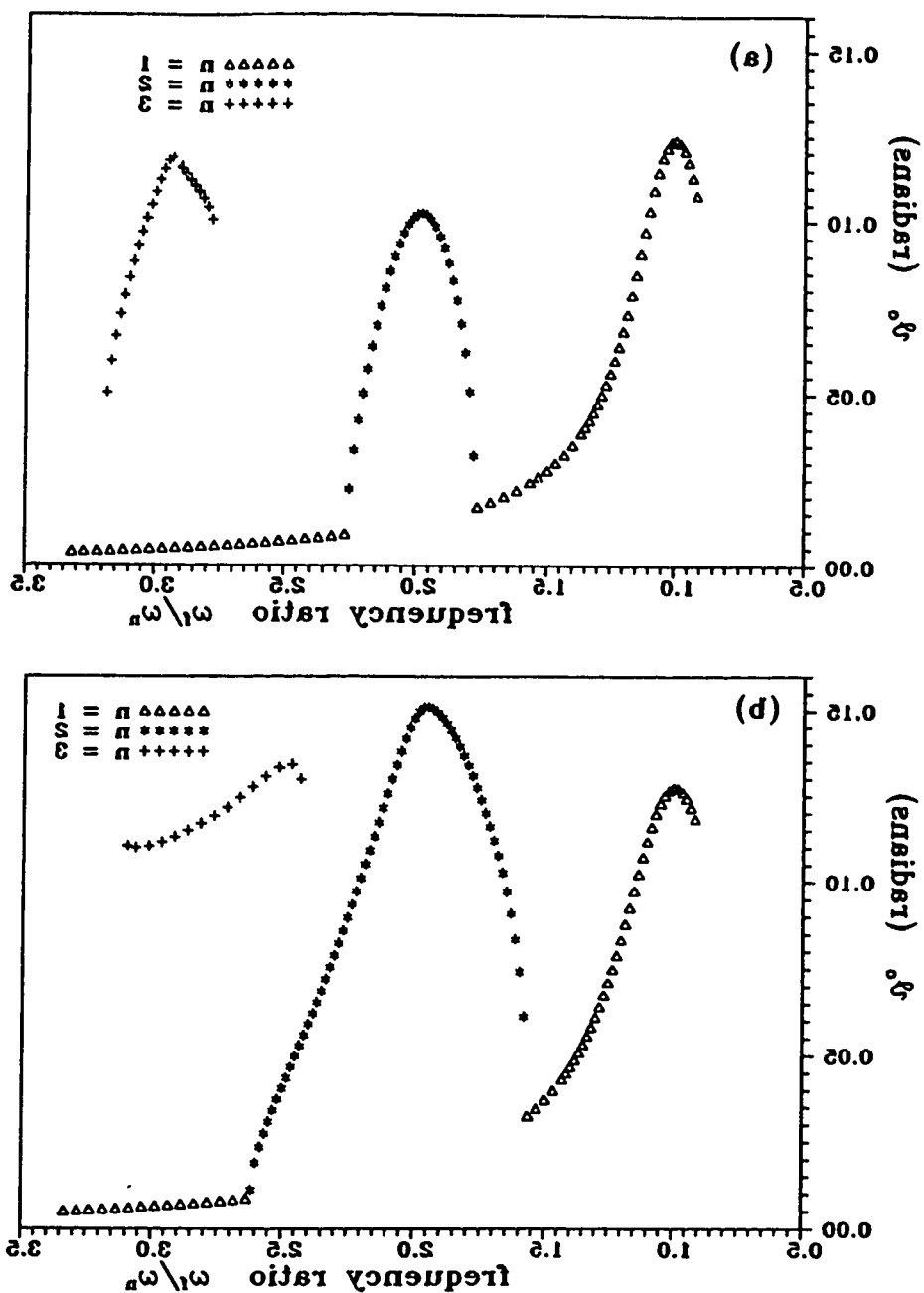


Figure 4.3: Comparison of the power response using total acceleration with bias terms: (a) Using $U = U_9t + U_9x$; (d) Using $U = U - xU_9x$. Parameters: $a = 100\omega$, $H = 10\omega$, $D = 5\omega$, $C_w = 3.0$, $C_d = 0.2$, $b = 0.5$, $\omega_0 = 0.6749/s$.

total acceleration expressions are used. The system parameters used are $a = 100\text{m}$, $H = 10\text{m}$, $D = 5\text{m}$, $C_a = 2.0$, $C_w = 0.5$, $\beta = 0.5$, and $\omega_n = 0.67\text{rad/s}$. It can be seen from this figure that when either form of the total acceleration expression is used, complex responses are predicted. The amplitude of the system response is predicted by the equation using $DU/Dt = 9U/g + (U - \dot{x})gU/g$ in the form $a = 9U/g + 0.67U/g$. This would mean that after plus the predicted using $DU/Dt = 9U/g + 0.67U/g$. This would mean that suppositions, chaos, nonlinear phenomena as well as instabilities problems in the case using the total acceleration form include a term which occurs even with larger values of the drag coefficient or smaller wave heights than those in the case using the total acceleration form without a term in which these phenomena may not appear.

For more comparison between please two see Figure 4.3 and 4.4. It can be seen that there is only small differences between the results of using two expressions for the fluid particle acceleration. The system parameters used in these two figures are: $a = 100\text{m}$, $H = 10\text{m}$, $D = 5\text{m}$, $C_a = 2.0$, $C_w = 0.5$, $\beta = 0.5$, $\omega_n = 0.67\text{rad/s}$; and $a = 100\text{m}$, $H = 5\text{m}$, $D = 5\text{m}$, $C_a = 2.0$, $C_w = 0.5$, $\beta = 0.5$, $\omega_n = 0.67\text{rad/s}$ respectively.

Because of the significant difference observed between the prediction of using either local or total acceleration, the remaining results in this chapter are obtained by numerically integrating the equation of motion with the use of the total acceleration expression $9U/g + U9U/g$. It is felt that results from either form of the total acceleration expression are a better model of what is really happening for this system.

4.3 Tredneuch Response

A tredneuch response curve is a very useful plot showing dynamical properties of a system. In this section tredneuch response curves obtained from numerical

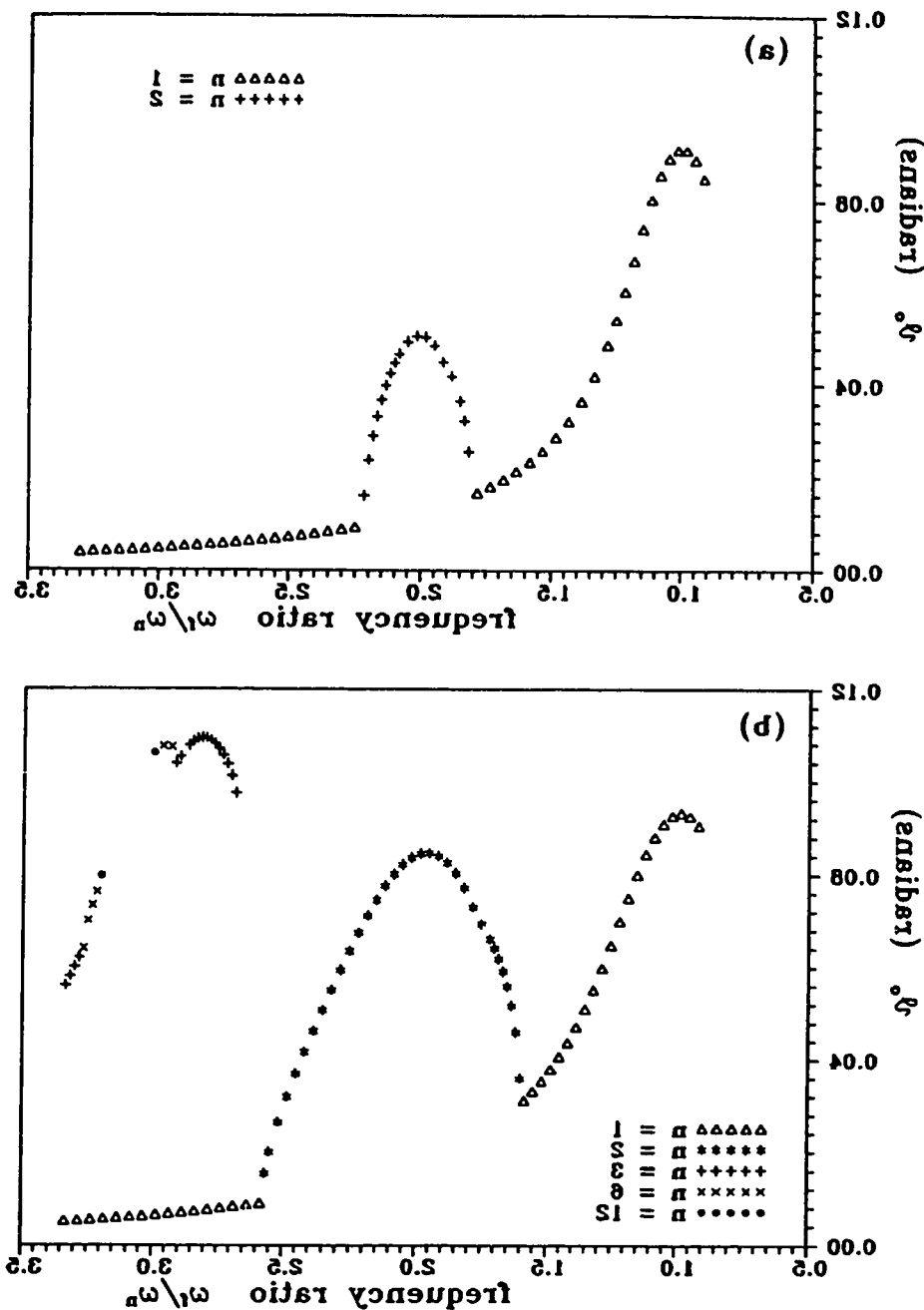


Figure 4.3: Comparison of the power response using total scattering with partial scattering. Parameters: $a = 100\text{m}$, $H = 10\text{m}$, $D = 5\text{m}$, $C_g = 5.0$, $C_q = 1.0$, $\beta = 3.0$, $\omega_0 = 0.05\text{rad/s}$. (a) Using $g_x + g_z$; (b) Using $g_x + (g_x - g_z)$.

wide variety of system parameters.

The importance of the convective term also can be seen from the discussion below. Recall that the fluid velocity in the direction of the tower motion, located at a vertical distance z from the base of the tower, is approximated by

$$(4.1) \quad u = \frac{\pi H}{T} e^{-(k-z)} \cos(\omega t - \varphi)$$

in which θ denotes along with the nondimensional parameter φ and z can be approximated by 1. In the case of deep water and higher frequency, such as in superharmonic resonance range, φ is large so that the variation of the fluid velocity with respect to θ may not be small, although the tower angular displacement θ is small. It is for this reason that two figures, Figure 4.1(a) and (b), differ greatly from each other in the superharmonic range. Considerably, the convective terms can not be neglected in the expression of fluid acceleration in deep water. The fact that peak value of the fundamental resonance in Figure 4.1(a) and (b) is about the same further supports the above argument that the nonlinear convective term only affects the system response in the higher frequency range.

If is worthwhile to note that in Figure 4.1(p) the peak values of superharmonic resonance are of the same magnitude as that of the fundamental resonance. Also note that in the range of ratio ω/ω_0 from 3.3 to 6.2 the period one resonance coexists with other superharmonic responses with different periods. Note that no coexistence of solutions have been found in the second resonance. This indicates that the period one solution becomes unstable in the fundamental range associated with the second resonance and becomes stable in the fundamental range associated with the second resonance. As will be shown in what follows this is a common phenomenon for all hydrodynamic responses with the exception that for some sets of parameters there exists a small instabilities range for period one solutions in the hydrodynamic range near the third resonance.

Figure 4.2 provides a comparison of the system response when two forms of the

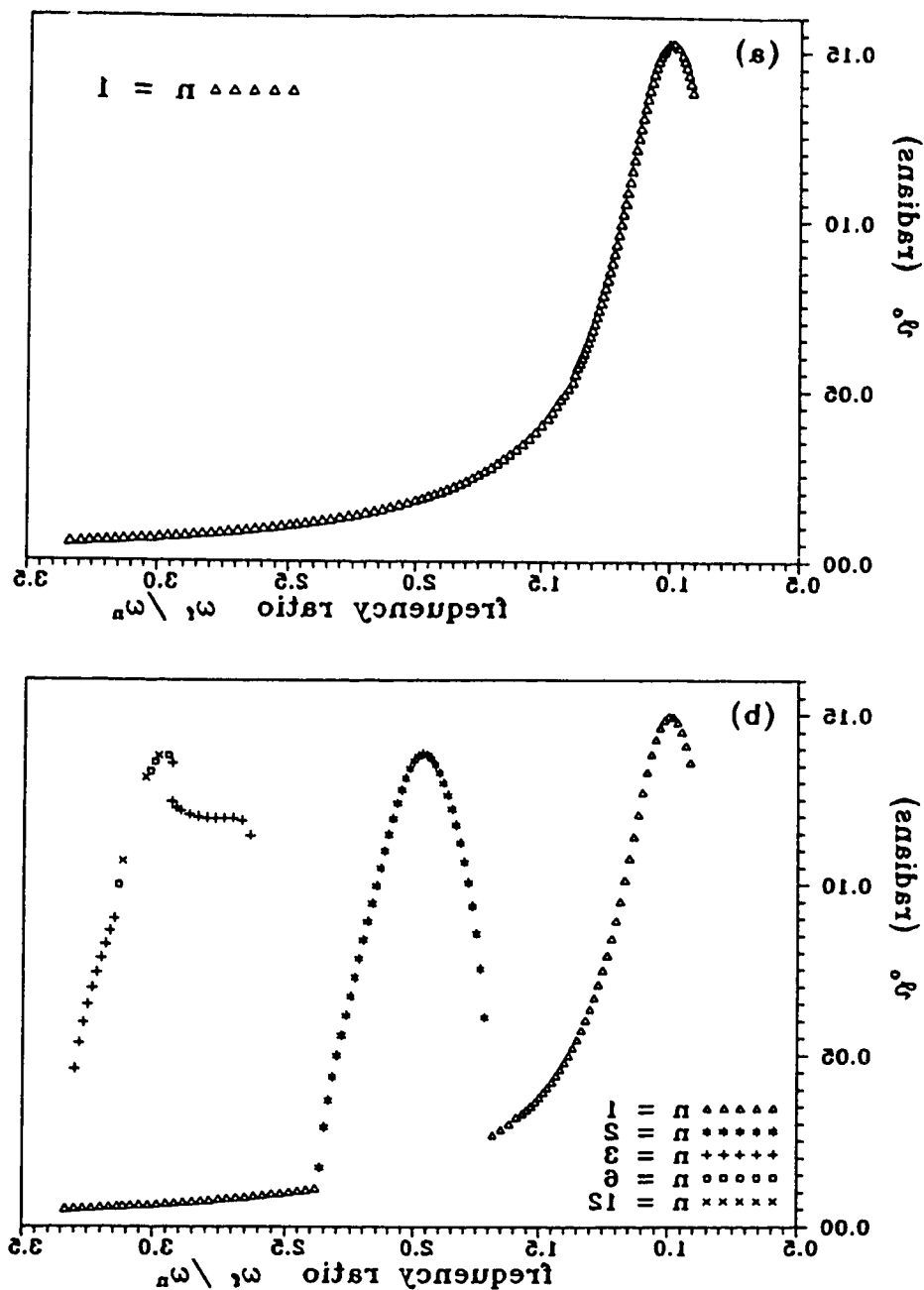


Figure 4.1: Frequency response of the filter using local and total acceleration with barometers: $a = 100\omega$, $H = 10\omega$, $D = 3\omega$, $C_w = 5.0$, $C_g = 0.5$, $\omega_0 = 0.01\omega_0$, $b = 0.5$. (a) Using gU/gt ; (b) Using $gU/gt + UgU/gx$.

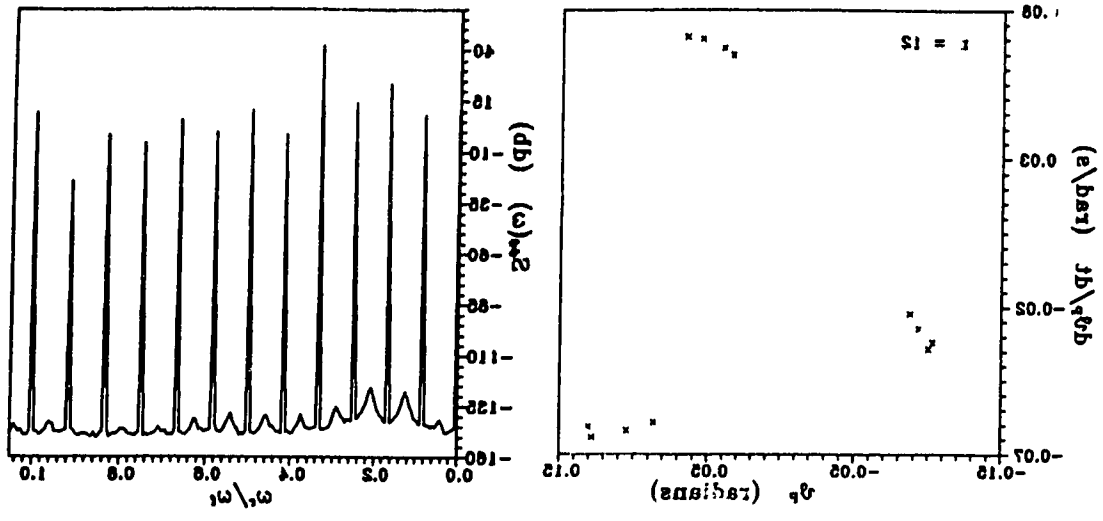
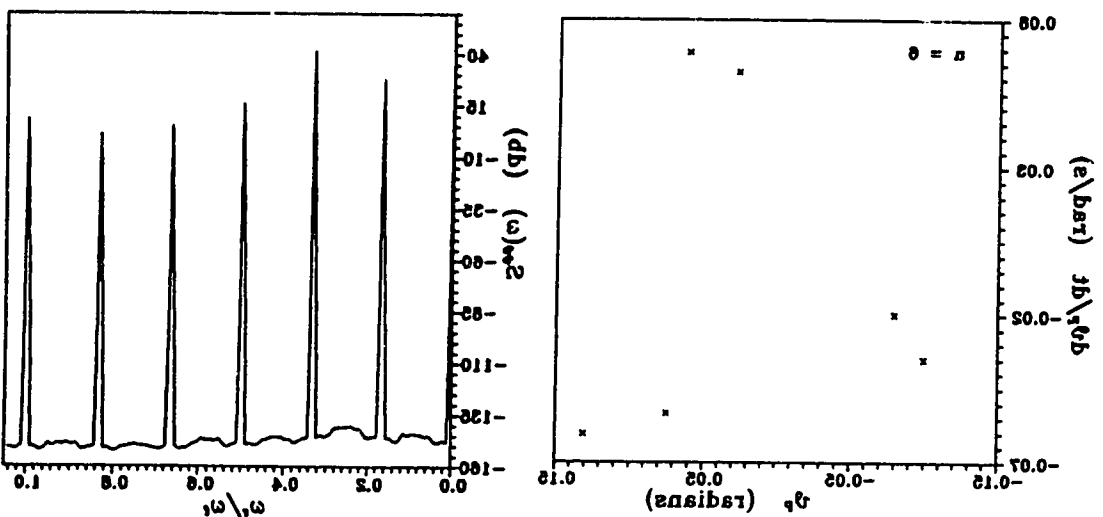
(b) $\omega_1 = 1.08 \text{ rad/s}$, berilio g solution(c) $\omega_1 = 1.967 \text{ rad/s}$, berilio f solution

Figure 4.14: Poincaré maps and power spectra (cont'd)

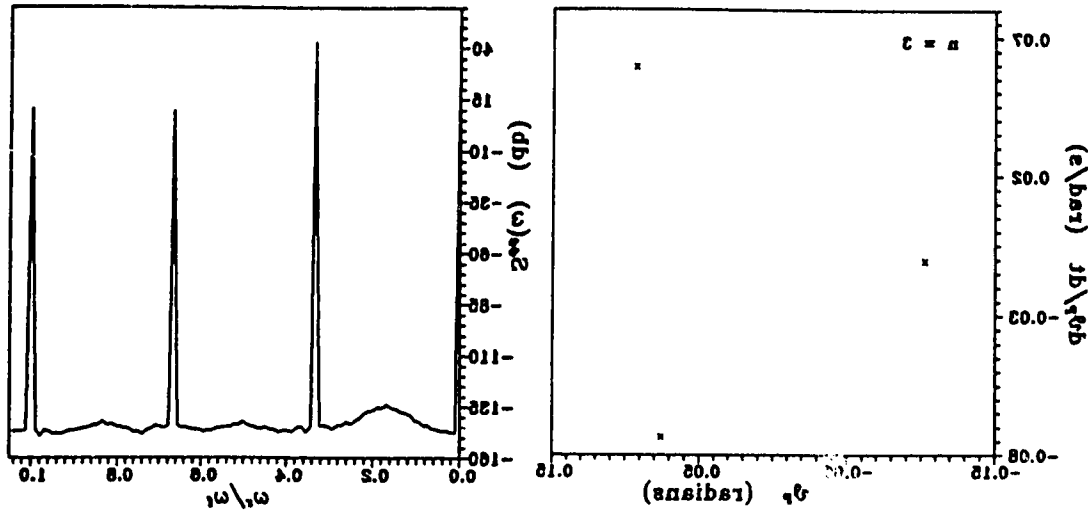


Figure 4.14(a): Poincaré map & period 3 solution
 $\theta = \pi$

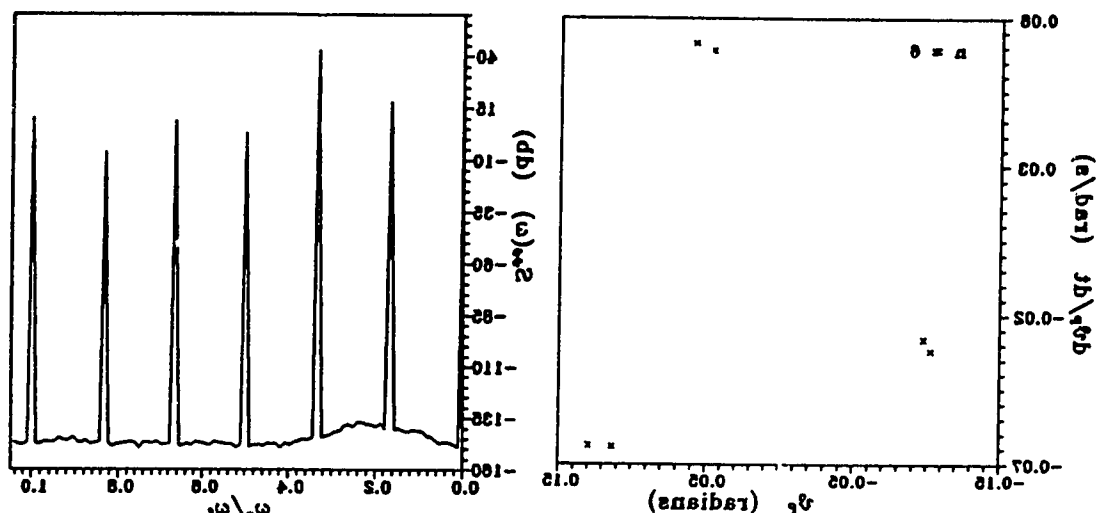


Figure 4.14(b): Poincaré map & period 6 solution
 $\theta = 0$

Figure 4.14: Poincaré maps and power spectra

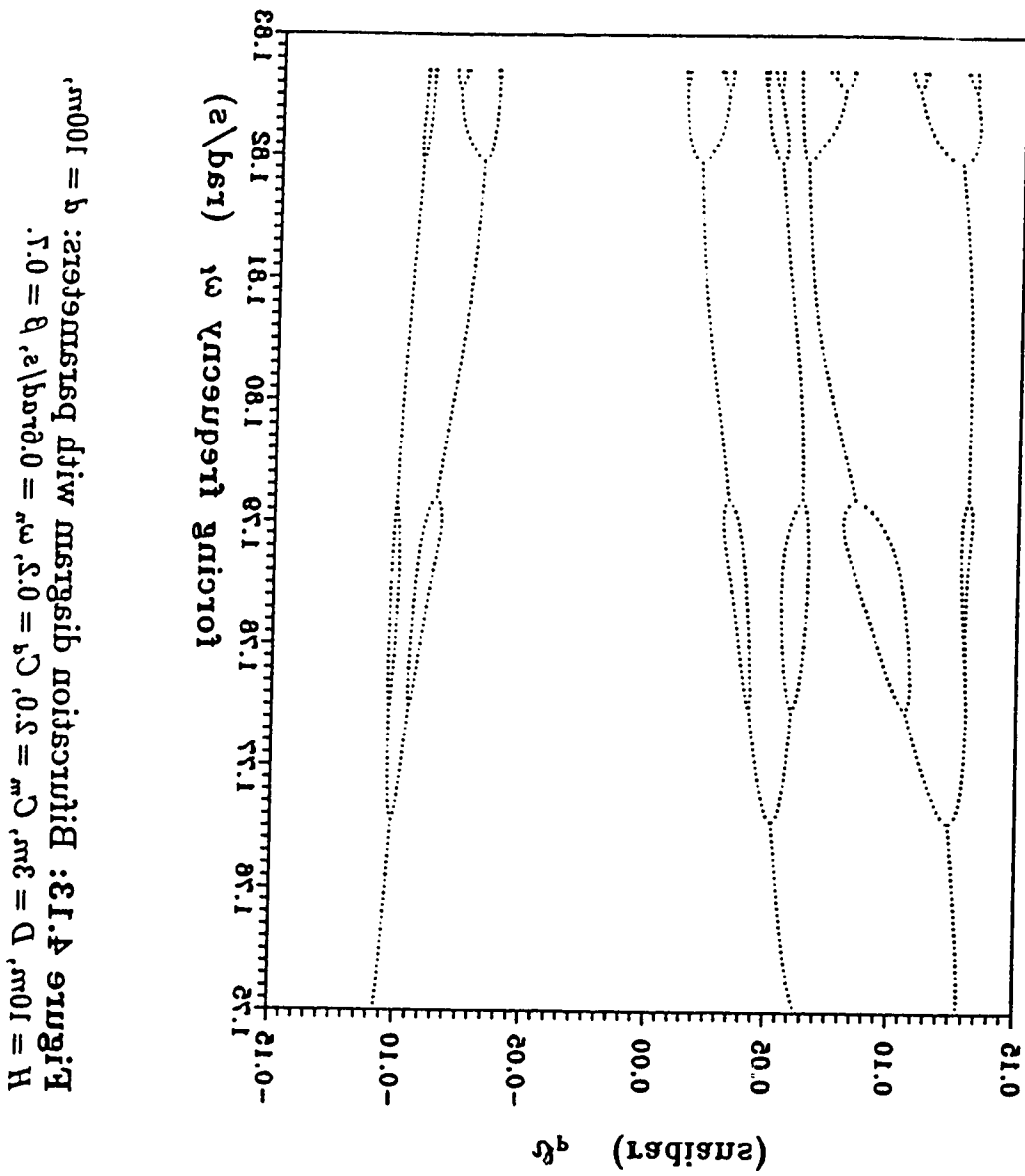


Figure A.13: Bifurcation diagram with parameter ω (s) on the horizontal axis and δ (sensibat) on the vertical axis:
 $H = 10\text{m}$, $D = 3\text{m}$, $C_m = 3\text{m}$, $C_a = 3\text{m}$, $C_b = 3\text{m}$, $C_c = 3\text{m}$, $C_d = 3\text{m}$, $\alpha = 0.0$, $\beta = 0.0$, $\gamma = 0.0$, $\delta = 0.0$, $\theta = 0.0$, $\lambda = 0.0$.

in Figure 4.13. This distribution diagram shows the global distribution of the system response for individual points located in the region. As can be seen in this figure, before the solution point, the response is zero. At $\omega = 0.1$, there is a sharp increase in the response to about 0.1. At $\omega = 0.2$, the response reaches a maximum value of approximately 0.25. At $\omega = 0.3$, the response begins to decrease and reaches a minimum value of about -0.1 at $\omega = 0.4$. At $\omega = 0.5$, the response increases again, reaching a maximum value of about 0.2 at $\omega = 0.6$. At $\omega = 0.7$, the response begins to decrease again, reaching a minimum value of about -0.1 at $\omega = 0.8$. At $\omega = 0.9$, the response increases again, reaching a maximum value of about 0.2 at $\omega = 1.0$. At $\omega = 1.1$, the response begins to decrease again, reaching a minimum value of about -0.1 at $\omega = 1.2$. At $\omega = 1.3$, the response increases again, reaching a maximum value of about 0.2 at $\omega = 1.4$. At $\omega = 1.5$, the response begins to decrease again, reaching a minimum value of about -0.1 at $\omega = 1.6$. At $\omega = 1.7$, the response increases again, reaching a maximum value of about 0.2 at $\omega = 1.8$. At $\omega = 1.9$, the response begins to decrease again, reaching a minimum value of about -0.1 at $\omega = 2.0$. At $\omega = 2.1$, the response increases again, reaching a maximum value of about 0.2 at $\omega = 2.2$. At $\omega = 2.3$, the response begins to decrease again, reaching a minimum value of about -0.1 at $\omega = 2.4$. At $\omega = 2.5$, the response increases again, reaching a maximum value of about 0.2 at $\omega = 2.6$. At $\omega = 2.7$, the response begins to decrease again, reaching a minimum value of about -0.1 at $\omega = 2.8$. At $\omega = 2.9$, the response increases again, reaching a maximum value of about 0.2 at $\omega = 3.0$. At $\omega = 3.1$, the response begins to decrease again, reaching a minimum value of about -0.1 at $\omega = 3.2$. At $\omega = 3.3$, the response increases again, reaching a maximum value of about 0.2 at $\omega = 3.4$. At $\omega = 3.5$, the response begins to decrease again, reaching a minimum value of about -0.1 at $\omega = 3.6$. At $\omega = 3.7$, the response increases again, reaching a maximum value of about 0.2 at $\omega = 3.8$. At $\omega = 3.9$, the response begins to decrease again, reaching a minimum value of about -0.1 at $\omega = 4.0$. At $\omega = 4.1$, the response increases again, reaching a maximum value of about 0.2 at $\omega = 4.2$. At $\omega = 4.3$, the response begins to decrease again, reaching a minimum value of about -0.1 at $\omega = 4.4$. At $\omega = 4.5$, the response increases again, reaching a maximum value of about 0.2 at $\omega = 4.6$. At $\omega = 4.7$, the response begins to decrease again, reaching a minimum value of about -0.1 at $\omega = 4.8$. At $\omega = 4.9$, the response increases again, reaching a maximum value of about 0.2 at $\omega = 5.0$. At $\omega = 5.1$, the response begins to decrease again, reaching a minimum value of about -0.1 at $\omega = 5.2$. At $\omega = 5.3$, the response increases again, reaching a maximum value of about 0.2 at $\omega = 5.4$. At $\omega = 5.5$, the response begins to decrease again, reaching a minimum value of about -0.1 at $\omega = 5.6$. At $\omega = 5.7$, the response increases again, reaching a maximum value of about 0.2 at $\omega = 5.8$. At $\omega = 5.9$, the response begins to decrease again, reaching a minimum value of about -0.1 at $\omega = 6.0$. At $\omega = 6.1$, the response increases again, reaching a maximum value of about 0.2 at $\omega = 6.2$. At $\omega = 6.3$, the response begins to decrease again, reaching a minimum value of about -0.1 at $\omega = 6.4$. At $\omega = 6.5$, the response increases again, reaching a maximum value of about 0.2 at $\omega = 6.6$. At $\omega = 6.7$, the response begins to decrease again, reaching a minimum value of about -0.1 at $\omega = 6.8$. At $\omega = 6.9$, the response increases again, reaching a maximum value of about 0.2 at $\omega = 7.0$. At $\omega = 7.1$, the response begins to decrease again, reaching a minimum value of about -0.1 at $\omega = 7.2$. At $\omega = 7.3$, the response increases again, reaching a maximum value of about 0.2 at $\omega = 7.4$. At $\omega = 7.5$, the response begins to decrease again, reaching a minimum value of about -0.1 at $\omega = 7.6$. At $\omega = 7.7$, the response increases again, reaching a maximum value of about 0.2 at $\omega = 7.8$. At $\omega = 7.9$, the response begins to decrease again, reaching a minimum value of about -0.1 at $\omega = 8.0$. At $\omega = 8.1$, the response increases again, reaching a maximum value of about 0.2 at $\omega = 8.2$. At $\omega = 8.3$, the response begins to decrease again, reaching a minimum value of about -0.1 at $\omega = 8.4$. At $\omega = 8.5$, the response increases again, reaching a maximum value of about 0.2 at $\omega = 8.6$. At $\omega = 8.7$, the response begins to decrease again, reaching a minimum value of about -0.1 at $\omega = 8.8$. At $\omega = 8.9$, the response increases again, reaching a maximum value of about 0.2 at $\omega = 9.0$. At $\omega = 9.1$, the response begins to decrease again, reaching a minimum value of about -0.1 at $\omega = 9.2$. At $\omega = 9.3$, the response increases again, reaching a maximum value of about 0.2 at $\omega = 9.4$. At $\omega = 9.5$, the response begins to decrease again, reaching a minimum value of about -0.1 at $\omega = 9.6$. At $\omega = 9.7$, the response increases again, reaching a maximum value of about 0.2 at $\omega = 9.8$. At $\omega = 9.9$, the response begins to decrease again, reaching a minimum value of about -0.1 at $\omega = 10.0$.

is about 1.8235.

Also the period doubling phenomenon can be seen from a sequence of Poincaré sections in Figure 4.14(a)-(b). These figures clearly show that a power spectrum shown in Figure 4.14(a) is a chaotic cascade in the response when varying forcing frequency ω , and the period doubling route to chaos.

The last Poincaré map for $\omega = 1.8235$ given in Figure 4.15 shows a chaotic response in which 2000 Poincaré points have been computed and plotted after 1000 forcing cycles transient. The power spectrum corresponding to each Poincaré map is shown on the right side of each map and is plotted on a logarithmic scale from 0 to 1. The ratio of the response frequency to the forcing frequency ω , m/ω , where $m = 1, 2, 3, \dots$, is the order of superimposed solutions. For the periodic response the power spectrum consists of a sequence of spikes at frequencies of (m/ω) , where $m = 1, 2, 3, \dots$, is the order, where there are spikes within the frequency solution. This for the solution of order n , there are n spikes within the frequency range from 0 to 1. For chaotic response, the power spectrum is continuous, showing "random like" behavior as in Figure 4.15. The chaotic attractor, as can be seen in Figure 4.15, is a variation one as the damping of the system in this case is very small.

A numerical test of period doubling cascade discovered by Feigenbaum [33] is the so-called Feigenbaum number. The Feigenbaum number associated with this

condition wasp will show a finer and finer structure on the boundary. Evidence of this can be seen in Figure 4.1 which shows that even a system with periodic response can exhibit a sensitive dependence on initial conditions. This makes the dynamic response of such structures difficult to predict.

4.2 Bifurcation to Chaos

To further investigate the frequency response curve of the bifurcated power and to identify the route to chaos by Hopf bifurcation, here, as an example, the frequency response curve for the case previously shown in Figure 4.1 (p) will be discussed in detail. For the frequency ratio range first this was been investigated before a brief time was in frequency ratio regions, each of them being associated with a resonant peak. The solutions are all period one solution in the range of frequency resonance peak. At point I.1 with the first resonance peak value (the fundamental frequency) being point I.12 and at a frequency ratio of point I.0. In the next resonance (point I.0.12) there is a double solution in twice of that of frequency ratio is point I.2 to A, the period of solution is twice of that of frequency ratio is point I.1. Following this frequency range the forcing and hence they are period two solutions. Following this frequency range with very small mean response amplitude. In the last period one solution range with this amplitude is a period two solution to be period three solution, period three, period six, period twelve solution, various sympathetic solutions coexist with the same solution and are observed. At $\omega_1 = 0.2$, there exist two different period three solution and phenomena is clearly seen at this value of frequency ratio. The period of frequency is clearly seen at this value of frequency ratio. An infinite period doubling cascade is formed and the solution of frequency ratio. An infinite period doubling cascade is formed and the solution of frequency ratio $\omega_1 = 3.1$. Note also that at the eventually becomes chaotic in the range $\omega_1 = 3.0 \sim 3.1$. The sympathetic solution. Higher frequency range period one solution coexist with the sympathetic solution. To see changes in response period clearly, the Poincaré points for each set of forcing frequency corresponding to this period doubling is plotted in Fig-

46

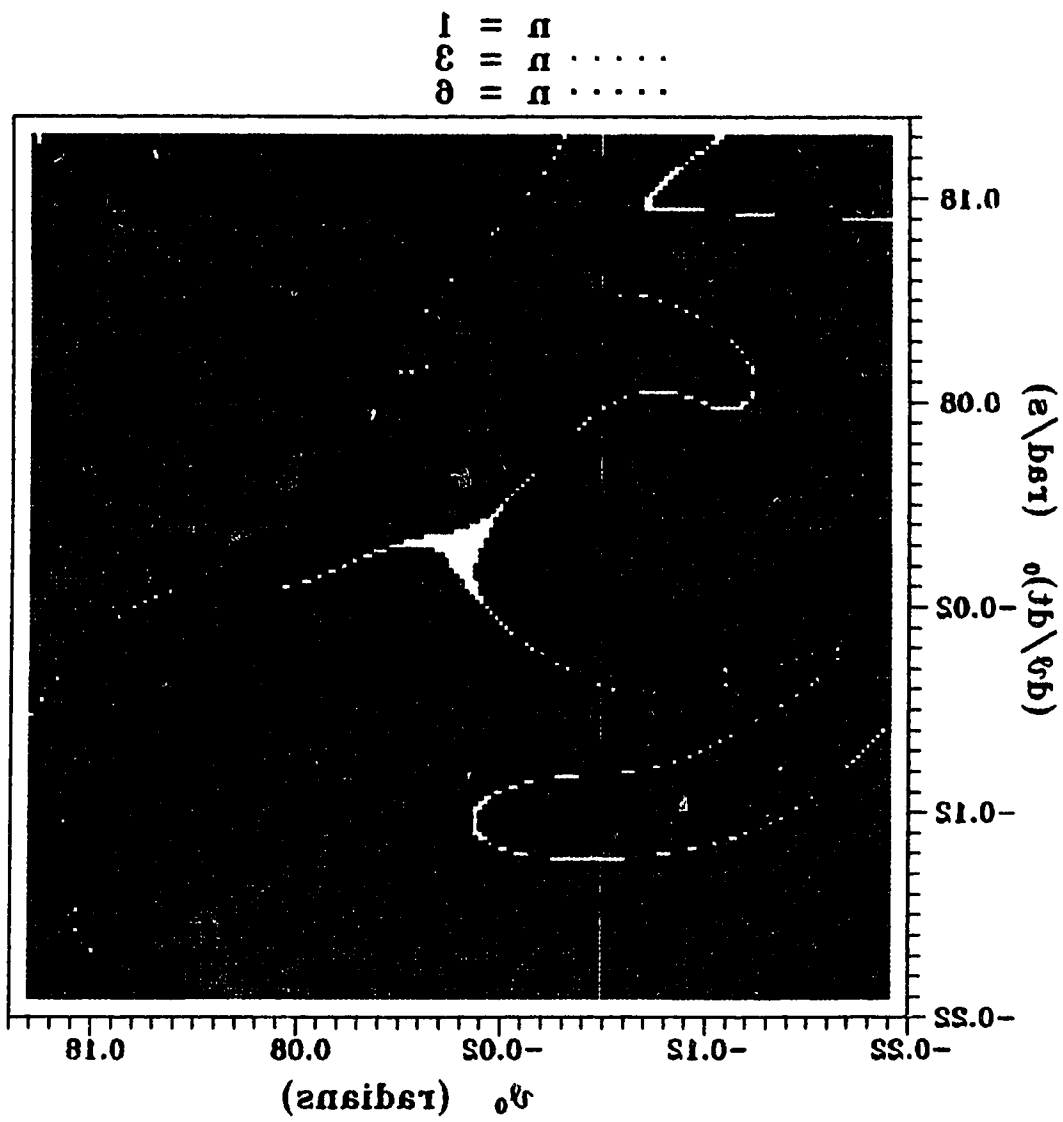
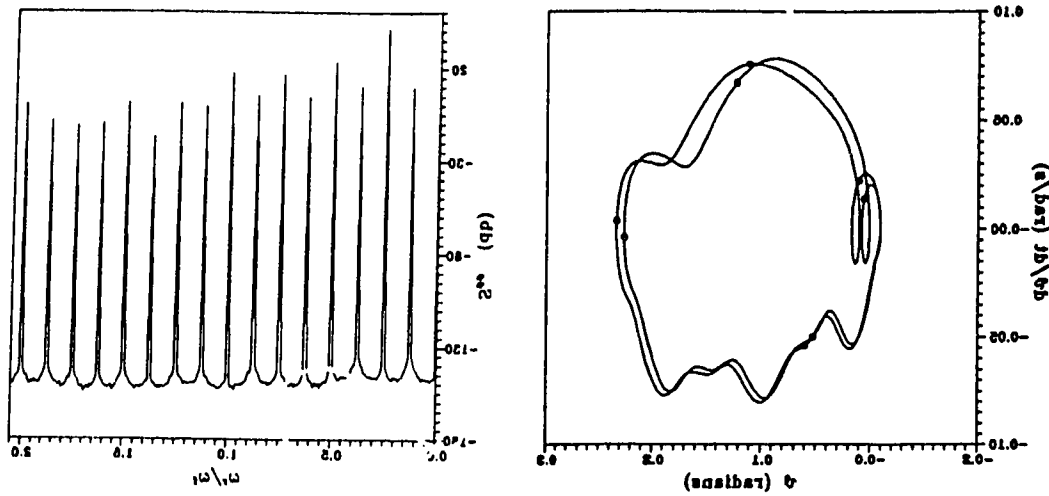
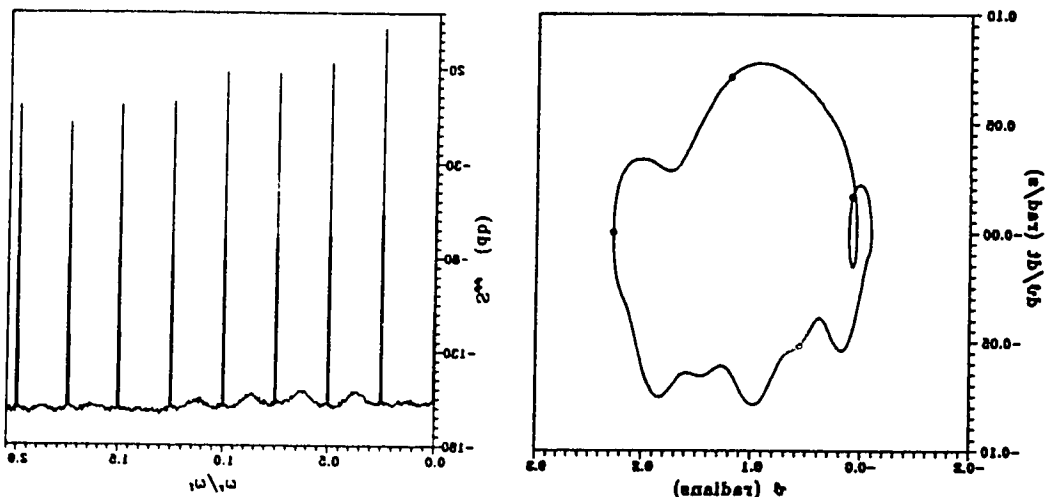


Figure 15 Basis of stiffening

parameters: $q=100\text{m}$, $H=10\text{m}$, $C_d=0.5$, $C_w=5$,
 $\omega_w=0.8\text{rad/s}$, $\omega_i=1.8\text{rad/s}$, $b=0.5$, $D=2\text{m}$



٤.١١(a) $\epsilon' / \epsilon_0 = \epsilon(t)$



٤.١١(b) $\epsilon' / \epsilon_0 = \epsilon(t)$

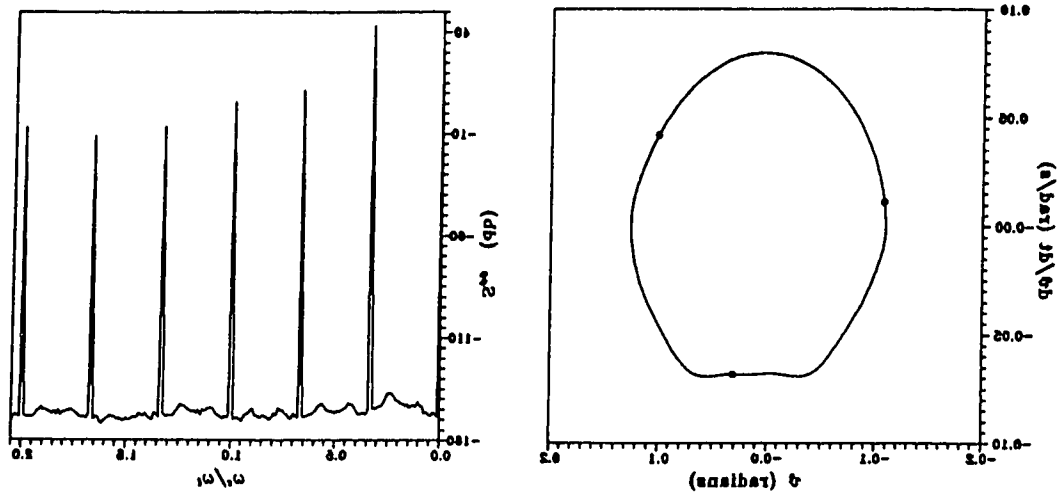
Figure 4.11: Periodic pinching polymerization with barostateters:
 $a = 100\text{nm}$, $H = 20\text{nm}$, $D = 3\text{nm}$, $C_w = 2.0$, $C_g = 0.5$, $\omega_0 = 0.67\text{rad/s}$,
 $\omega_p = 0.5$.

graph to Fig. 4.11 shows a period halving phenomenon to 1/8 of the forcing frequency. Figure 4.11 shows a period doubling phenomenon to 1/4 of the forcing frequency with an increase in forcing frequency from period eight to four solution with an increase in forcing frequency from 100 rad/s to 200 rad/s. Values of the system parameters for Figure 4.11 are: $a = 100\text{m}$, $H = 3\text{m}$, $C_d = 2.0$, $C_w = 0.5$, $\omega_a = 0.01\text{rad/s}$, and $\omega = 1.0\text{rad/s}$, the response is a period eight solution; if ω is increased slightly to 1.01 rad/s, the response changes to period four solution.

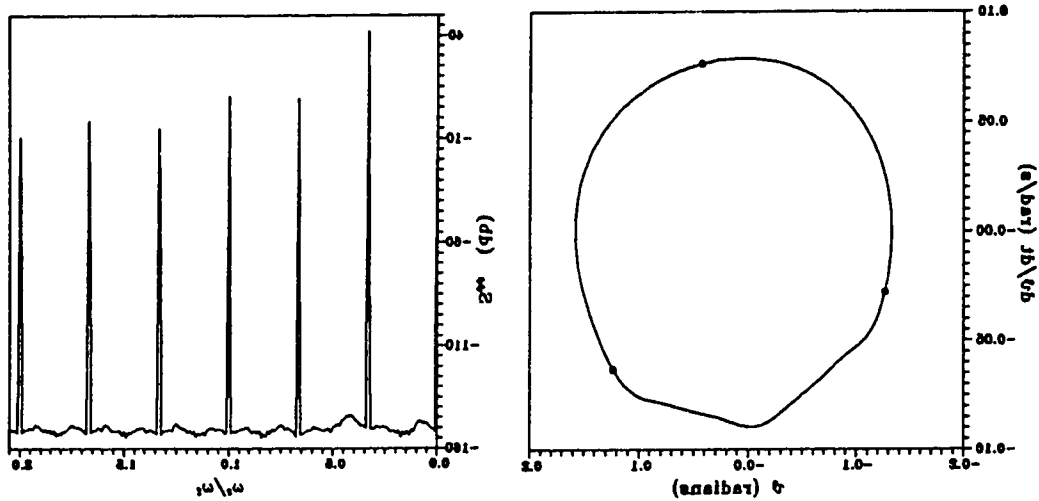
These figures clearly show the dependence of the response on initial conditions and system parameters and steady-state response of the system.

If this pendulum shows that superharmonic response and coexisting multiple solutions are common for complex off-resonance situations. To see the dependence of coexisting steady-state solution for three different initial conditions, passing of three coexisting solutions on initial conditions, plotted in Fig. 4.12. System parameter values for this figure are: $a = 100\text{m}$, $H = 10\text{m}$, $D = 5\text{m}$, $C_d = 0.5$, $C_w = 2.0$, $\omega_a = 1.0\text{rad/s}$, $\omega = 1.0\text{rad/s}$, and $\theta = 0^\circ$. The step size of this was for both axes, the initial velocity is 0.0 m/s and 0.088 rad/s, is different initial conditions and initial angular velocity is 0.0 m/s and 0.0200 rad/s respectively. The motion starts with a steady state to follow this pendulum motion. The motion starts with a steady state to follow this pendulum motion. Similarly, the motion starts with a steady state to follow this pendulum motion. As can be seen in this case shows only dependent on the initial conditions. The shape of passes of attractor is very complicated and the stretching and folding of the attractor is very complex. For the case of the parameters used here, pass in boundary effects are clearly shown. In general, the pass in boundary effects as smooth, conjugate lines, implying that it is motion starts away from the boundary, small uncertainties in them will not affect the final response. However, if this pendulum shows in many nonlinear systems that, in general, the pass in boundary effects are not smooth and have a fractal nature (see for example, Kapitaniak [41]). In this case, and small uncertainties in initial conditions may lead to uncertainties in the outcome of the system. As the step size becomes smaller and smaller, the initial

16



(a) starting point $(-0.0, 0.5)$



(d) starting point $(-0.5, 0.5)$

Figure 4.10: Two coexisting $n = 3$ solutions with parameter values: $q = 100\text{m}$, $H = 10\text{m}$, $D = 5\text{m}$, $C_q = 0.5$, $C_w = 2.0$, $\omega_s = 0.6\pi\text{rad/s}$, $\beta = 0.5$, $\omega_1 = 1.772\pi\text{rad/s}$.

Table 4.3: Solutions for $D = 3$ using $DU/Dt = g_{UU} + U g_{Ug}$

H = 1 m							
q = 100 m				q = 200 m			
parameters	$C_g = 0.3$	$C_g = 0.5$	$C_g = 1.0$	$C_g = 0.3$	$C_g = 0.5$	$C_g = 1.0$	$C_g = 1.0$
$\delta = 0.3$	$u=1, 3$	$u=1, 3$	$u=1$	$u=1$	$u=1$	$u=1$	$u=1$
$\delta = 0.5$	$u=1, 3$	$u=1, 3$	$u=1$	$u=1$	$u=1$	$u=1$	$u=1$
$\delta = 1$	$u=1, 3$	$u=1, 3$	$u=1$	$u=1$	$u=1$	$u=1$	$u=1$
$\delta = 2$	$u=1, 3$	$u=1, 3$	$u=1$	$u=1$	$u=1$	$u=1$	$u=1$
H = 10 m							
q = 100 m				q = 200 m			
parameters	$C_g = 0.3$	$C_g = 0.5$	$C_g = 1.0$	$C_g = 0.3$	$C_g = 0.5$	$C_g = 1.0$	$C_g = 1.0$
$\delta = 0.3$	$u=1, 3$	$u=1, 3$	$u=1$	$u=1$	$u=1$	$u=1$	$u=1$
$\delta = 0.5$	$u=1, 3$	$u=1, 3$	$u=1$	$u=1$	$u=1$	$u=1$	$u=1$
$\delta = 1$	$u=1, 3$	$u=1, 3$	$u=1$	$u=1$	$u=1$	$u=1$	$u=1$
$\delta = 2$	$u=1, 3$	$u=1, 3$	$u=1$	$u=1$	$u=1$	$u=1$	$u=1$
H = 20 m							
q = 100 m				q = 200 m			
parameters	$C_g = 0.3$	$C_g = 0.5$	$C_g = 1.0$	$C_g = 0.3$	$C_g = 0.5$	$C_g = 1.0$	$C_g = 1.0$
δ, chaos	$u=1, 3$	$u=1, 3$	$u=1$	$u=1$	$u=1$	$u=1$	$u=1$
δ, chaos	$u=1, 3$	$u=1, 3$	$u=1$	$u=1$	$u=1$	$u=1$	$u=1$
δ, chaos	$u=1, 3$	$u=1, 3$	$u=1$	$u=1$	$u=1$	$u=1$	$u=1$
δ, chaos	$u=1, 3$	$u=1, 3$	$u=1$	$u=1$	$u=1$	$u=1$	$u=1$

Table A.2: Solutions for $D = 1\text{m}$ using $D\backslash D_f = 9U\backslash g + (19U\backslash g)^2$

$b=100\text{ m}$							
$H=10\text{ m}$				$H=5\text{ m}$			
parameters	$C_a = 0.3$	$C_a = 0.5$	$C_a = 1.0$	$C_a = 0.3$	$C_a = 0.5$	$C_a = 1.0$	$C_a = 1.0$
$\beta = 0.3$	$u=1, \frac{3}{2}$	$u=1$	$u=1, \frac{3}{4}$	$u=1$	$u=1$	$u=1$	$u=1$
$\beta = 1$	$u=1$	$u=1$	$u=1, \frac{3}{4}$	$u=1$	$u=1$	$u=1$	$u=1$
$\beta = 5$	$u=1, \frac{3}{2}$	$u=1$	$u=1$	$u=1$	$u=1$	$u=1$	$u=1$

for deeper water depth $a = 500\text{m}$ where fluid damping is very large.

The solutions for $D = 1\text{m}$ and $D = 3\text{m}$ are listed in Tables A.2 and A.3 respectively. The same conclusions as above can be drawn from these tables. It also can be seen that complex responses are unlikely to occur when decreasing D , as the fluid damping is inversely proportional to the water diameter D . It has been shown that fluid damping often implies the generation of a beat frequency coupling cascade and beat frequency often leads to chaotic motion, even though these do not necessarily to occur. Operation of such phenomena is important for identifying chaotic motion.

Shown in Figure A.10 are two coexisting beat frequency solutions, one with a smaller amplitude (Figure A.10 (a)) and the other with a larger amplitude (Figure A.10 (b)) corresponding to a lump boundary. Dots in the phase plane illustrate leapfrog corroboration to a lump boundary. Operation of Figure A.10 are as follows: $a = 100\text{m}$, $H = 10\text{m}$, $D = 5\text{m}$, $C_a = 0.3$, $\omega_r = 0.6\text{rad/s}$, $\omega_l = 1.73\text{rad/s}$, and $\beta = 0.3$. Starting from point $(-0.05, 0.5)$, the motion of the system is attracted to the smaller amplitude solution; while starting from point $(-0.5, 0.5)$, the final motion of the system converges to the larger amplitude solution, indicating the dependence on initial conditions. Power spectra in the right side of each phase plot in Figure A.10 show that the response is mainly the component with frequency

Table 4.1: Solutions for D given using $D_U/D_t = g_U/g_t + U g_U/g_x$

decreases significantly when the power diameter D decreases since decreasing the power diameter will increase fluid damping significantly. This indicates that large damping can eliminate the existence of complex nonlinear resonance.

4.4 Supharmonic Response

For all values of parameters that have been investigated in this thesis for vibration of motion using the total acceleration expression $D\ddot{y} + \dot{D}\dot{y} + W_y y = 0$, supharmonic response has been observed in most of them. Various supharmonic solutions with different multiples of the forcing period have been seen in hydrodynamic response curves for different parameter values. The dependence of the supharmonic solution is a symbol of the dissipative change of the system response. Such a dissipative change is called a pitchfork and can be an indicator of the transition of the system response from order to chaos. Oscillation and investigation of such solutions are fundamental to identify the route to chaos.

The solutions that are distinguished power system can have in some parameter range for power diameter $D = 5$ m are listed in Table 4.1. In this table it is possible to determine the order of the supharmonic solution and all other parameters that define periodic. It can be seen from this table that as the wave height increases, an increasing number of supharmonic solutions and possibly the chaotic response can appear. Chaotic motion occurs when the drag coefficient C_d is small and the wave height is large. Since values of the drag coefficient are usually in the range from 0.0 to 2.0 for real structures, a drag coefficient of 0.3 is not typical, as mentioned before. This implies that chaotic motion may not be a common phenomenon in a real damped offshore structure for the parameter range that was investigated here. However chaotic response could occur when wave height is very large for a set of parameters. The supharmonic response is definitely a common phenomenon for the investigated power system and it occurs in a range of parameter range even

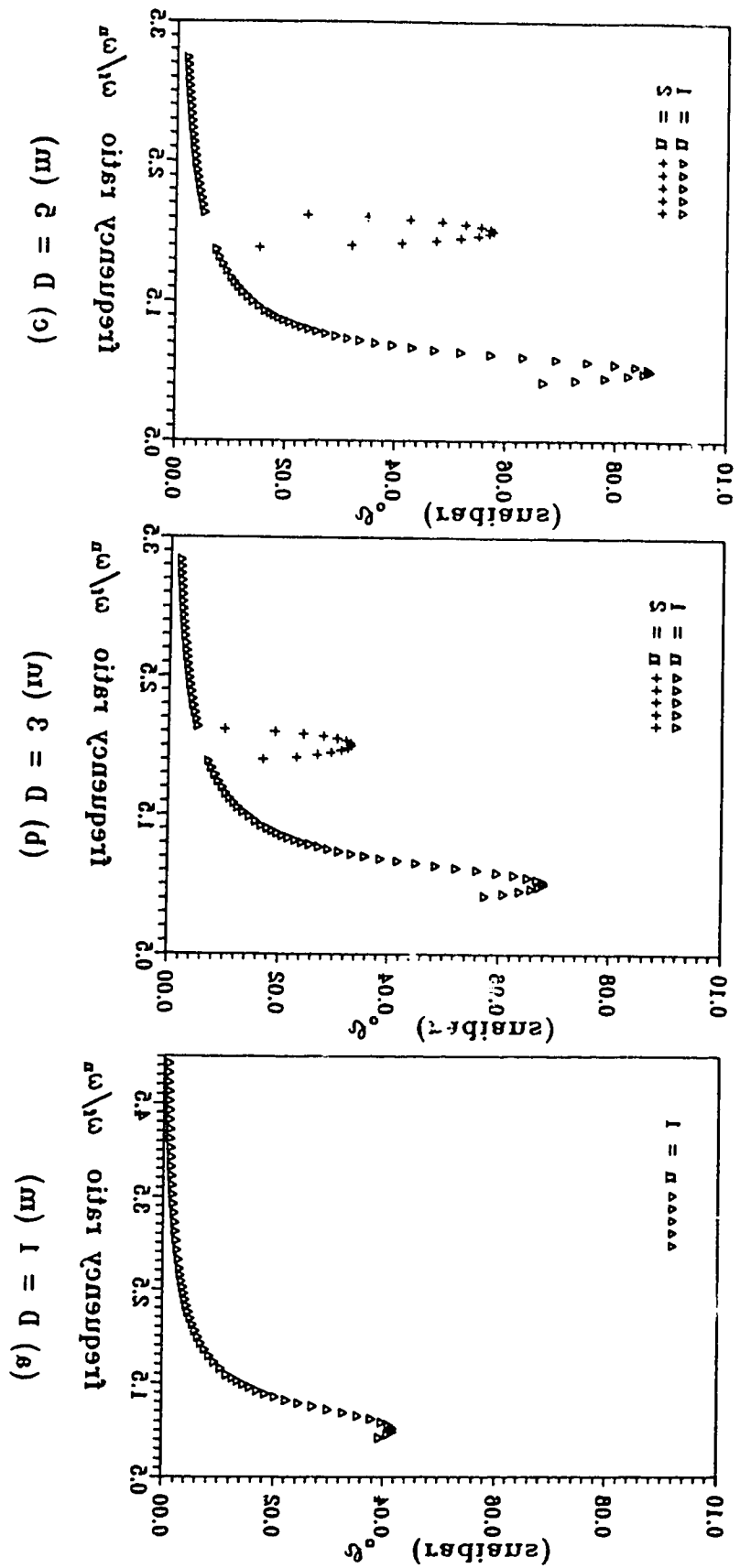


Figure 4.8: Frequency response for different values of D . Parameters: $\lambda = 100\pi$, $H = 5\pi$, $C_w = 5\pi$, $C_a = 5\pi$, $\omega_0 = \omega_w$, $W_{\text{rip}} = 0.0$.

- [10] Gottlieb, O., "Bifurcations and Routes to Chaos in Wave-Structure Interactions", *Journal of Guidance, Control, and Dynamics*, Vol. 19, No. 4, pp. 835-836, July-August, 1997.
- [11] Thompson, J. M. T., Bokasa, A. R. and Chakraborti, R., "Spiral Instability and Chaotic Motions of Coupled Oscillators Subjected to Structural and Aerodynamic Motions", *Journal of Fluids Resources Technology*, ASME, Vol. 100, pp. 191-198, June, 1984.
- [12] Sarpkaya, T. and Isaacson, M., "Mechanics of Wave Forces on Oscillating Structures", *Journal of Fluid Mechanics Reprint*, 1981.
- [13] Chakraborti, S. K., "Recent Advances in High Frequency Wave Forces", *Proceedings of Fourth International Offshore Mechanics and Applied Mechanics Conference*, Vol. 1, pp. 125-141, Dallas, Texas, 1982.
- [14] Kondratenko, B. I. and Gribeneva, L. H., "Forces on Circular Cylinders and Plates in an Oscillating Flow", *Journal of Research of the National Bureau of Standards*, Vol. 60, No. 5, pp. 433-440, 1958.
- [15] Chakraborti, S. K. and Coffey, D., "Hydrodynamic Coefficients of a Moving Cylinder", *Journal of Fluids Resources Technology*, ASME, Vol. 100, pp. 183-190, June, 1984.
- [16] Williamson, C. H. K., "In-line Response of a Cylinder in Oscillatory Flow", *Applied Ocean Research*, Vol. 5, No. 3, pp. 93-106, 1982.
- [17] Kostylevskaya, W. and Nakamura, M., "Wave Forces Acting on a Moving Cylinder", *Journal of Offshore Mechanics and Arctic Engineering*, ASME, Vol. 110, pp. 315-319, November, 1988.
- [18] Newmark, J. N., *Marine Hydrodynamics*, The MIT Press, 1972.
- [19] Sapsis, P.-T. and Chen, T. W., "Response of a Dynamic System to Low-Induced Loads", *International Journal of Non-Linear Mechanics*, Vol. 15, pp. 115-125, 1980.
- [20] McNamara, J. E. and Lane, M., "Practical Modelling for Aerodynamic Risks and Loading Conditions", *Journal of Fluids Resources Technology*, ASME, Vol. 106, pp. 444-450, December, 1984.
- [21] Chakraborti, S. K. and Coffey, D. C., "Motions of Aerodynamically Induced Flapwise Motions of Joints", *Journal of Fluids Resources Technology*, ASME, Vol. 108, pp. 333-341, August, 1986.

References

- [1] Gee, G. C., "Recent Advances in Design and Construction of Deepwater Pipelines", Part I, Ocean Industry, pp. 71-88, November, 1980.
- [2] Thollon, D., "A General Review of Future Problems and Their Solution", Proceedings of Second International Conference on Behaviour of Offshore Structures, London, pp. 773-783, 1979.
- [3] Pate, M. H., Dynamics of Offshore Structures, Butterworths, 1982.
- [4] Massou, M., "Recent Developments in the Construction of Hull-in-Hull Ships", Interactions with Offshore Structures, The Second International Conference on Civil Ship Methods in Offshore Engineering, Halifax, Canada, Vol. Civil Engineering, pp. 73-82, 1984.
- [5] Moon, E. C., Offshore Applications: A Introduction for Applied Scientists and Engineers, John Wiley & Sons, 1982.
- [6] Morison, J. R., O'Brien, M. P., Johnson, I. W. and Sefcik, S. A., "The Force Exerted by Waves on Ships", Transactions of the American Institute of Mining and Metallurgical Engineers, Vol. 148, pp. 148-154, 1950.
- [7] May, R. M., "Simple Mathematical Models with Very Complicated Dynamics", Nature, Vol. 261, pp. 459-462, June, 1976.
- [8] Thompson, J. M. T. and Stewart, H. B., Nonlinear Dynamics and Chaos: Geometric Methods for Engineers and Scientists, John Wiley & Sons, 1986.
- [9] Bishop, S. R. and Rubin, I. N., "The Use of Chaotic Models of a Moorey Semi-Supersolid", Journal of Offshore Mechanics and Arctic Engineering, ASME, Vol. 110, pp. 205-209, August, 1988.

resonates the central dynamic performance of such structure. The associations that have been made for this structure are bipolar and relational. Numerous simulations are very ready and this time consumers since the same proportion needs to be proportional to each set of stable parameters. Further investigation is indispensable to understand the dynamics of the power system.

The final development is a more complex system which includes the power generation system. This system consists of three main components: a hydroelectric power plant, a wind farm, and a solar panel array. The hydroelectric power plant uses the water flow from the river to generate electricity. The wind farm consists of several turbines located along the riverbank,利用风能发电。The solar panel array is located on the roof of the building,利用太阳能发电。The system is designed to be highly efficient, able to generate enough electricity to power the entire building and even sell excess power back to the grid. The system also includes a battery storage unit, allowing for power to be stored during peak production times and released during peak demand times. This system represents a significant step forward in sustainable energy generation, providing a reliable and renewable source of power for the building.

of system parameters has been investigated to provide a basic understanding of the behavior of this coupled resistive power.

It has been found that the nonlinear wave exciting force, arising from the non-linear convective terms in wave kinematics, plays a crucial role in the complex behaviors in the system parameter range investigated here. Over two hundred cases with different sets of system parameters have been investigated using the local form is used, the nonlinear drag force is form of fluid acceleration. When the local form is used, the nonlinear drag force is the only nonlinearly in the system and it is significant to note that sympathetic or chaotic responses are not found yet in this case. It seems that complex nonlinear responses are uniquely to occur when the inertia forcing terms corresponding to the convective terms are neglected. This is in contrast to the results of Gottlieb et al. [3]. It may be that the proper composition of the system parameters to operate complex response and chaotic response has not yet been considered.

For the system parameter range that has been studied here, chaotic response was found when the drag coefficient is small and wave height is large. This occurs for cases that $DU/Dt = 9U/g + UgU/g$ is used to evaluate the fluid particle acceleration. Since the drag coefficient for real structures rapidly is much larger than those where chaos has been found in this thesis, the chaos is probably due a common phenomenon for real structures except when the wave height is very large. At this level, when $DU/Dt = 9U/g + (U - \dot{x})gU/g$ is used, the numerical simulations have shown that chaotic response may occur at slightly larger values of the drag coefficient and slightly smaller wave heights. Thus when either form of the total acceleration expression considered in this thesis is used, nonlinear response can be anticipated. It is felt that inclusion of convective terms in the expression for the fluid particle acceleration is redundant to accurately model the fluid kinematics. This is the case even when the magnitude of the total oscillation is small. It has also been shown that the nonlinear convective terms only affect the system response in the sympathetic range and does not significantly affect the

Chapter 5

Summary and Conclusions

A single-degree-of-freedom model of the articulated tower subjected to regular wave excitation is studied in this thesis. Linear wave theory and the relative velocity formulation of the Morison equation have been used to obtain the wave forces acting on the structure. The exact form of the drag force is retained so that the model presented here can predict responses accurately during motion. The resulting equations of motion are nonlinear in both the drag force and wave exciting forces when the total acceleration of fluid particle is used. The drag force is a nonlinear damping function of the relative velocity between the fluid particle displacement and tower displacement so that the resulting motion of the articulated tower is a coupled system. In order to study the influence of each nonlinear function of the tower displacement displacement, the local expression of fluid particle acceleration is used so that the behavior, the local expression of fluid particle acceleration is used so that the nonlinear damping drag force is only nonlinearly in the displacement of motion. Thus different dampings of motion have been considered each with a different form of the fluid particle acceleration. An Adams-Basheff-Moulton numerical method has been used to obtain the solutions of different dampings of motion. A large variety

the computed Lipschitz exponent was positive, it was observed from time history that the response was out chaotic but periodic. A common outcome for these two cases is that the response amplitude is very small and it takes very long time to converge to steady state. The reason for this discrepancy could result from an error in the computer program. For this reason the program has been checked with a number of well known nonlinear systems, such as Duffing's equation [9], Van der Pol's equation [41], and a driven pendulum system given by Basker [42]. The computation of Lipschitz exponent in each case were in good agreement with the results shown in some literature references. Much effort has also been made to test the computer program of calculating the Lipschitz exponent by varying parameters, such as the total number of forcing cycles, initial length of the numerical axis, as well as the Lipschitz time step size. However, the calculated Lipschitz exponent was found to be independent of these parameters and showed very good convergence in all cases. Despite these program checks the reasons for the calculated Lipschitz exponent being out consistent with the type of motion that the system usually experiences are as yet unknown. Problems in calculating the Lipschitz exponent have also been reported by Plasschaert et al. [43], who studied the transition of a low-dimensional cylinder vibration system. Further work is needed to find out the reasons for this inconsistency. For reference the method used to calculate the largest Lipschitz exponent is given in Appendix B.

81

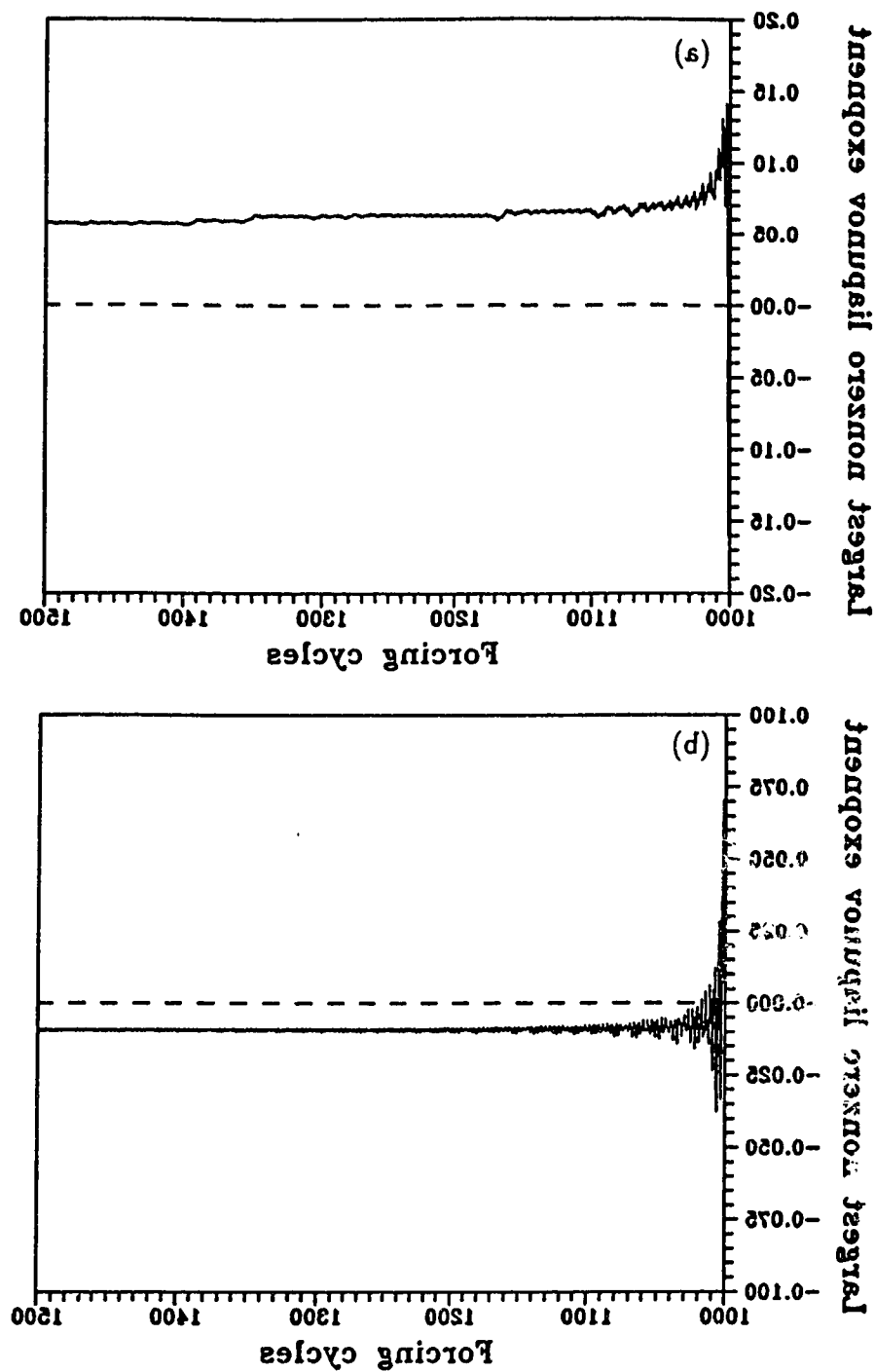


Figure 4.17: Time evolution of the largest non-zero Lyapunov exponent for (a) soft and (b) bimodal responses.

are given in Appendix B, or references [5, 36].

Figure 4.15. Figure 4.15 shows the time evolution of the largest Lyapunov exponent as a function of the number of forcing cycles. The total time used to calculate the largest Lyapunov exponent is 500 forcing cycles after transient phase dieas a function of the number of forcing cycles. The motion starts from initial point $\theta = 0.149400$, $\dot{\theta} = 0.0$ is subjected to chaotic motion and the corresponding largest Lyapunov exponent is shown in Figure 4.15. Motion starts from initial point $\theta = 0.149400$, $\dot{\theta} = 0.0$ is subjected to chaotic motion and the corresponding largest Lyapunov exponent is positive as shown in Figure 4.15. This indicates the sensitivity dependence on initial conditions.

implies the convergence to periodic motion, in this case the period one solution.

is also calculated as shown in Figure A.17 (p). The negative exponent in this case

coexists during the solution, with initial conditions $\theta = 0.7\pi$ and $\dot{\theta} = 0.1\sqrt{g/a}$,

one solution (see Figure A.1 (p)). The largest negative Lyapunov exponent for

observed chaotic response. Note that observed chaotic motion coexists with both

The computed positive largest negative Lyapunov exponent further verifies the

If shown in Figure 4.1, the first case being the second from solution to period one solution and the second from solution to period two solution. All four points plotted are positive at $t = 0$, which shows that the system is stable. The steady-state value is approximately 1.25. The transient values fluctuate around this steady-state value, with the amplitude of the oscillations decreasing over time.

47

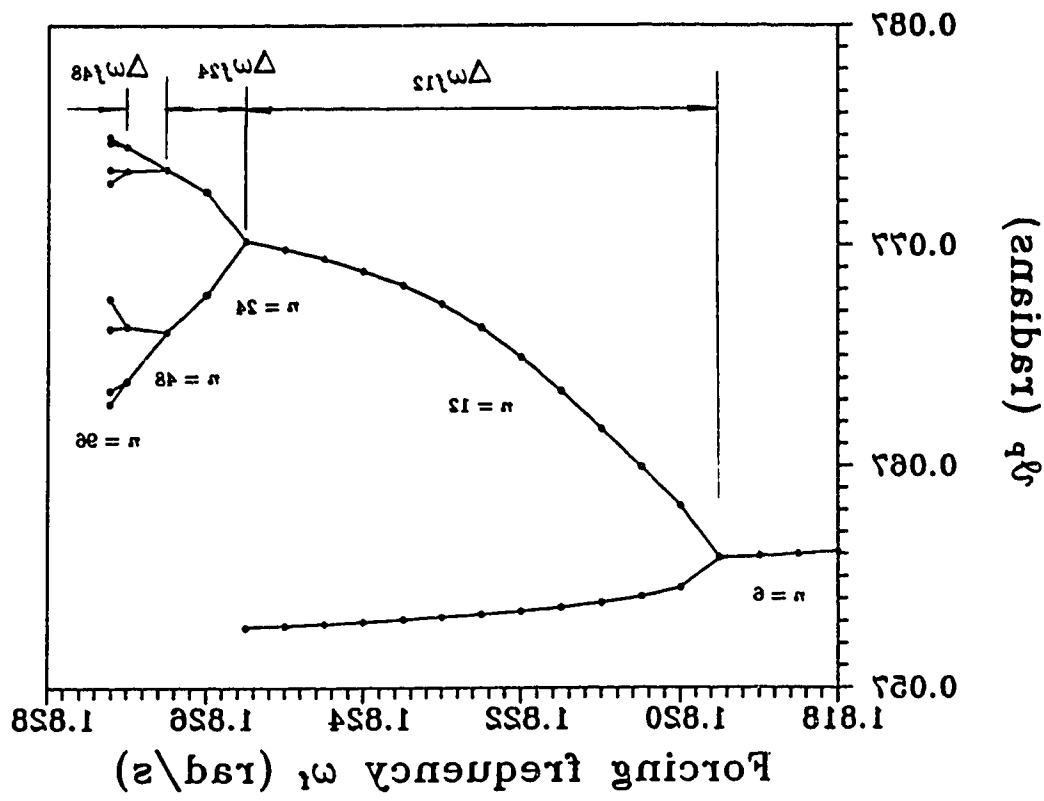


Figure 4.16: Partial enlargement of polarization dispersion diagram

period damping ratio which leads to chaotic response has also been calculated and approximation and one pitch excitation shown in Figure 4.13 has been evaluated and shown in Figure 4.16. These combined Feigenbaum numbers are

$$(4.4) \quad \Delta = \frac{18\pi\omega}{48} = 0.062, \quad \delta = \frac{\pi\omega}{18\Delta} = 28.4, \quad \epsilon = \frac{\pi\omega\Delta}{48} = 1.8$$

It can be seen that these values show the global coupling to the universal Feigenbaum number of 4.66920..., which is obtained for the logistic endomorphism and has also been observed in various nonlinear systems and experimental studies. It also can be expected that, with this fixed ratio, the pitchfork bifurcation cascade will finally reach an accumulation point where the observed chaotic response occurs.

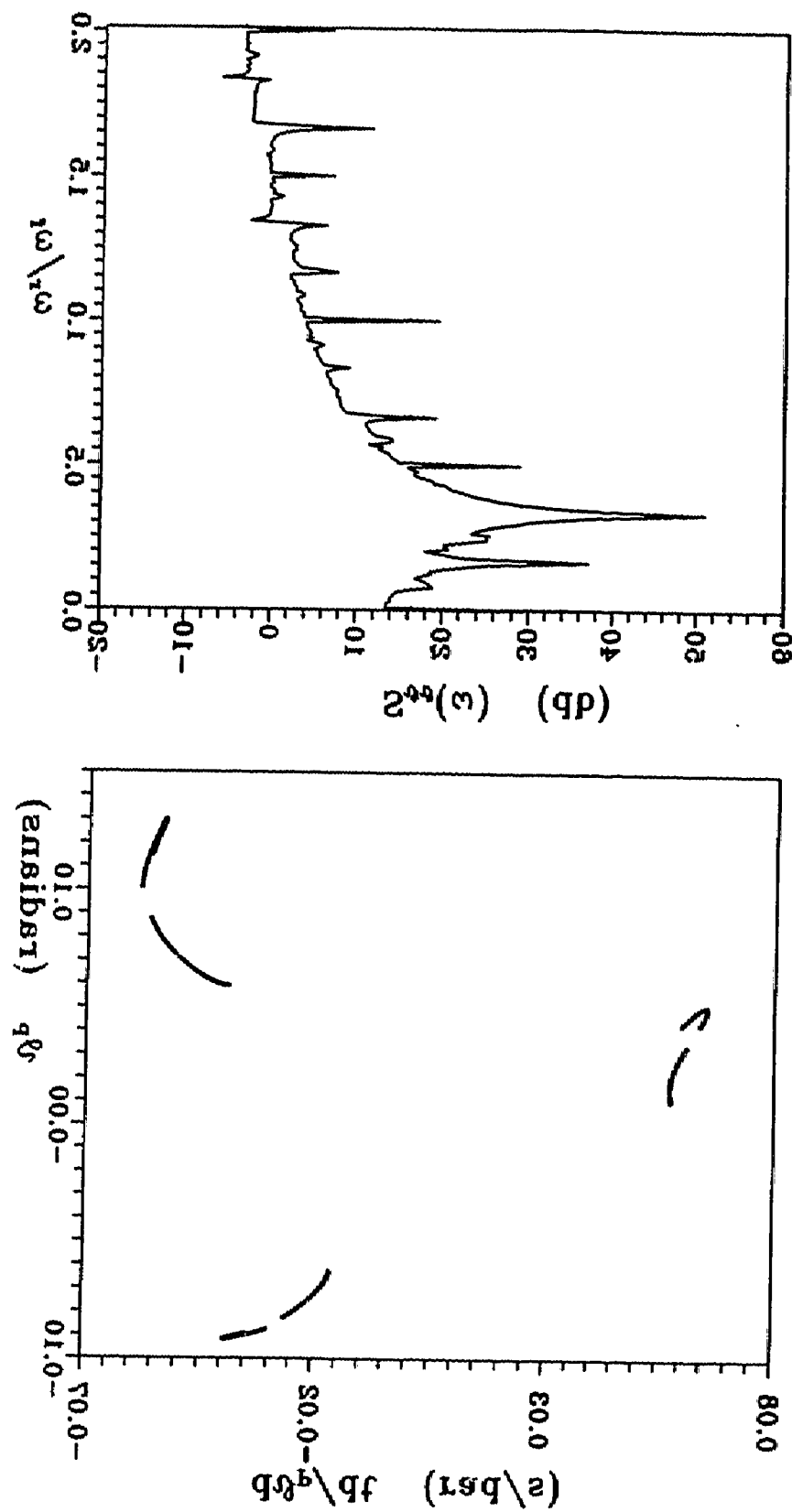
4.6 Numerical Calculation of Liapunov Exponent

The existence of a solution with stability long period does not necessarily imply chaotic motion. The defining characteristic of a chaotic system is its sensitivity dependence on initial conditions. As discussed before, the Liapunov exponent is used as a quantitative test of the divergence of nearby points and measures the sensitivity of the system to changes in initial conditions. Since the system considered here is a second order dissipative differential equation, there is no Liapunov exponents for this system, one is negative to ensure that the system is dissipative, and one has to be zero since there is no stretching, contraction and divergence. Thus the sign of the largest non-zero Liapunov exponent will decide whether the system is positive, this implies chaotic response, whereas if the largest non-zero Liapunov exponent is negative, it indicates periodic response.

The algorithm used to calculate the largest non-zero Liapunov exponent here uses the original definition of original difference. The variation is as follows:

5

Figure 4.15: Bounce rate and power spectrum for crositic responses



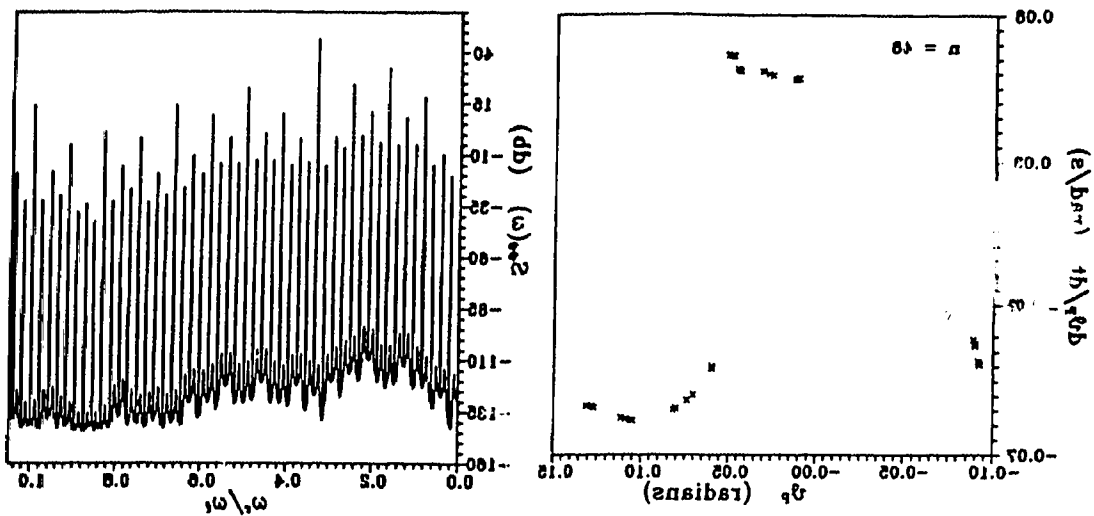
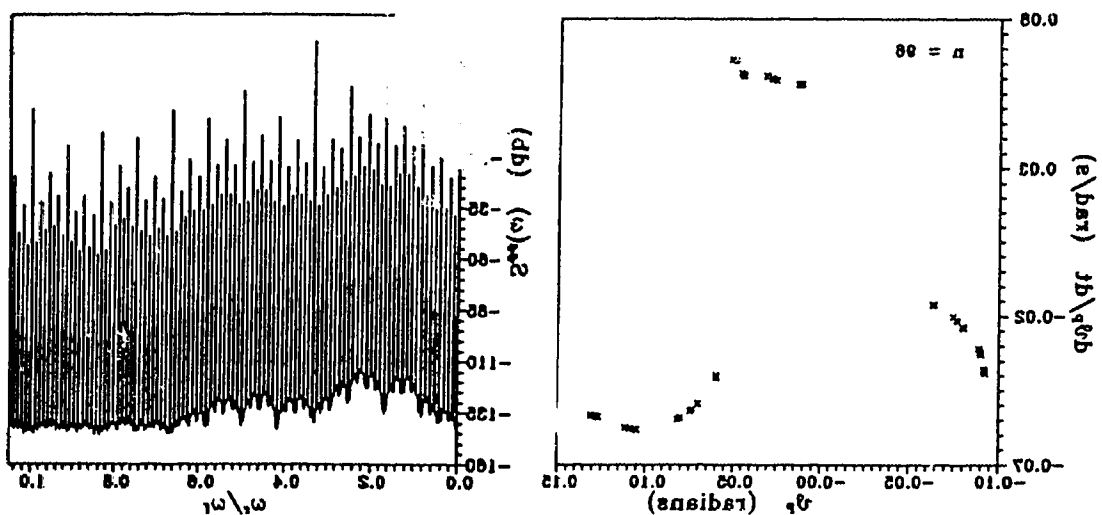
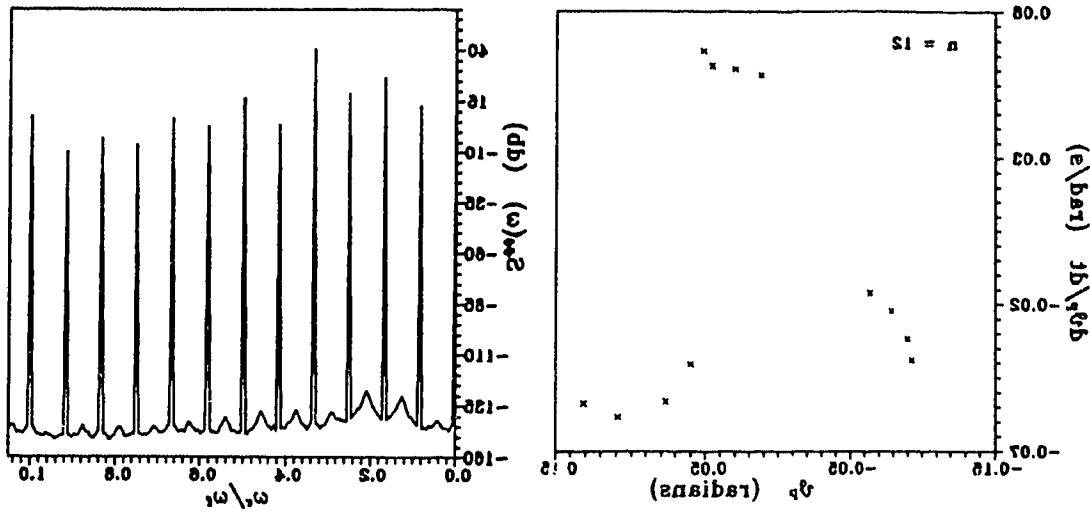
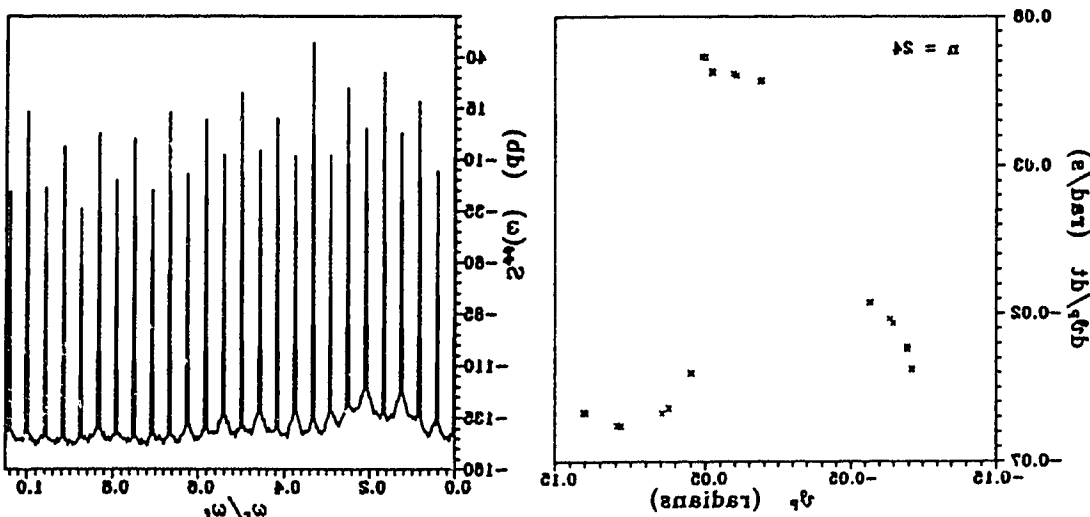
(a) $\omega_1 = 1.83715 \text{ rad/s}$, before 48 solution(b) $\omega_1 = 1.8375 \text{ rad/s}$, before 66 solution

FIGURE 4.14: Poincaré maps and power spectra (cont'd)

07



پولاریزد دامنه های، برابر با ۱.۸۳۵ را در سلول I می باشد (e)



پولاریزد دامنه های، برابر با ۰.۸۳۵ را در سلول II می باشد (f)

فیگچه ۴.۱۴: پولاریزد دامنه های و طیف قدرت (cont'd)

- [22] Lipsett, A. W., *Nonlinear Response of Structures to Regular and Random Waves*, Ph. D. Dissertation, University of British Columbia, 1985.
- [23] Yagasaki, K., "Chaos in a Weakly Nonlinear Oscillator with Parametric and External Resonances", *Journal of Applied Mechanics*, ASME, Vol. 58, pp. 244-250, March, 1991.
- [24] Yagasaki, K., Sakata, M. and Kimura, K., "Dynamics of a Weakly Nonlinear System Subjected to Combined Parametric and External Excitation", ASME, Vol. 57, pp. 209-217, March, 1990.
- [25] HaQuang, N., Mook, D. T. and Plaut, R. H., "A Non-linear Analysis of the Interactions Between Parametric and External Excitations", *Journal of Sound and Vibration*, Vol. 118, pp. 425-439, 1987.
- [26] Choi, H. S. and Lou, J. Y. K., "Nonlinear Behaviour of an Articulated Offshore Loading Platform", *Applied Ocean Research*, Vol. 13, No. 2, pp. 63-74, 1991.
- [27] Gottlieb, O. , Yim, S. C. S. and Hudspeth, R. T., "Analysis of Nonlinear Responses of an Articulated Tower", *Proceedings of the First International Offshore and Polar Engineering Conference*, pp. 384-390, Edinburgh, 1991.
- [28] Liaw, C. Y., "Chaotic and Periodic Responses of a Coupled Wave-Force and Structure System", *Computers and Structures*, Vol. 30, No. 4, pp. 985-993, 1988.
- [29] Fujino, M. and Sagara, N., "An Analysis of Dynamic Behaviour of an Articulated Column in Waves - Effects of Nonlinear Hydrodynamic Drag Force on the Occurrence of Subharmonic Oscillation", *Journal of the Society of Naval Architects of Japan*, pp. 103-112, 1990 (in Japanese).
- [30] Nayfel, A. H. and Khdeir, A. A., "Nonlinear Rolling of Ships in Regular Beam Seas", *International Shipbuilding Progress*, Vol. 33, pp. 40-49, 1986.
- [31] Nayfel, A. H. and Khdeir, A. A., "Nonlinear Rolling of Biased Ships in Regular Beam Waves", *International Shipbuilding Progress*, Vol. 33, pp. 84-93, 1986.
- [32] Liaw, C. Y., "Numerical Modelling and Subharmonic Bifurcations of a Compliant Cylinder Exposed to Waves", *Journal of Offshore Mechanics and Arctic Engineering*, ASME, Vol. 111, pp. 29-36, February, 1989.
- [33] Feigenbaum, M. J., "Quantitative Universality for a Class of Nonlinear Transformations", *Journal of Statistical Physics*, Vol. 19, No. 1, pp. 25-52, 1978.
- [34] Feigenbaum, M. J., "Universal Behaviour in Nonlinear Systems", *Physica*, Vol. 9D, pp. 433-438, 1983.

- [35] Haken, H., " At Least One Lyapunov Exponent Vanishes if the Trajectory of an Attractor Does Not Contain a Fixed Point", *Physics Letters*, Vol. 94A, pp. 71-72, 1983.
- [36] Wolf, A., Swift, J. B., Swinney, H. L. and Vastano, J. A., " Determining Lyapunov Exponents From a Time Series ", *Physica*, Vol. 16D, pp. 285-317, 1985.
- [37] Press, W. H., Flannery, B. P., Teukosky, S. A. and Vetterling, W. T., *Numerical Recipes: The Art of Scientific Computing (FORTRAN version)*, Cambridge University Press, 1989.
- [38] Isaacson, M., " Nonlinear Inertia Forces on Bodies ", *Journal of the Waterway, Port, Coastal and Ocean Division*, ASCE, Vol. 105, No. WW3, pp. 213-227, August, 1979.
- [39] Piessens, R., de Doncker-Kapenga, E., Überhuber, C. W. and Kahaner, D. K., *QUADPACK: A Subroutine Package for Automatic Integration*, Springer-Verlag, 1983.
- [40] Shampine, L. F. and Gordon, M. K., *Computer Solution of Ordinary Differential Equations*, W. H. Freeman and Company, 1975.
- [41] Kapitaniak, T., *Chaotic Oscillations in Mechanical Systems*, Manchester University Press, 1991.
- [42] Baker, G. L. and Gollub, J. P., *Chaotic Dynamics: an introduction*, Cambridge University Press, 1990.
- [43] Plaschko, P., Berger, E. and Brod, K., " The Transition of Flow-Induced Cylinder Vibrations to Chaos ", *Nonlinear Dynamics: An International Journal of Nonlinear Dynamics and Chaos in Engineering Systems*, Vol. 4, No. 3, June, pp. 251-268, 1993.

Appendix A

Solutions Using Local Acceleration Only

Shown in this Appendix are tables which list possible solutions in a variety of the system parameters that have been investigated in this thesis for using local form of fluid particle acceleration $DU/Dt = \partial U/\partial t$.

The results show that complex responses of the articulated tower system are unlikely to occur if the local acceleration only is used to evaluate the fluid particle acceleration.

Table A.1:Solutions for $D = 5m$ using $DU/Dt = \partial U/\partial t$

H=5 m						
d=100 m				d=500 m		
parameters	$C_d = 0.2$	$C_d = 0.5$	$C_d = 1.0$	$C_d = 0.2$	$C_d = 0.5$	$C_d = 1.0$
$\beta = 0.2$	n=1	n=1	n=1	n=1	n=1	n=1
$\beta = 0.5$	n=1	n=1	n=1	n=1	n=1	n=1
$\beta = 0.7$	n=1	n=1	n=1	n=1	n=1	n=1
H=10 m						
d=100 m				d=500 m		
parameters	$C_d = 0.2$	$C_d = 0.5$	$C_d = 1.0$	$C_d = 0.2$	$C_d = 0.5$	$C_d = 1.0$
$\beta = 0.2$	n=1	n=1	n=1	n=1	n=1	n=1
$\beta = 0.5$	n=1	n=1	n=1	n=1	n=1	n=1
$\beta = 0.7$	n=1	n=1	n=1	n=1	n=1	n=1
H=20 m						
d=100 m				d=500 m		
parameters	$C_d = 0.2$	$C_d = 0.5$	$C_d = 1.0$	$C_d = 0.2$	$C_d = 0.5$	$C_d = 1.0$
$\beta = 0.2$	n=1	n=1	n=1	n=1	n=1	n=1
$\beta = 0.5$	n=1	n=1	n=1	n=1	n=1	n=1
$\beta = 0.7$	n=1	n=1	n=1	n=1	n=1	n=1
H=30 m						
d=100 m				d=500 m		
parameters	$C_d = 0.2$	$C_d = 0.5$	$C_d = 1.0$	$C_d = 0.2$	$C_d = 0.5$	$C_d = 1.0$
$\beta = 0.2$	n=1	n=1	n=1	n=1	n=1	n=1
$\beta = 0.5$	n=1	n=1	n=1	n=1	n=1	n=1
$\beta = 0.7$	n=1	n=1	n=1	n=1	n=1	n=1

Table A.2:Solutions for $D = 3m$ using $DU/Dt = \partial U/\partial t$

H=5 m						
d=100 m				d=500 m		
parameters	$C_d = 0.2$	$C_d = 0.5$	$C_d = 1.0$	$C_d = 0.2$	$C_d = 0.5$	$C_d = 1.0$
$\beta = 0.2$	n=1	n=1	n=1	n=1	n=1	n=1
$\beta = 0.5$	n=1	n=1	n=1	n=1	n=1	n=1
$\beta = 0.7$	n=1	n=1	n=1	n=1	n=1	n=1
H=10 m						
d=100 m				d=500 m		
parameters	$C_d = 0.2$	$C_d = 0.5$	$C_d = 1.0$	$C_d = 0.2$	$C_d = 0.5$	$C_d = 1.0$
$\beta = 0.2$	n=1	n=1	n=1	n=1	n=1	n=1
$\beta = 0.5$	n=1	n=1	n=1	n=1	n=1	n=1
$\beta = 0.7$	n=1	n=1	n=1	n=1	n=1	n=1
H=20 m						
d=100 m				d=500 m		
parameters	$C_d = 0.2$	$C_d = 0.5$	$C_d = 1.0$	$C_d = 0.2$	$C_d = 0.5$	$C_d = 1.0$
$\beta = 0.2$	n=1	n=1	n=1	n=1	n=1	n=1
$\beta = 0.5$	n=1	n=1	n=1	n=1	n=1	n=1
$\beta = 0.7$	n=1	n=1	n=1	n=1	n=1	n=1
H=30 m						
d=100 m				d=500 m		
parameters	$C_d = 0.2$	$C_d = 0.5$	$C_d = 1.0$	$C_d = 0.2$	$C_d = 0.5$	$C_d = 1.0$
$\beta = 0.2$	n=1	n=1	n=1	n=1	n=1	n=1
$\beta = 0.5$	n=1	n=1	n=1	n=1	n=1	n=1
$\beta = 0.7$	n=1	n=1	n=1	n=1	n=1	n=1

Table A.3:Solutions for $D = 1m$ using $DU/Dt = \partial U/\partial t$

H=5 m						
d=100 m						
parameters	$C_d = 0.2$	$C_d = 0.5$	$C_d = 1.0$	$C_d = 0.2$	$C_d = 0.5$	$C_d = 1.0$
$\beta = 0.2$	n=1	n=1	n=1	n=1	n=1	n=1
$\beta = 0.5$	n=1	n=1	n=1	n=1	n=1	n=1
$\beta = 0.7$	n=1	n=1	n=1	n=1	n=1	n=1
H=10 m						
d=100 m				d=500 m		
parameters	$C_d = 0.2$	$C_d = 0.5$	$C_d = 1.0$	$C_d = 0.2$	$C_d = 0.5$	$C_d = 1.0$
$\beta = 0.2$	n=1	n=1	n=1	n=1	n=1	n=1
$\beta = 0.5$	n=1	n=1	n=1	n=1	n=1	n=1
$\beta = 0.7$	n=1	n=1	n=1	n=1	n=1	n=1
H=20 m						
d=100 m				d=500 m		
parameters	$C_d = 0.2$	$C_d = 0.5$	$C_d = 1.0$	$C_d = 0.2$	$C_d = 0.5$	$C_d = 1.0$
$\beta = 0.2$	n=1	n=1	n=1	n=1	n=1	n=1
$\beta = 0.5$	n=1	n=1	n=1	n=1	n=1	n=1
$\beta = 0.7$	n=1	n=1	n=1	n=1	n=1	n=1
H=30 m						
d=100 m				d=500 m		
parameters	$C_d = 0.2$	$C_d = 0.5$	$C_d = 1.0$	$C_d = 0.2$	$C_d = 0.5$	$C_d = 1.0$
$\beta = 0.2$	n=1	n=1	n=1	n=1	n=1	n=1
$\beta = 0.5$	n=1	n=1	n=1	n=1	n=1	n=1
$\beta = 0.7$	n=1	n=1	n=1	n=1	n=1	n=1

Appendix B

Numerical Calculation of the Largest Liapunov Exponent

This appendix contains a description of the method for the numerical calculation of the largest Liapunov exponent for a set of first order time dependent differential system. The algorithm here follows that given by Wolf et al. [36] and Moon [5].

B.1 Definition

For an n-dimensional time-dependent differential system, we monitor the long term evolution of an infinitesimal n-sphere of initial conditions. The sphere will become an n-ellipsoid due to the local deformation. If $d_i(t)$ denotes the length of the i^{th} ellipsoidal principal axis, then the i^{th} Liapunov exponent is defined as (see for example, Wolf et al. [36]),

$$\lambda_i = \lim_{t \rightarrow \infty} \frac{1}{(t - t_0)} \ln \frac{d_i(t)}{d_i(t_0)}. \quad (\text{B.1})$$

The λ_i , $i = 1, 2, \dots, n$, ordered from largest to smallest, are related to the stretching and contracting nature of different directions in phase space. If $d(t)$ denotes the

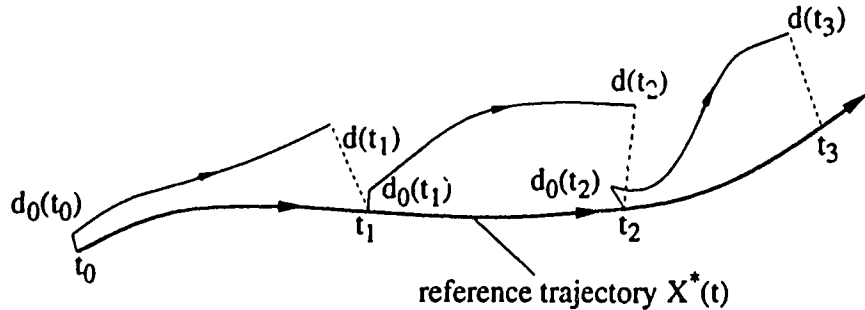


Figure B.1: Calculation of the largest Lyapunov exponent from time series

largest length of ellipsoidal principal axis, the largest Lyapunov exponent is then defined as

$$\lambda_1 = \lim_{t \rightarrow \infty} \frac{1}{(t - t_0)} \ln \frac{d(t)}{d(t_0)} \quad (\text{B.2})$$

A problem arises for using this definition directly to calculate λ_1 . The divergence of chaotic trajectories can only be locally exponential as $d(t)$ cannot go to infinity if the system is bounded as is the case for a dissipative system, such as the articulated tower system discussed in this thesis. In practice, to obtain a measure of this divergence, averaging must be used to estimate the exponential growth at many points along a reference trajectory as shown in Figure B.1. Thus the procedure to measure this divergence of trajectories goes as follows. Beginning with a reference trajectory and a point on a nearby trajectory, measure $d(t)/d(0)$. When $d(t)$ grows too large, take a new “nearby” trajectory and define a new $d(0)$. In Equation B.2, let $t - t_0 = \tau$, and take N samples. After averaging we have

$$\lambda_1 = \frac{1}{N} \sum_{i=1}^N \frac{1}{\tau} \ln \frac{d(t_i)}{d_0(t_{i-1})}$$

$$\begin{aligned}
&= \frac{1}{N\tau} \sum_{i=1}^N \frac{d(t_i)}{d_0(t_{i-1})} \\
&= \frac{1}{t_N - t_0} \sum_{i=1}^N \frac{d(t_i)}{d_0(t_{i-1})}.
\end{aligned} \tag{B.3}$$

It can be seen that the main idea to calculate λ_1 is to be able to determine the ratio $d(t_i)/d_0(t_{i-1})$.

B.2 Algorithm for Computing the Largest Liapunov Exponent λ_1

The method described below to compute the largest Liapunov exponent follows that given in [5]. For a set of first order n-dimensional differential equations of the form

$$\dot{\mathbf{x}} = \mathbf{f}(\mathbf{x}, t), \tag{B.4}$$

integration gives a reference solution $\mathbf{x}^*(t)$. The integrating time should be long enough to get rid of the transients. Then take $\mathbf{x}^*(t_k)$ and a nearby point $\mathbf{x}^*(t_k) + \Delta\mathbf{x}(t_k)$ as initial conditions, where $\Delta\mathbf{x}(t_k)$ is the initial divergence vector with each component along each principal axis and can be obtained by solving the following variational equations.

Substitute $\mathbf{x}^*(t_k) + \Delta\mathbf{x}(t_k)$ into Equation B.4 to get

$$\dot{\mathbf{x}}^*(t_k) + \Delta\dot{\mathbf{x}}(t_k) = \mathbf{f}(\mathbf{x}^* + \Delta\mathbf{x}, t). \tag{B.5}$$

Expanding $\mathbf{f}(\mathbf{x}^* + \Delta\mathbf{x}, t)$ in Taylor series in the vicinity of $\mathbf{x}^*(t_k)$ and retaining the linear terms, we have

$$\Delta\dot{\mathbf{x}}(t_k) = \left. \frac{\partial \mathbf{f}}{\partial \mathbf{x}} \right|_{\mathbf{x}=\mathbf{x}^*} \Delta\mathbf{x}(t_k) \tag{B.6}$$

or

$$\Delta \dot{\mathbf{x}}(t_k) = \mathbf{J}|_{\mathbf{x}=\mathbf{x}^*} \Delta \mathbf{x}(t_k) \quad (\text{B.7})$$

where $\partial \mathbf{f} / \partial \mathbf{x}|_{\mathbf{x}=\mathbf{x}^*} = \mathbf{J}$ is the Jacobian matrix evaluated at $\mathbf{x} = \mathbf{x}^*$. Equation B.7 is called variational equations, and it represents the linearization of vector field along a trajectory. Thus at each time step, called the Liapunov time step, $\tau = t_{k+1} - t_k$ should be small to minimize the error.

In practice, we can integrate Equations B.4 and B.7 simultaneously, taking into account the change in \mathbf{J} through $\mathbf{x}^*(t)$. After a given time interval $\tau = t_{k+1} - t_k$, take

$$\frac{d(t_{k+1})}{d(t_k)} = \left| \frac{\Delta \mathbf{x}(\tau, t_k)}{\Delta \mathbf{x}(0, t_k)} \right|. \quad (\text{B.8})$$

For next step, use the direction of $\Delta \mathbf{x}(\tau, t_k)$ and normalize it to get

$$\Delta \mathbf{x}(0, t_{k+1}) = \frac{\Delta \mathbf{x}(\tau, t_k)}{|\Delta \mathbf{x}(0, t_k)|}. \quad (\text{B.9})$$